

**UNIVERSITY OF MISSOURI,
COLUMBIA**

Synthesis and Reactivity of Actinide Phosphorano-Stabilized Carbene and Phosphido
Complexes

DISSERTATION

Submitted in partial satisfaction of the requirements

For the degree of

DOCTOR OF PHILOSOPHY

in Chemistry

by

Pokpong Rungthanaphatsophon

University of Missouri, Columbia

May 2018

Portions of Chapter 1 © 2017 Wiley-VCH Verlag GmbH & Co. KGaA, Weinheim

Portions of Appendix A © 2016 Royal Society of Chemistry

All other materials © 2018 Pokpong Rungthanaphatsophon

The dissertation of Pokpong Rungthanaphatsophon is approved and is acceptable in quality and form for publication on microfilm and digital formats:

Committee Chair

Acknowledgements

I would like to thank my advisor, Justin Walensky, for the guidance and mentorship he provided.

Charles Barnes, Wei Wycoff, and Steven Kelley for their technical support at the University of Missouri-Columbia.

The computational portion of this dissertation would not be possible without the help of Adrien Bathelier, Ludovic Castro, Patrick Huang, Laurent Maron, Thomas Duignan, Jochen Autschbach, Enrique Batista, and Ping Yang.

Special thanks to the Walensky group: Robert Ward, Matthew Vollmer, Andrew Lane, Andrew Behrle, Andrew Breshears, Kira Behm, Sean Vilanova, Alex Myers, Michael Tarlton, and Michael Murray.

Table of Contents

Acknowledgements.....	ii
Table of Figures	vi
Table of Tables	x
Abstract of Dissertation	1
Introduction.....	3
Chapter 1: Formation of Methane vs. Benzene in the Reactions of $(C_5Me_5)_2Th(CH_3)_2$ with $[CH_3PPh_3]X$, $X = Cl, Br, I$, Yielding Thorium-Carbene or Thorium-Ylide Complexes.....	8
Introduction.....	8
Experimental.....	10
General Considerations	10
Crystal structure determination and refinement.....	13
Computational details.....	14
Results and Discussion	15
Density Functional Theory (DFT) and Mechanistic Investigations.....	18
Conclusion	24
Chapter 2: Phosphorano-Stabilized Carbene Complexes with Short Thorium(IV) and Uranium(IV)-Carbon Bonds	26
Introduction.....	26

Experimental.....	27
General Considerations.....	27
Crystal structure determination and refinement.....	31
Computational Details.....	32
Results and Discussion.....	33
Syntheses.....	33
Spectroscopy.....	34
Structural Analysis.....	35
Electronic Structure Calculations.....	37
Conclusion.....	44
Chapter 3: Four Electron Reduction Chemistry Using an Uranium(III) Phosphido Complex.....	46
Introduction.....	46
Experimental.....	47
General Considerations.....	47
Crystallographic data collection and structure determination.....	50
Result and discussion.....	53
Conclusions.....	57
Chapter 4: Influence of Substituents on Electronic Structure of Mono- and Bis(Phosphido) Thorium(IV) Complexes.....	58
Introduction.....	58

Experimental.....	59
General considerations.....	59
Computational Details.	65
Crystal structure determination and refinement.....	65
Results and Discussion	68
Syntheses.	68
Structural Analysis.....	70
Spectroscopy and TD-DFT Calculations.	74
Conclusion	79
Appendix A: Copper(I) Clusters with Bulky Dithiocarboxylate, Thiolate, and Selenolate Ligands	81
Introduction.....	81
Experimental.....	82
General Considerations.....	82
Appendix B: Reactivity of U(IV) Phosphido Complexes with Organic Azide and Isocyanide.	112
Introduction.....	112
Experimental Section.....	112
General Considerations.....	112
References.....	125
Vita	157

Table of Figures

Figure 1-1. Phosphorano-stabilized carbene ligands previously used with thorium and/or uranium.	9
Figure 1-2. Thermal ellipsoid plots of 2 (left) and 3 (right) shown at the 50% probability level. Only the hydrogen atom connected to the carbene carbon is shown for clarity. ...	17
Figure 1-3. DFT computed enthalpy profile (298 K) in kcal/mol. The blue pathway refers to the benzene elimination pathway to form 1 while the green pathway refers to the carbene formation, 3	20
Figure 1-4. 3D representation of the σ (a) and π (b) bonds in complex 1	24
Figure 2-1. Thermal ellipsoid plots of 1 (left) and 2 (right) shown at the 50% probability level. The hydrogen atoms, except for H21, have been omitted for clarity.....	36
Figure 2-2. Natural bond orbitals (NBOs) in complex 4 . The uranium-carbene bond is composed of a σ -type (left) and π -type (right) NBO. The α - and β -spin NBOs are indistinguishable on this scale so only the α -spin NBOs are shown. The π -type NBO mixes with a P–C antibonding σ -NBO, thus extending the effects of spin polarization due to the paramagnetic uranium to the P–C centers.	38
Figure 2-3. Summary of relevant reported ^{13}C NMR resonances and thorium-carbon bond distances. Those with only one of the two characteristics have been omitted.....	43
Figure 3-1. Thermal ellipsoid plots of 1 shown at the 50% probability level. The hydrogen atoms have been omitted for clarity.....	54
Figure 3-2. Thermal ellipsoid plots of 2 shown at the 50% probability level. The hydrogen atoms have been omitted for clarity.....	56

Figure 4-1. Thermal ellipsoid plots of 1 (left) and 4 (right) shown at the 50% probability level. The hydrogen atoms have been omitted for clarity.....	72
Figure 4-2. Thermal ellipsoid plot of 2 shown at the 50% probability level. The hydrogen atoms have been omitted for clarity.....	73
Figure 4-3. Thermal ellipsoid plot of 6 shown at the 50% probability level. The hydrogen atoms have been omitted for clarity.....	73
Figure 4-4. Thermal ellipsoid plot of 7 shown at the 50% probability level. The hydrogen atoms have been omitted for clarity.....	74
Figure 4-5. Molecular orbital (MO) diagram of related thorium complexes. 6d and 5f indicate at least 5% total thorium character in the molecular orbital with the larger contribution taking precedent in the coloring scheme. Ligand denotes less than 5% thorium character. Isosurfaces (± 0.03 au) of LUMO (above) and HOMO (below).....	77
Figure 4-6. Comparison of experimental and theoretical absorption spectra for $(C_5Me_5)_2Th[PH(Mes)]_2$ and $(C_5Me_5)_2Th[P(Mes)(CH_3)]_2$, 2 . Observable features of the experimental spectra are reproduced well by the calculations. Inlaid on the spectra are isosurfaces (± 0.03 au) of natural transition orbitals (NTOs) positioned to correspond to the spectral features observed.	79
Figure A-1. Active site of CusA is shown.	81
Figure A-2. General drawing of the terphenyl ligands used in this manuscript.	82
Figure A-3. Thermal ellipsoid plot of 1 shown at the 50% probability level. All hydrogen atoms and residual solvent molecule are omitted for clarity.	101
Figure A-4. Thermal ellipsoid plot of 2 shown at the 50% probability plot. All hydrogen atoms are omitted for clarity.	103

Figure A-5. Thermal ellipsoid plot of 3 shown at the 50% probability level. All hydrogen atoms, carbon atoms on PEt_3 , and residue solvent molecule are omitted for clarity.	103
Figure A-6. Thermal ellipsoid plot of 4 shown at the 50% probability level. All hydrogen atoms and residue solvent molecule are omitted for clarity.	104
Figure A-7. Thermal ellipsoid 30% probability plot of 5 . All hydrogen atoms are omitted for clarity.....	105
Figure A-8. Thermal ellipsoid plot of 7 shown at the 50% probability level. All hydrogen atoms are omitted for clarity.	105
Figure A-9. Thermal ellipsoid plot of 8 shown at the 50% probability level. All hydrogen atoms and residue solvent molecule are omitted for clarity..	106
Figure A-10. Thermal ellipsoid plot of 9 shown at the 50% probability level. All hydrogen atoms are omitted for clarity.	107
Figure A-11. Thermal ellipsoid plot of 10 shown at the 50% probability level. All hydrogen atoms are omitted for clarity.	108
Figure A-12. Thermal ellipsoid plot of 11 shown at the 50% probability level. All hydrogen atoms are omitted for clarity.	108
Figure A-13. Thermal ellipsoid plot of 12 shown at the 50% probability level. All hydrogen atoms are omitted for clarity.	110
Figure A-14. Thermal ellipsoid plot of 13 shown at the 50% probability level. All hydrogen atoms are omitted for clarity..	110
Figure B-1. Thermal ellipsoid plot of $(\text{C}_5\text{Me}_5)_2\text{Th}[\text{P}(\text{C}_6\text{H}_5)(\text{SiMe}_3)]_2$ shown at the 50% probability level. All hydrogen atoms are omitted for clarity.	114

Figure B-2. Thermal ellipsoid plot of $(C_5Me_5)_2Th[P(C_6H_5)(SiMe_3)]_2$ shown at the 50% probability level. All hydrogen atoms are omitted for clarity.	115
Figure B-3. Thermal ellipsoid plot of $(C_5Me_5)_2Th(CN^tBu)[(\eta^2-N,C)-(^tBuNCPPh)]$ shown at the 50% probability level. All hydrogen atoms are omitted for clarity.	116
Figure B-4. Thermal ellipsoid plot of $(C_5Me_5)_2Th(CN^tBu)[(\eta^2-N,C)-(^tBuNCPPh)]$ shown at the 50% probability level. All hydrogen atoms are omitted for clarity.	117
Figure B-5. Thermal ellipsoid plot of $(C_5Me_5)_2U(CH_3)[P(C_6H_2Me_3-2,4,6)(SiMe_3)]$ shown at the 50% probability level. All hydrogen atoms are omitted for clarity.	118
Figure B-6. Thermal ellipsoid plot of $(C_5Me_5)_2Th[^tBuNCCH_2C=N^tBuCN^tBu]$ shown at the 50% probability level. All hydrogen atoms are omitted for clarity.	120
Figure B-7. Thermal ellipsoid plot of $(C_5Me_5)_2Th[^tBuNCCH_2C=N^tBuCN^tBu]$ shown at the 50% probability level. All hydrogen atoms are omitted for clarity.	121
Figure B-8. Thermal ellipsoid plot of $(C_5Me_5)_2U(\kappa^2-N,N)-[(N(SiMe_3))_2P(C_6H_2Me_3-2,4,6)]$ shown at the 50% probability level. All hydrogen atoms are omitted for clarity.	122
Figure B-9. Thermal ellipsoid plot of $(C_5Me_5)_2U(CH_3)[-N=P(SiMe_3)_2(C_6H_5)]$ shown at the 50% probability level. All hydrogen atoms are omitted for clarity.	124

Table of Tables

Table 1-1. X-ray crystallographic data shown for complexes 1-3	14
Table 1-2. Calculated and experimental geometrical parameters of Prod, 3 . Distance and angles are reported in Å and degrees (°) respectively.....	23
Table 2-1. X-ray crystallographic data shown for complexes 1-4	31
Table 2-2. ¹ H, ¹³ C, and ³¹ P NMR resonances for the phosphorano-stabilized carbene ligand.....	34
Table 2-3. Selected bond distances (Å) and angles (deg) for thorium and uranium carbene complexes.	36
Table 2-4. Analysis of the uranium-carbene bond in (C ₅ Me ₅) ₂ U(X)(CHPPh ₃) complexes, X = Cl, 2 ; Br, 3 ; I, 4 , as derived from DFT-ZORA: percent uranium composition of natural bond orbitals (NBO), QTAIM bond critical point parameters (ρ , $\nabla^2\rho$, H , ϵ), and bond index parameters (Wiberg index in the NAO basis and delocalization index over the U–C atomic basins).....	39
Table 3-1. Crystallography data for complexes 1, 2 , and 4	53
Table 4-1. X-ray crystallographic data shown for complexes 1-7	66
Table 4-2. Selected bond distances (Å) and angle (deg) for complexes 1, 2, 4-7	71
Table 4-3. ³¹ P NMR resonances for metallocene thorium phosphido complexes, Mes = C ₆ H ₂ Me ₃ -2,4,6.	76
Table A-1. Select ¹ H, ¹³ C, and ³¹ P NMR resonances (in ppm) for complexes 1, 3-13 ..	100

Abstract of Dissertation

Synthesis and Reactivity of Actinide Phosphido and Phosphorano-Stabilized Carbene
Complexes

By

Pokpong Rungthanaphatsophon

University of Missouri, Columbia, 2018

Professor Justin R. Walensky, Chair

Nuclear power plants have been operated in the United States for over 60 years, generating over 800 terawatt-hours of energy per year. However, there is still no reliable process to recycle the spent nuclear fuel. This dissertation looks at the formation of actinide-ligand multiple bonds, which may give us insights into how to improve the process of separation of actinides from the spent nuclear fuels contaminated with lanthanides. This is because lanthanides cannot participate in multiple bonding and a difference in coordination chemistry between actinides and lanthanides is important in separation methods. This dissertation contains two parts, both of which involve using phosphorus to create new actinide complexes. Chapters 1 and 2 outline the use of phosphorano-stabilized carbene complexes to make short actinide-carbon bonds. In fact,

these complexes exhibit the shortest uranium and thorium-carbon bonds reported in the literature.

Chapter 3 revolves around investigating the synthesis, characterization, and reactivity of actinide phosphido (monoanionic phosphine) complexes. In this regard, I have synthesized the first trivalent uranium phosphido complex, $(C_5Me_5)_2U[P(SiMe_3)(2,4,6-Me_3C_6H_2)](THF)$. The investigation of its reactivity revealed that the complex is capable of 4-electron reduction chemistry. For example, the reaction of $(C_5Me_5)_2U[P(SiMe_3)(2,4,6-Me_3C_6H_2)](THF)$ with azidotrimethylsilane, N_3SiMe_3 , produces a U(VI) complex. Three electrons are from the metal center, U(III) to U(VI), and one electron is from reductive coupling of the phosphido ligand.

The phosphido chemistry can also be extended to tetravalent uranium and thorium. Chapter 4 outlines the synthesis of thorium phosphido complexes which exhibit an unusual absorption in the visible region which we contributed to a ligand to metal charge transfer. Just by varying the ligand design, we were able to manipulate the HOMO/LUMO gap, which results in an absorption in a different part of the visible region.

Appendix A summarizes the synthesis of copper(I) complexes with bulky terphenyl ligands. The steric properties of the complex center can be tuned by changing the substituent on the terphenyl. By carefully controlling the steric properties, different coordinating environments around the metal center can be achieved. Finally, Appendix B describes the reactivity of U(IV) phosphido complexes with organic azide and *tert*-butyl isocyanide.

Introduction

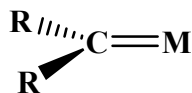
Over the past few decades, organoactinide complexes have been studied due to their potential to perform unique chemical transformations both stoichiometrically and catalytically¹. This unique property is due to its high Lewis acidity and large size, which lead to the formation of complexes with high coordination numbers², allowing for binding of multiple substrates with unique coordination environments. Another key factor to its unique properties is the presence of the 5f orbitals, which have been shown to be able to participate in bonding, unlike 4f orbitals of the lanthanides³⁻⁵. However, the degree of participation of the 5f orbitals still remains unclear. The area of metal-ligand multiple bonding in actinides gives rise to an opportunity to study this characteristic. However, the area is severely underdeveloped when compared to that of transition metals. Transition metal complexes with metal-ligand multiple bonds have been proposed as intermediates and in some cases direct catalysts for multiple important chemical transformations⁶⁻⁹. As mentioned previously, unlike transition metals, due to their large ionic radii and high Lewis acidity, actinide complexes with metal-ligand multiple bonds have been shown to give rise to unique chemical properties¹⁰. A comprehensive study and understanding of these complexes could give rise to a better separation process or novel reactivity.

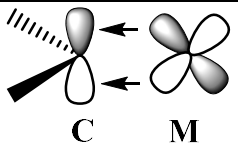
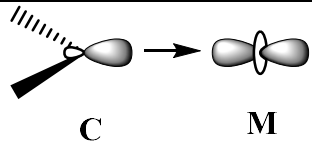
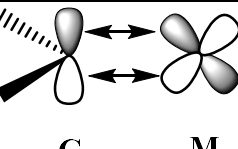
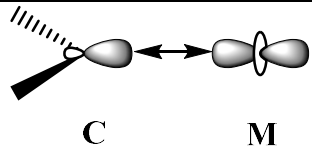
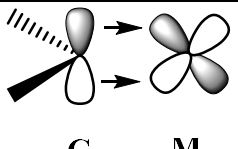
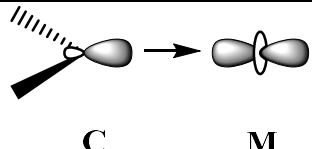
The first actinide pentamethylcyclopentadienyl (Cp*) complex was reported in 1979¹¹, along with other compounds including Cp*₂An(CH₃)₂ (An = Th or U)¹², which proved to be important starting materials for several chemical processes. There are several factors that contribute to its usefulness. First, the steric crowding provided by the Cp* ligand

leaves only the frontal orbitals of the metal to be accessible for other substrates. In addition, due to its poor overlap with the orbitals on the metal center, electron density from other substrates must be provided, enhancing metal-ligand bond along the frontal orbitals.

The study of metal-ligand multiple bonds in actinide chemistry has been dominated by uranyl (UO_2^{2+}) chemistry¹³⁻¹⁴. The first non-oxo actinide complex, which contains some multiple bond character, was synthesized in the early 1980s by Gilje featuring a phosphorano-stabilized carbene¹⁵. It has been shown that complexes of actinides with multiple bond character can perform a remarkable chemical transformation¹.

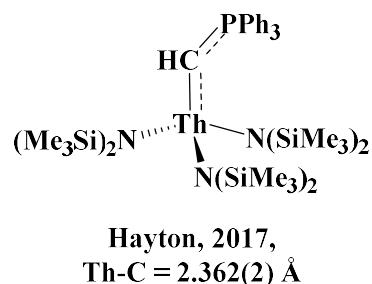
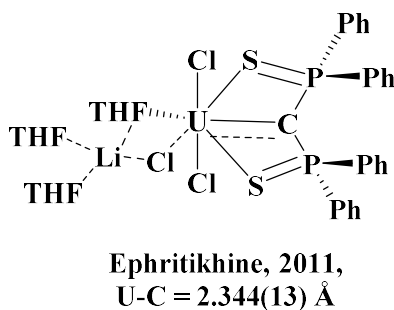
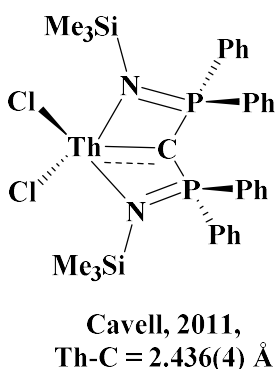
In organometallic chemistry, the term carbene is used to describe metal complexes containing the $\text{M}=\text{CRR}'$ moiety. The most well studied of this class of ligand are Fischer carbenes and Schrock alkylidenes. In a Fischer carbene, the $\text{M}=\text{C}$ bond is formed from σ donation of the filled orbital on the carbon to the empty orbital on the metal center and π back bonding from the metal center. On the other hand, Schrock alkylidenes are formed from a coupling of metal and ligand triplet state¹⁶. In contrast to these two major types of carbene, the phosphorano-stabilized carbene complex isolated by Gilje, all four electrons used to form metal carbon bonds originated from the ligand¹⁷.



	R	π	σ
Fischer carbene	Electron donating		
Schrock alkylidene	Alkyl		
Phosphorano-stabilized carbene	Electron Withdrawing		

As mentioned previously, the first actinide carbene complex was synthesized by Gilje in the early 80s featuring a significantly shorter U-C bond length (2.29 Å) than other complexes. In addition, U-C-P bond angle is larger than 140° together with the short U-C bond this indicates a significant degree of multiple bond character in the U-C bond¹⁵. The compound is also highly reactive toward small molecules such as carbon monoxide¹⁸, isocyanates¹⁹, and nitriles²⁰. The field was rejuvenated again when Ephritikhine isolated uranium carbene complexes with methandiide pincer ligand²¹. However, these complexes exhibit a much longer U-C bond compare to that of Gilje's. Nevertheless, these methandiide pincer complexes exhibit a highly polarized U-C and readily react with small molecules such as nitriles and carbonyls²²⁻²³, which demonstrated the nucleophilic

nature of the methandiide carbon. Built upon Ephritikhine's work, Liddle and Cavell independently isolated actinide carbene complexes using methandiide ligand²⁴⁻²⁵. Hayton was also able to isolate actinide carbene complexes by using $U(NR_2)_3$ or $(NR_2)_2Th[CH_2SiMe_2NR]$ ($An = Th^{26}, U^{27}$; $R = SiMe_3$).



To date, no true alkylidene has been successfully isolated. However, multiple attempts to generate the compound using diazoalkanes have yielded interesting results, such as the formation of metal hydrazido complex²⁸ and a reduction on the diazoalkane to form a radical anion fragment²⁹.

Another aspect of this dissertation is the synthesis of actinide phosphido ($M-PR_2$) complexes and their reactivity, but continuing the theme of using phosphorus to produce novel actinide complexes. Due to a weak actinide-phosphorus bond, such complexes are rare in the actinide chemistry. The reactivity and properties of these complexes are not well understood but are interesting due to their potential use in catalysis and small molecule activation.

The first ever reported actinide-phosphorus bonds is $(C_5Me_5)_2Th(PPh_2)_2$ ³⁰. The compound exhibits a dark purple color, which is unusual given its diamagnetic nature. While dark purple thorium compounds had been reported before, such species are

typically associated with either Th(III)³¹ or contain a radical-based ligand³². In contrast, $(C_5Me_5)_2Th[PH(C_6H_2(CH_3)_3-2,4,6)]$ and $(C_5Me_5)_2Th[PH(C_6H_2(iPr)_3-2,4,6)]$ both exhibited a pale yellow to orange color. This suggests that the electronic structure of these complexes ties in very closely to the substituent on the phosphorus.

In recent years, bond formation involving phosphorus has become increasingly more important in organic synthesis due to its potential use in stereo-controlled bond formation reaction³³. Although synthesis of these compounds can be done, metal-mediated reactions have proven to be much easier. Better understanding of these reactions can lead to a new synthetic route for useful bioactive molecules.

Chapter 1: Formation of Methane vs. Benzene in the Reactions of $(C_5Me_5)_2Th(CH_3)_2$ with $[CH_3PPh_3]X$, $X = Cl, Br, I$, Yielding Thorium-Carbene or Thorium-Ylide Complexes¹

Introduction

Due to their large size and high Lewis acidity, actinides have the ability to demonstrate coordination chemistry and reactivity not seen elsewhere on the periodic table³⁴⁻³⁸. This is in part due to the relatively poor overlap of metal-ligand orbitals, thus making steric properties of the ligands coordinated to the metal paramount in the stability of the overall complex. In addition, due to their being highly electropositive metals, actinide alkyl and hydride complexes tend to be reactive towards a variety of substrates³⁹⁻⁴².

Thorium and uranium metallocene complexes have been extensively studied, providing a plethora of reactivity patterns⁴³. One recurring theme in $(C_5Me_5)_2AnR_2$, $An = Th, U$; $R =$ alkyl, is their ability to facilitate C-H bond activation reactions as well as the capability to perform protonolysis reactions. For example, $(C_5Me_5)_2ThMe_2$ reacts with *N*-pyridine oxide to liberate methane by C-H bond activation of the pyridine ring⁴⁴ and can also be used to make metal-ligand multiple bonds with anilines such as $H_2N(2,6-Me_2C_6H_3)$ to produce $(C_5Me_5)_2Th=N(2,6-Me_2C_6H_3)(THF)$ ⁴⁵.

Several groups have synthesized complexes featuring actinide-carbon multiple bonds, and these compounds feature a phosphorano-stabilized carbene moiety of some form, Figure 1-1. Gilje and Cramer reported the first uranium-carbene compound,

¹ A version of this chapter has been published: See: *Angew. Chem. Int. Ed.*, 2017, 56, 12925 –12929.

(C₅H₅)₃UCHPPh(CH₃), from the salt metathesis reaction of (C₅H₅)₃UCl with Li[κ²-(C,C')-(CH₂)(CH₂)PPh(CH₃)]¹⁵. The Ephritikhine^{22, 46-47} and Liddle^{23, 48-54} groups have produced several U(IV), U(V), and U(VI) complexes in subsequent years from salt metathesis reactions with a dilithium methandiide, Li₂[C(PPh₂E)₂], E = NSiMe₃ or S, starting material. Additionally, the Hayton group used the reaction of U[N(SiMe₃)₂]₃ with an ylide, Ph₃P=CH₂, to produce [(Me₃Si)₂N]₃UCHPPh₃²⁷. In all of these examples, short actinide-carbon bonds are observed only when the carbene is terminally bound to the actinide.

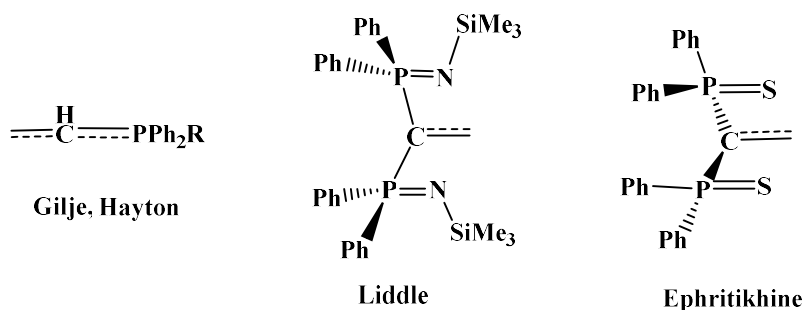


Figure 1-1. Phosphorano-stabilized carbene ligands previously used with thorium and/or uranium.

Whether these complexes, that feature zwitterions with metal-carbon bond distances similar to metal-alkyl complexes, qualify as metal-ligand multiple bonds has also been discussed⁵⁵. For example, in terminal phosphorano-stabilized carbene complexes, the U-C bond distances are 2.29(3)^{15, 56} and 2.278(8) Å,²⁷ respectively. The shortest bond distance reported for a supported carbene has a uranium(IV)-carbon bond length of 2.310(4) Å⁵¹. Only when uranium is in a penta- or hexavalent oxidation state does the uranium-carbon distance shorten to ~2.18-2.45(1) Å⁵⁴. In the case of thorium, Liddle has synthesized a thorium carbene complex with Th-C distances from 2.41-2.51 Å^{48, 50}.

Recently, a terminal thorium phosphorano-stabilized carbene was reported by Hayton and has a Th-C bond distance of 2.362(2) Å²⁶. Herein, we report two new phosphorano-stabilized carbene complexes with short, 2.299(6) and 2.3137(18) Å, thorium-carbon distances.

Experimental

General Considerations. All syntheses were carried out using standard Schlenk and glovebox techniques under a nitrogen atmosphere. All solvents were dried over activated molecular sieves and alumina column in solvent purification system by MBRAUN, USA. Methylolithium, methyltriphenylphosphonium iodide, methyltriphenylphosphonium bromide, and methyltriphenylphosphonium chloride (Aldrich) were used as received. (C₅Me₅)Th(CH₃)₂ was synthesized following literature procedures¹². Elemental analyses were performed by Microanalysis Facility, College of Chemistry, University of California, Berkeley. Deuterated solvent was obtained from Cambridge Isotope Laboratories, Inc. Benzene-*d*₆ was dried over molecular sieves, and degassed by three cycles of freeze-pump-thaw. Infrared spectra were recorded as KBr pellets on Perkin-Elmer Spectrum One FT-IR spectrometer. ¹H and ¹³C NMR data were obtained using 500 and 300 MHz DRX Bruker spectrometer. ³¹P NMR data were obtained using 300 MHz DRX Bruker spectrometer. ¹H and ¹³C chemical shifts are reported in ppm referenced to solvent impurities and ¹³C resonances as internal standards.⁵⁷ ³¹P chemical shifts are reported in ppm relative to 85% H₃PO₄ external standard. NMR multiplicities are indicated s (singlet), d (doublet), t (triplet), and m (multiplet).

Caution! Thorium-232 is an alpha-emitting radiometal with a half-life of 1.4×10^{10} years. It was used in a radiological laboratory with appropriate personal protective and counting equipment.

Synthesis of $(C_5Me_5)Th(Cl)[(CH_2)(CH_2)PPh_2]$, **1.** Brown powder of **1** was synthesized by using $(C_5Me_5)Th(CH_3)_2$ (248 mg, 0.47 mmol) and methyltriphenylphosphonium chloride (146 mg, 0.47 mmol) in 1:1 toluene/THF mixture at 75 °C for 18 hours (140 mg, 40%). Crystals suitable for X-ray crystal analysis were obtained from a concentrated solution of **1** at -45 °C after several days. 1H NMR (500 MHz, C_6D_6): δ 0.51 (d, 1H, $^2J_{H-P} = 13.5$ Hz, $(CH_2)(CH_2)PPh_2$), 0.69 (d, 1H, $^2J_{H-P} = 7.5$ Hz, $(CH_2)(CH_2)PPh_2$), 2.01 (s, 30 H, $C_5(CH_3)_5$), 6.95-7.03 (m, 6H, *m*- and *p*- Ph), 7.59-7.63 (m, 4H, *o*- Ph). $^{13}C\{^1H\}$ NMR (C_6D_6): 12.3 ($C_5(CH_3)_5$), 16.0 ($^1J_{C-P} = 47$ Hz, $(CH_2)(CH_2)PPh_2$), 19.5 ($^1J_{C-P} = 38$ Hz, $(CH_2)(CH_2)PPh_2$), 123.4 ($C_5(CH_3)_5$), 128.6 (d, $^3J_{C-P} = 10.2$ Hz, *m*- Ph), 130.5 (d, $^2J_{C-P} = 10.4$ Hz, *o*- Ph), 131.0 (d, $^4J_{C-P} = 3.4$ Hz, *p*- Ph), 138.7 (d, $^1J_{C-P} = 57.6$ Hz, *ipso*-Ph). $^{31}P\{^1H\}$ NMR (C_6D_6): δ 15.6. IR (KBr, cm^{-1}): 3051 (w), 2901 (vs), 2855 (s), 2725 (w), 1484 (w), 1437 (vs), 1377 (m), 1102 (s), 1024 (m), 999 (w), 941 (w), 826 (w), 793 (s), 751 (s), 738 (s), 695 (s), 517 (s), 485 (m).

Synthesis of **1**, alternative method. Complex **1** was synthesized in a manner similar to **1** by using $(C_5Me_5)_2Th(Cl)(CH_3)$ (280 mg, 0.51 mmol) and CH_2PPh_2Me (prepared by reacting equimolar amounts of $[(CH_3)_2PPh_2]I$ with $K[N(Si(CH_3)_3)_2]$ (109 mg, 0.51 mmol) in 1:1 toluene/THF mixture at 75 °C for 18 hours (250 mg, 66%).

Synthesis of (C₅Me₅)Th(Br)[CHPPh₃], 2. Yellow powder of **2** was synthesized by using (C₅Me₅)Th(CH₃)₂ (250mg, 0.47 mmol) and methyltriphenylphosphonium bromide (168 mg, 0.47 mmol) in THF at 65°C for 18 hours (240 mg, 60%). Crystals suitable for X-ray crystal analysis were obtained from a concentrated solution of **2** at -45 °C after several days. ¹H NMR (500 MHz, C₆D₆): δ 1.88 (d, 1H, ²J_{H-P} = 21 Hz, CHPPh₃), 2.14 (s, 30 H, C₅(CH₃)₅), 7.07-7.15 (m, 9H, *m*- and *p*- Ph), 7.76-7.80 (m, 6H, *o*- Ph). ¹³C{¹H} NMR (C₆D₆): 12.3 (C₅(CH₃)₅), 107.6 (d, ¹J_{C-P} = 18.9Hz, CHPPh₃), 124.9 (C₅(CH₃)₅), 128.4 (d, ³J_{C-P} = 10.9 Hz, *m*- Ph), 130.6 (d, ⁴J_{C-P} = 2.5 Hz, *p*- Ph), 133.0 (d, ²J_{C-P} = 9.2 Hz, *o*- Ph), 136.6 (d, ¹J_{C-P} = 80.9 Hz, *ipso*-Ph). ³¹P{¹H} NMR (C₆D₆): δ 15.7. IR (KBr, cm⁻¹): 3048 (w), 2958 (m), 2900 (s), 2855 (s), 2726 (w), 1482 (m), 1436 (vs), 1378 (m), 1309 (w), 1261 (w), 1180 (w), 1103 (vs), 1078 (m), 1067 (m), 1026 (m), 998 (m), 953 (vs), 840 (w), 791 (w), 748 (s), 709 (s), 695 (s), 587 (w), 528 (vs), 517 (vs). Anal. Calcd for C₃₉H₄₆Th₁Br₁P₁: C, 54.61; H, 5.41. Found: C, 54.40; H, 5.44.

Synthesis of (C₅Me₅)Th(I)[CHPPh₃], 3. A mixture of (C₅Me₅)Th(CH₃)₂ (156 mg, 0.29 mmol), methyltriphenylphosphonium iodide (119 mg, 0.29 mmol), and 30 mL of THF was heated to 65 °C in a sealed bomb under vigorous stirring for 18 h, during which the pale yellow liquid phase turned from yellow to orange. The remaining unreacted methyltriphenylphosphonium iodide was removed with filtration, and the solvent was removed *in vacuo*. The dark brown residue was taken into toluene (5 mL), filtered through Celite, and solvent was removed *in vacuo*. Pentane (3 mL) was added, and the suspension was stirred for 5 min followed by filtration to collect the solid. Solvent evaporation *in vacuo* afforded the product as yellow powder (133mg, 50%). Crystals suitable for X-ray crystal analysis were obtained from a concentrate solution of **3** at -45

°C after several days. ^1H NMR (500 MHz, C_6D_6): δ 2.07 (d, 1 H, $^2J_{\text{H-P}} = 21.5$ Hz, CHPh_3), 2.17 (s, 30 H, $\text{C}_5(\text{CH}_3)_5$), 7.07-7.15 (m, 9H, *m*- and *p*- Ph), 7.77-7.81 (m, 6H, *o*- Ph). $^{13}\text{C}\{^1\text{H}\}$ NMR (C_6D_6): 12.9 ($\text{C}_5(\text{CH}_3)_5$), 113.7 (d, $^1J_{\text{C-P}} = 19.9$ Hz, CHPh_3), 125.2 ($\text{C}_5(\text{CH}_3)_5$), 128.4 (d, $^3J_{\text{C-P}} = 12.4$ Hz, *m*- Ph), 130.7 (d, $^4J_{\text{C-P}} = 2.6$ Hz, *p*- Ph), 133.1 (d, $^2J_{\text{C-P}} = 9.3$ Hz, *o*- Ph), 135.9 (d, $^1J_{\text{C-P}} = 80.9$ Hz, *ipso*-Ph). $^{31}\text{P}\{^1\text{H}\}$ NMR (C_6D_6): δ 14.6. IR (KBr, cm^{-1}): 3054 (w), 2984 (m), 2957 (m), 2898 (s), 2854 (s), 2725 (w), 1481 (m), 1436 (vs), 1376 (m), 1308 (w), 1103 (vs), 1080 (s), 1025 (m), 999 (m), 950 (vs), 819 (w), 792 (w), 749 (s), 710 (s), 695 (vs), 618 (w), 588 (w), 528 (vs), 516 (vs). Anal. Calcd for $\text{C}_{39}\text{H}_{46}\text{Th}_1\text{I}_1\text{P}_1$: C, 51.78; H, 5.12. Found: C, 51.45; H, 5.08.

Crystal structure determination and refinement. The selected single crystal of 1-3 was mounted on a nylon cryoloop using viscous hydrocarbon oil. X-ray data collection was performed at 100(2) or 150(2) K. The X-ray data were collected on a Bruker CCD diffractometer with monochromated Mo-K α radiation ($\lambda = 0.71073$ Å). The data collection and processing utilized Bruker Apex2 suite of programs⁵⁸. The structures were solved using direct methods and refined by full-matrix least-squares methods on F 2 using Bruker SHELX-97 program⁵⁹. All nonhydrogen atoms were refined with anisotropic displacement parameters. All hydrogen atoms were placed at calculated positions and included in the refinement using a riding model. Thermal ellipsoid plots were prepared by using Olex2⁶⁰ with 50% of probability displacements for nonhydrogen atoms. Crystal data and details for data collection for complexes **1-3** are provided in Table 1-1.

Table 1-1. X-ray crystallographic data shown for complexes **1-3**.

	1	2	3
CCDC deposit number	1540800	1540799	1540801
Empirical formula	C ₃₄ H ₄₄ ClPTh	C ₃₉ H ₄₆ BrPTh	C ₃₉ H ₄₆ IPTh
Formula weight (g/mol)	751.15	857.68	904.67
Crystal habit, color	Needle, colorless	Prism, yellow	Plate, yellow
Temperature (K)	150(2)	100(2)	100(2)
Space group	<i>P2</i> ₁	<i>P2</i> ₁ / <i>n</i>	<i>P2</i> ₁ / <i>n</i>
Crystal system	Monoclinic	Monoclinic	Monoclinic
Volume (Å ³)	3113.0(2)	3472.9(4)	3508.9(10)
<i>a</i> (Å)	9.8192(4)	12.4502(9)	12.2719(19)
<i>b</i> (Å)	21.5053(8)	17.1675(12)	17.321(3)
<i>c</i> (Å)	15.1301(6)	16.2632(12)	16.524(3)
α (°)	90	90	90
β (°)	103.0040(10)	92.455(2)	92.541(2)
γ (°)	90	90	90
<i>Z</i>	4	4	4
Calculated density (Mg/m ³)	1.603	1.640	1.712
Absorption coefficient (mm ⁻¹)	4.948	5.516	5.200
Final R indices [<i>I</i> > 2σ(<i>I</i>)]	R1 = 0.0648, wR2 = 0.1091	R1 = 0.0142, wR2 = 0.0348	R1 = 0.0401, wR2 = 0.0853

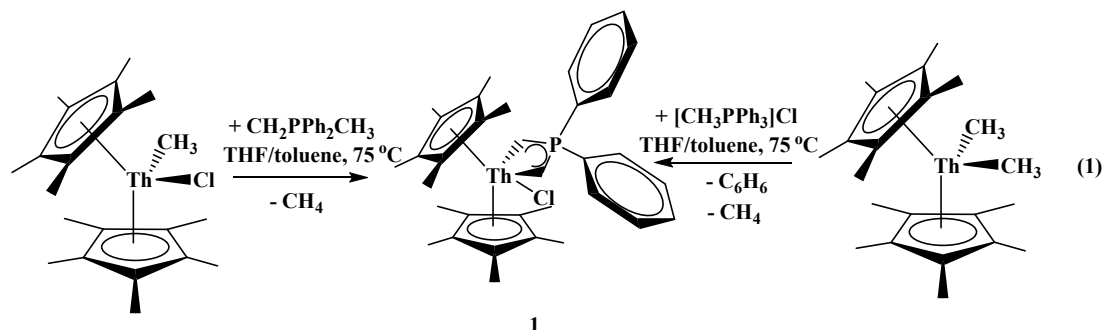
Computational details.

All calculations were carried out with the Gaussian 09 suite of programs.⁶¹ Thorium atoms were treated with a 5f-in-core effective core potential to describe their +4 oxidation state, associated with its adapted basis set.⁶² Carbon and hydrogen atoms were described with a 6-31G(d,p) double- ζ basis set.⁶³ Phosphorus and iodine atoms were both treated with their respective small core relativistic effective core potential of Stuttgart and

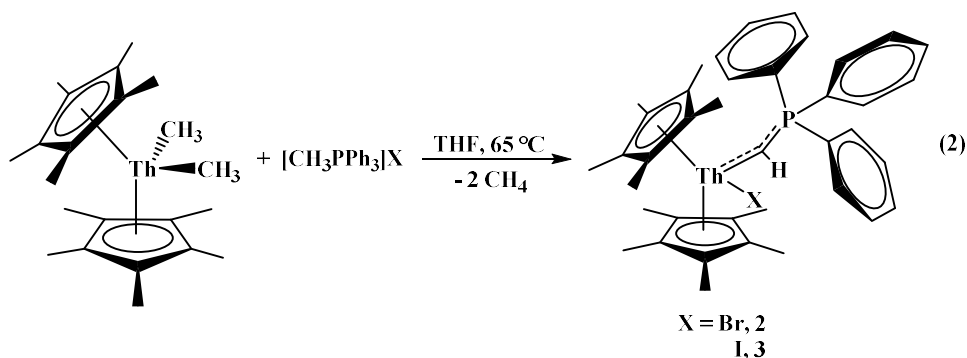
their adapted basis sets.⁶⁴⁻⁶⁵ Calculations were carried out at the DFT level of theory with the hybrid functional B3PW91.⁶⁶⁻⁶⁷ Geometries were optimized without any symmetry restriction and the nature of the extrema was verified by analytical frequency calculations. The calculation of electronic energies and enthalpies of the extrema of the potential energy surface (minima and transition states) were performed at the same level of theory as the geometry optimizations. IRC calculations were performed to confirm the connections of the optimized transition states. The electronic charges and the electronic structure (at the DFT level) were computed using the natural population analysis (NPA) and the natural bond orbital (NBO) techniques respectively.⁶⁸

Results and Discussion

We began by investigating the reactivity of $(C_5Me_5)_2ThMe_2$ with phosphonium halide salts. Due to solubility issues, a 1:1 mixture of THF:toluene was used for the reaction of $(C_5Me_5)_2ThMe_2$ and $[CH_3PPh_3]Cl$, and heated to 75 °C, eq 1. The 1H NMR spectrum of this reaction showed a $(C_5Me_5)^{1-}$ resonance at 2.01 ppm. In addition, the ^{13}C DEPT experiment showed two methylene carbons. The structure of $(C_5Me_5)_2Th(Cl)[\kappa^2-(CH_2)(CH_2)PPh_2]$, **1**, was determined by X-ray crystallographic analysis. Unfortunately, the data was not sufficient to discuss bond distances, but the connectivity of the molecule could be established. Surprisingly, this complex was reported by Gilje *et al*¹⁵. from the salt metathesis reaction of $(C_5Me_5)_2ThCl_2$ with $Li[(CH_2)(CH_2)PPh_2]$, and the NMR spectra from **1** and the Gilje group are nearly identical since the original report was in toluene-*d*₈. This was an unexpected result, since it involves a loss of a phenyl group from phosphorus.



The reaction of $(C_5Me_5)_2Th(CH_3)_2$ with $[CH_3PPh_3]Br$ and $[CH_3PPh_3]I$ in THF at $65\text{ }^\circ C$, eq 2, produced similar NMR resonances to each other. Both reactions show a gradual change from pale yellow to orange over the course of 18 hours. The 1H NMR spectra revealed one resonance at 1.88 and 2.07 ppm for the bromide and iodide, respectively, and had $^2J_{P-H}$ coupling constants of 21 Hz, indicative of two-bond coupling. A single proton was observed at 2.14 ppm for Br and 2.17 ppm for I. In addition, the ^{13}C NMR spectrum showed that the resonance of the carbon coordinated to the proton and phosphorus was located at 107.6 and 113.7 ppm ($^1J_{P-C} = 20$ Hz), which is an unusual shift downfield from a typical alkyl carbon resonance.



Both structures were determined by X-ray crystallography to be $(C_5Me_5)_2Th[CHPPh_3](X)$, X = Br, **2**; I, **3**, Figure 1-2, which are viewed as phosphorano-stabilized carbene or metalated ylide⁶⁹ complexes. The Th-C(carbene) bond distance of 2.299(6) Å in **3**, Table 1-2, is the shortest reported. In **2**, the Th-C(carbene) distance is

slightly longer at 2.3137(18) Å, making this the second shortest thorium-carbon distance. The shortening of the Th-C bond in both **2** and **3** is due to the terminal nature of the carbene, whereas in previously isolated thorium complexes, the carbene was supported, and had Th-C bond lengths in the range of 2.41-2.50 Å^{23, 49-51, 70-73}. We believe the Th-C bond distance reported in **3** is shorter than Hayton's [(Me₃Si)₂N]₃Th(CHPh₃) due to the higher donating strength of the amide ligands in comparison to the metallocene and halide ligands in **3**.

The Th-C21-P1 bond angle in **2** is 162.05(11)°, and is more bent than those seen in Th-N-C angles of imido complexes, 168.3(2) in (1,2,4-*t*-Bu₃C₅H₂)₂ThN(4-CH₃C₆H₄)⁷⁴ and 171.5(7)° in (C₅Me₅)₂ThN(2,6-Me₂C₆H₃)(THF),⁴⁵ which contain multiple bonding character. The Th-Br distance of 2.8669(2) Å is slightly longer than the 2.800(2) Å in (C₅Me₅)₂ThBr₂⁷⁵ and 2.785(1) Å in (1,2,4-*t*-Bu₃C₅H₂)₂ThBr₂.⁷⁴ The Th-C21-P1 bond angle is 163.1(4)°, while the Th-I bond distance of 3.1052(6) Å is similar to those previously reported.⁷⁶

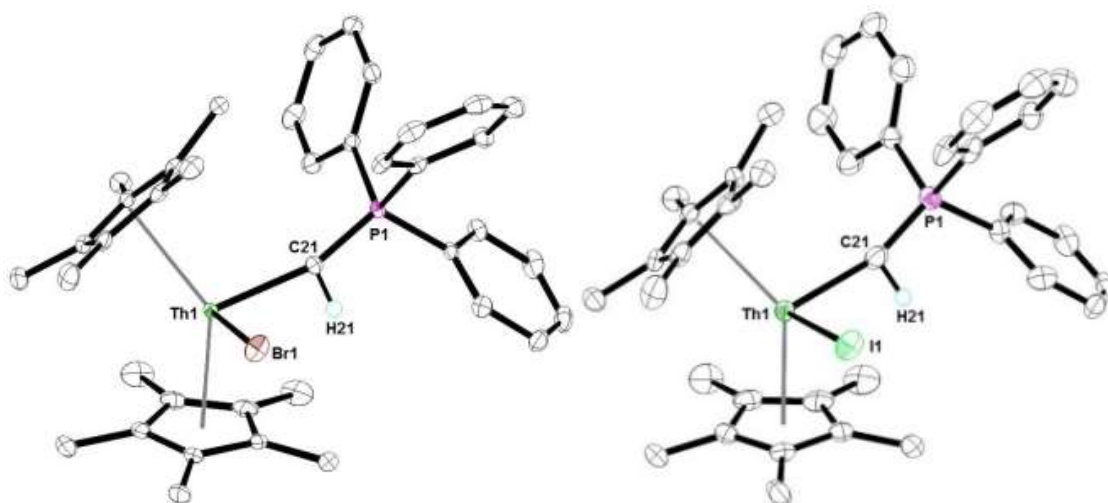
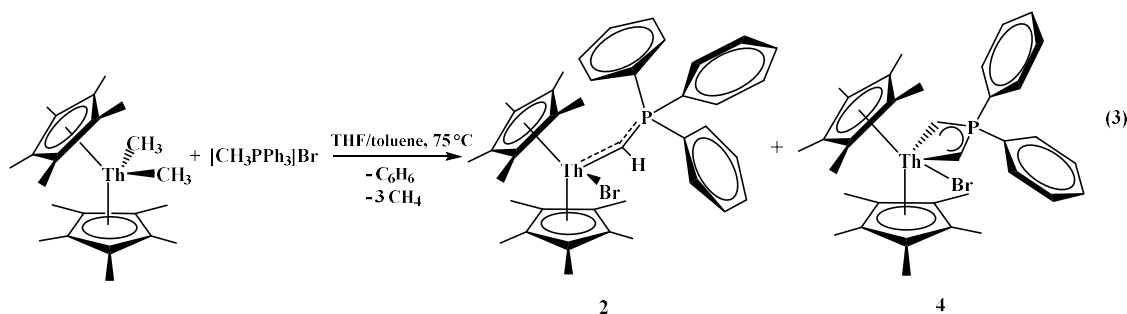


Figure 1-2. Thermal ellipsoid plots of **2** (left) and **3** (right) shown at the 50% probability level. Only the hydrogen atom connected to the carbene carbon is shown for clarity.

Since the reaction conditions differed between the phosphonium salts used, the reactions of the iodide and bromide salts in a 1:1 THF:toluene mixture were heated to 75 °C as well. Interestingly, for the bromide salt, the major product in the ^1H NMR spectrum was similar to the spectrum obtained for **1**, and we therefore identified it as $(\text{C}_5\text{Me}_5)_2\text{Th}(\text{Br})[\kappa^2\text{-(CH}_2\text{)(CH}_2\text{)PPh}_2]$, **4**, eq 3. Formation of benzene was also observed in the ^1H NMR spectrum. An unidentified decomposition byproduct was also observed so the distribution of **2** and **4** was difficult to assess. With respect to the reaction with the iodide salt, **3** is the exclusive product.



Density Functional Theory (DFT) and Mechanistic Investigations

In order to get insight on this peculiar influence of the halogen salt on the product formation, DFT calculations were conducted to determine reaction energy profiles since DFT has proven its ability to properly account for the reactivity of thorium complexes.⁷⁷⁻

⁸⁰ First, the reactivity of the chloride salt was investigated by computing the formation of both the carbene complex and the chelating phosphoylide complex, **1**. For the formation of $(\text{C}_5\text{Me}_5)_2\text{Th}[\text{CHPPh}_3]\text{Cl}$, two pathways were considered depending on whether there was or was not a nucleophilic assistance of the chloride on the C-H activation reactions. The putative carbene formation pathways appear to be less kinetically and thermodynamically favorable than the experimentally observed benzene elimination

pathway. Therefore, only the latter pathway will be described here. The reaction begins by the formation of a marginally stabilized adduct of $[\text{Ph}_3\text{PCH}_3]^+$ to $(\text{C}_5\text{Me}_5)_2\text{Th}(\text{CH}_3)_2$, **adduct**. This adduct is stabilized when the chloride interacts with the strongly Lewis acidic thorium center, reducing the electrostatic repulsion between thorium and $[\text{Ph}_3\text{PCH}_3]^+$. As in the $[\text{Ph}_3\text{PCH}_3]^+$, the positive charge is mainly located at the phosphorus center. Due to the interaction of the chloride with the thorium (nucleophilic assistance), either a methyl Nucleophilic Addition (NA) at the phosphorus or an Electrophilic Substitution (ES) at the carbon of the methyl group can occur, and the associated transition state (**TS1**) was located on the Potential Energy Surface (PES). The associated activation barrier is low (15.3 kcal/mol) and is in line with the charges carried out by the phosphorus atom (+1.78), the thorium metal (+1.99) and the methyl group (-0.48).

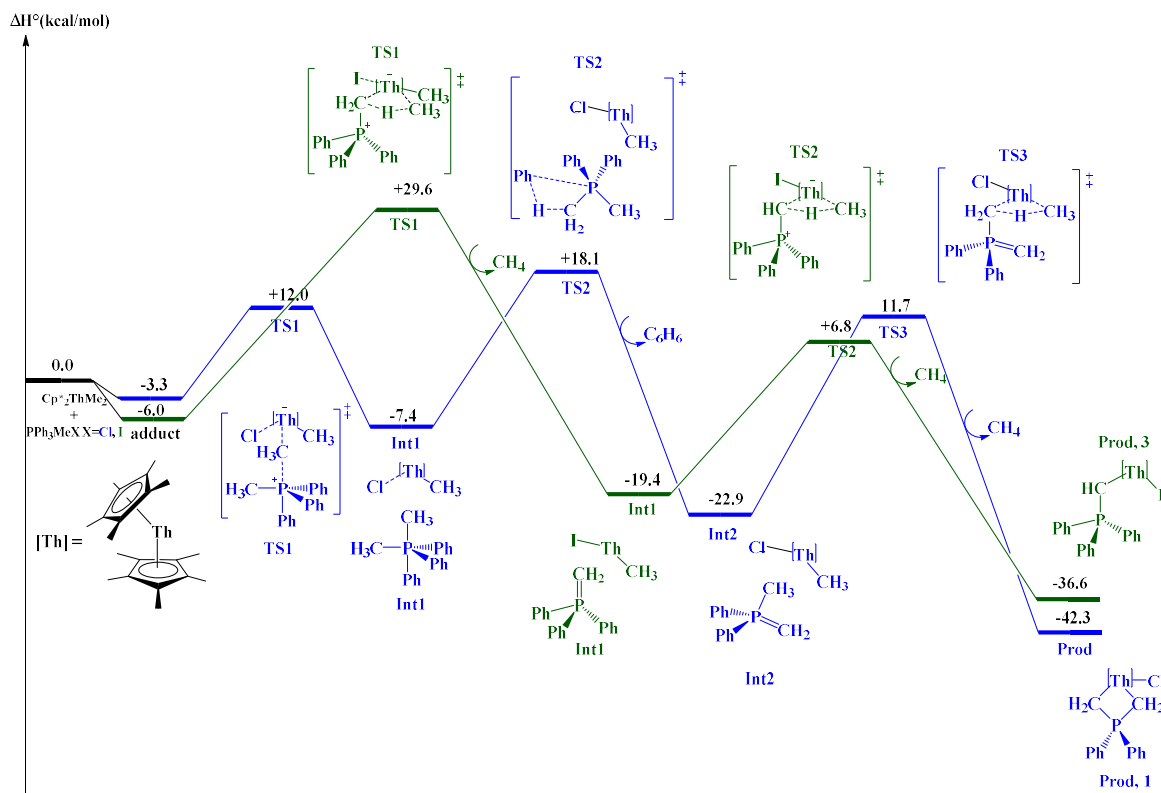


Figure 1-3. DFT computed enthalpy profile (298 K) in kcal/mol. The blue pathway refers to the benzene elimination pathway to form **1** while the green pathway refers to the carbene formation, **3**.

Following the intrinsic reaction coordinates, a thorium for phosphorus exchange occurs at the carbon center of the methyl group, and it leads to the formation of a Van der Waals adduct of the P(V) molecule $\text{PPh}_3\text{P}(\text{CH}_3)_2$ to $(\text{C}_5\text{Me}_5)_2\text{Th}(\text{Cl})(\text{CH}_3)$, **TS1**. At **TS1**, there is a trigonal bipyramid arrangement around the phosphorus with the incoming methyl occupying the apical position, in line with a NA, but the methyl group is planar with a $\text{Th}\cdots\text{CH}_3$ distance of 2.73 Å, and a P-CH₃ distance also of 2.73 Å, so that the reaction is an ES one. At the same time, the Th-Cl bond is formed (2.85 Å). The result, **Int1**, is mainly stabilized due to the formation of the strongly ionic Th-Cl bond, as the P(V) molecule is fleetingly interacting with the thorium complex. The “bond” dissociation

energy of this adduct is 0.5 kcal/mol. Interestingly, this P(V) molecule appears to be quite unstable and undergoes a benzene elimination, **TS2**, yielding **Int2**, the ylide $\text{H}_2\text{C}=\text{P}(\text{CH}_3)(\text{Ph})_2$. The decomposition of $\text{Ph}_3\text{P}(\text{CH}_3)_2$ has been previously investigated and benzene was observed,⁸¹ giving further evidence for this reaction pathway. As in the chloride case, and at first sight, the benzene elimination seems to be the lowest energy pathway over the carbene formation. However, analyzing in details the ES step of the benzene elimination in the iodide case, it appears that this step is not thermodynamically favored and is just an equilibrium. As the benzene elimination barrier (24.0 kcal/mol) is higher than the barrier of the first step (16.8/17.0 kcal/mol), this step is therefore not productive, and the P(V) molecule can be viewed in this case as a dormant species or a reservoir of $[\text{PPh}_3\text{Me}]^+$. This difference between the chloride and iodide salt is due to the nucleophilicity of the halide. While the iodide is more covalent than chloride and stabilizes the ionic thorium center to a lesser extent, as found at the Natural Bonding Orbital (NBO) level, this stabilization is also evidenced by comparing the two profiles of the carbene formation. Indeed, the iodide NA appears not to favor the reaction (but rather slightly disfavoring it) whereas it was the opposite in the chloride case (decrease of roughly 8 kcal/mol of the barrier). Therefore, only the carbene reaction is productive and will be described in detail.

In the reaction pathway of the iodide, the first transition state, **TS1**, corresponds to the C-H activation of the methyl group of the substrate. The proton is transferred to one of the methyl ligands of the thorium complex to give **Int1** and the concomitant release of a methane molecule. The substrate does not bind between the two methyl groups in order to avoid steric repulsions between its phenyl groups and the methyl substituents of the

(C₅Me₅)¹⁻ ligands of the thorium complex. **TS1** is a classic four-center σ -bond metathesis transition state, with CH₂, H and CH₃ almost aligned (176.5°). The activation barrier is calculated to be +29.6 kcal/mol, which corresponds to a kinetically accessible reaction at 60 °C. The charge alternation (calculated with the NPA technique) at the transition state level is quite good: +2.30 for Th, -0.69 for CH₂, +0.25 for H and -0.43 for CH₃. Once the methane molecule is released, the complex relaxes to give **Int1**, whose formation is thermodynamically favored (-19.4 kcal/mol). During these two steps, the iodide continues to interact with the thorium atom.

The second transition state, **TS2**, is the C-H activation leading to the formation of the final product of the reaction and another methane molecule. The proton is transferred to the second methyl group of the thorium complex. **TS2** is another classic four-center σ -bond metathesis transition state, with CH, H and CH₃ almost aligned (166.6°). The relative activation barrier is calculated to be +25.9 kcal/mol, which is also kinetically accessible experimentally. The charge alternation at the transition state level is very good: +2.36 for Th, -1.31 for CH, +0.24 for H and -0.39 for CH₃. Moreover, this second and last step is thermodynamically very favorable (-36.6 kcal/mol with respect to the separated reactants). Once the methane molecule is released, the iodide can fill a vacant coordination site of the thorium center to form the very stable product, **Prod, 3**. The comparison between optimized and experimental geometrical parameters of **3** is reported in Table 2. There is an excellent agreement between the computed and the observed structures. While the reaction between (C₅Me₅)₂Th(CH₃)₂ and [Ph₃PCH₃]Br was not calculated, the energetics associated with methane versus benzene elimination should be

closer and therefore at 65 °C, **2** is formed, but going to 75 °C, a mixture of **2** and **4** are observed.

While we relied on DFT calculations for step 1 to form $(C_5Me_5)_2Th(CH_3)I$, the second step was investigated experimentally by the reaction of $(C_5Me_5)_2Th(CH_3)I$ with $Ph_3P=CH_2$. This reaction was monitored in C_6D_6 at 300 K by 1H NMR spectroscopy and afforded **3** in 90% yield after 9 hours. Methane was found in the 1H NMR spectrum. The reaction was observed to be overall second order, first order in $(C_5Me_5)_2Th(CH_3)I$ and first order in $Ph_3P=CH_2$, with slope, k , of 0.293. This corresponds to a ΔG^\ddagger of approximately 0.73 kcal/mol, which when compared to 7.4 kcal/mol as predicted by DFT calculations when done with a toluene solvation model, supports that this reaction occurs at room temperature with a low activation barrier.

Table 1-2. Calculated and experimental geometrical parameters of **Prod, 3**. Distance and angles are reported in Å and degrees (°) respectively.

	Calculated structure	Experimental structure
Th1-C21 distance	2.33	2.299(6)
Th1-H21 distance	2.60	2.51(5)
Th1-I1 distance	3.13	3.1052(6)
C21-Th1-I1 angle	95.9	96.70(15)

The electronic structure of the carbene product **3** has been studied theoretically with the NBO technique. One strongly polarized covalent σ bond (15.9% Th – 84.1% C) is found at the first order analysis. A π -type doublet of electrons is also found on the carbon atom (occupation of 1.72), and a strong donor-acceptor interaction between this doublet and empty d-f hybrid orbitals of the thorium center appear at the second-order perturbation analysis (the largest contribution being 102 kcal/mol), in line with a polarized π bond,

Figure 1-4. A Th-I σ bond is also found, which is polarized in favor of Th (75.6%), in line with iodide being more covalent.

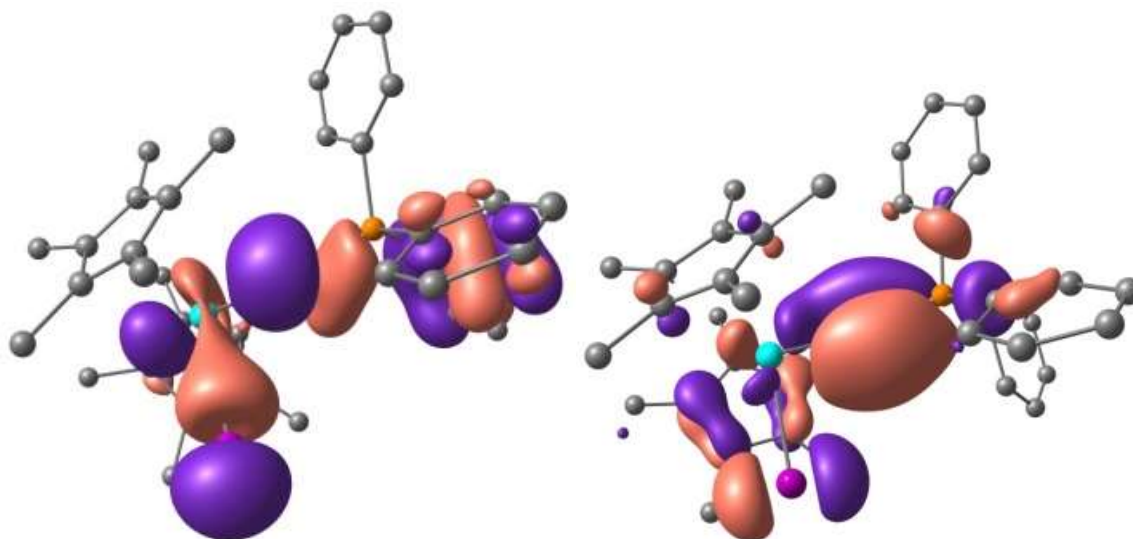


Figure 1-4. 3D representation of the σ (a) and π (b) bonds in complex **1**.

Conclusion

In summary, we have produced rare thorium phosphorano-stabilized carbene complexes, $(C_5Me_5)_2Th(CHPPH_3)X$, $X = Br, I$, with the shortest thorium-carbon bond distances of $\sim 2.30 \text{ \AA}$ from the reaction of $(C_5Me_5)_2Th(CH_3)_2$ with either $[CH_3PPh_3]I$ or $[CH_3PPh_3]Br$. When $[CH_3PPh_3]Cl$ is used, the ylide complex, $(C_5Me_5)_2Th(CH_2CH_2PPh_2)$, is produced. The mechanism of carbene formation involves two sigma-bond metathesis reactions on the methyl group of $[Ph_3PCH_3]^+$ while benzene elimination was observed from the putative $Ph_3P(CH_3)_2$ species. This intermediate, $Ph_3P(CH_3)_2$, forms due to the nucleophilicity of chloride versus iodide. The interplay of these factors has been examined using density functional theory calculations to provide insight into the reaction pathways and show a logical rationale for the differences in reactivity. The terminal nature of these zwitterionic ligands gives them thorium-carbon

bond distances that are much shorter than those seen in thorium-alkyl species and we therefore conclude that these are carbene complexes with true thorium-carbon multiple bonding.

Chapter 2: Phosphorano-Stabilized Carbene Complexes with Short Thorium(IV) and Uranium(IV)-Carbon Bonds

Introduction

Metal-ligand multiple bonding has attracted a great amount of attention in the f element community due to the interest in exploring the extent of covalent bonding of these understudied metals.⁸² These complexes provide insight into the role that the valence orbitals (5f and 6d) play in bonding.⁸³⁻⁸⁴ While no alkylidene complexes are known with the f elements, terminal phosphorano-stabilized carbene complexes were first realized by Gilje and Kramer in 1981, and have become increasingly used due to their tendency to form short metal-carbon bonds.^{15, 26-27, 85-86} Shorter bond distances are due to the resonance between an alkyl and metalated ylide forms of the ligand, eq 1.



In terminal phosphorano-stabilized carbene complexes, the metal-carbon bond is significantly shorter than tetravalent actinide-carbon(alkyl) bonds, which is typically not the case for supported methandiide systems.⁵⁴ This brings into question the extent to which methandiide complexes show multiple bonding character.⁵⁵

In the past, the covalent character of actinide-ligand bonding has been examined mostly using structural methods coupled with density functional theory (DFT) calculations.⁸⁷⁻⁹³ However, some groups have fused spectroscopic and computational methods. Kiplinger has used spectroscopic methods⁹⁴⁻⁹⁵ as well as electrochemical measurements, to probe actinide-ligand bonding.⁹⁶⁻⁹⁷ X-ray Absorption Near-Edge Spectroscopy (XANES) has become increasingly popular,⁹⁸⁻¹⁰² but limited by expertise

and beam time. Electron Paramagnetic Resonance (EPR) spectroscopy has also been used, but also requires synchrotron radiation.¹⁰³ Only recently, has the use of NMR spectroscopy been used to probe thorium-ligand bonding since a diamagnetic metal is required to correlate with Quantum Theory of Atoms in Molecules (QTAIM).^{26, 104} This treatment originally forged by Bader,¹⁰⁵ has been pioneered by Kaltsoyannis and has quickly become the standard measure in assessing covalent bonding character in f element complexes.^{3, 106-107} Herein, we examine, in an identical fashion to Hayton and Hrobarik,⁶ actinide-carbon bonds by combining ¹³C NMR spectroscopy and DFT calculations to compare phosphorano-stabilized carbene complexes with methandiide complexes of thorium.

Previously, we examined the reactivity of (C₅Me₅)₂Th(CH₃)₂ with phosphonium salts, [CH₃PPh₃]₃X, X = Cl, Br, I.⁷ When X = Br and I, the carbene was isolated, however, when X = Cl, an ylide-complex, (C₅Me₅)₂Th(Cl)[κ²-(C,C)-CH₂CH₂PPh₂], was made due to a difference in formation. From the reaction pathway calculations, it was realized that the carbene complex, (C₅Me₅)₂Th(X)(CHPPh₃), could be formed from direct reaction of (C₅Me₅)₂Th(CH₃)X with the ylide, CH₂=PPh₃. Here, we generalize this reaction for thorium and uranium by investigating the reaction of (C₅Me₅)₂AnX(CH₃); An = Th, U; X = Cl, Br, I, with CH₂PPh₃. In addition, we use ¹H, ¹³C, and ³¹P NMR spectroscopy as well as density functional theory calculations to examine the bonding in these complexes.

Experimental

General Considerations. All syntheses were performed under an inert atmosphere of N₂ by using glovebox and Schlenk technique. All solvents were dried over activated molecular sieves and alumina in solvent purification system by MBRAUN, USA.

$(C_5Me_5)_2Th(CH_3)(Cl)$,¹² $(C_5Me_5)_2U(CH_3)(Cl)$,¹² $(C_5Me_5)_2U(CH_3)_2$,¹² and $CH_2=PPh_3$ ²⁷ were prepared according to published literature procedure. Copper(I) iodide and copper(I) bromide (Aldrich) were used as received. Elemental analyses were performed by Microanalysis Facility, College of Chemistry, University of California, Berkeley. 1H and ^{13}C NMR spectra were collected using either 600 or 500 MHz Bruker Advance Spectrometer. 1H and ^{13}C NMR chemical shifts are reported in ppm referenced to solvent impurities as internal standard.⁵⁷ ^{31}P NMR spectra were collected using 300 MHz Bruker AvII Spectrometer. ^{31}P NMR chemical shifts are reported in ppm referenced externally to 85% H_3PO_4 at 0 ppm. All NMR data were collected in benzene- d_6 (Cambridge Isotope) which were dried over activated molecular sieves and degassed by three cycles of freeze-pump-thaw. NMR multiplicities are indicated s (singlet), d (doublet), t (triplet), and m (multiplet). IR spectra were collected as KBr pellets on Perkin-Elmer Spectrum One FT-IR spectrometer.

Caution! *Thorium-232 is an alpha-emitting radiometal with a half-life of 1.4×10^{10} years. U-238 is an alpha-emitting radiometal with a half-life of 4.5×10^9 years. They were used in a radiological laboratory with appropriate personal protective and counting equipment.*

Synthesis of $(C_5Me_5)_2Th(Cl)[CHPPh_3]$, **1.** A sealed bomb flask was charged with $(C_5Me_5)_2Th(CH_3)(Cl)$ (347 mg, 0.63 mmol), $CH_2=PPh_3$ (173 mg, 0.63 mmol), and THF (20 mL) was heated to 60-62 °C while stirring overnight. The resulting orange solution was dried *in vacuo* and washed with pentane. All volatiles were removed *in vacuo* to afford a product as yellow powder (274 mg, 54%). Crystals suitable for X-ray crystal analysis were obtained from a concentrated toluene solution of **1** at -45 °C after several days. 1H NMR (500 MHz, C_6D_6): δ 1.70 (d, 1 H, $^2J_{H-P} = 20$ Hz, $CHPPh_3$), 2.11 (s, 30 H,

C_5Me_5), 7.07-7.15 (m, 9H, *m*- and *p*- Ph), 7.75-7.80 (m, 6H, *o*-Ph). $^{13}C\{^1H\}$ NMR (C_6D_6): 12.0 ($C_5(CH_3)_5$), 104.1 (d, $^1J_{C-P} = 19.5$ Hz, $CHPPh_3$), 124.6 ($C_5(CH_3)_5$), 128.4 (d, $^3J_{C-P} = 11.4$ Hz, *m*-Ph), 130.5 (d, $^4J_{C-P} = 2.6$ Hz, *p*-Ph), 132.9 (d, $^2J_{C-P} = 9.5$ Hz, *o*-Ph), 137.0 (d, $^1J_{C-P} = 80$ Hz, *ipso*-Ph). $^{31}P\{^1H\}$ NMR (C_6D_6): δ 16.5. IR (KBr, cm^{-1}): 3052.7 (w), 2958 (m), 2901 (s), 2855 (s), 1481 (m), 1436 (vs), 1377 (m), 1101 (vs), 1063 (m), 1024 (m), 998 (m), 953 (vs), 830 (w), 803 (w), 748 (s), 709 (s), 696 (vs), 528 (vs), 516 (vs). Anal. Calcd for $C_{39}H_{46}Th_1Cl_1P_1$: C, 57.60; H, 5.70. Found: C, 57.35; H, 5.89.

Synthesis of $(C_5Me_5)_2U(Cl)[CHPPh_3]$, 2. A sealed bomb flask was charged with $(C_5Me_5)_2U(CH_3)(Cl)$ (305 mg, 0.55 mmol), $CH_2=PPh_3$ (151 mg, 0.55 mmol), and THF was heated to 60-62 °C while stirring overnight. The resulting deep red solution was dried *in vacuo* to yield the product as deep red microcrystalline powder (430 mg, 96%). Crystals suitable for X-ray crystal analysis were obtained from a concentrated toluene solution of 1 at -45 °C after several days. 1H NMR (500 MHz, C_6D_6): δ -17.3 (s, 1H, $CHPPh_3$), 4.99 (br-t, 6H, $^3J_{H-H} = 8.2$ Hz, *m*-Ph), 5.4 (s, 30H, C_5Me_5), 5.95 (t, 6H, $^3J_{H-H} = 7.4$ Hz, *o*-Ph), 6.49 (t, 3H, $^3J_{H-H} = 7.8$ Hz, *p*-Ph). ^{13}C DEPT135 (C_6D_6): -35.3 ($C_5(CH_3)_5$), 129.5 (d, $^2J_{C-P} = 10.3$ Hz, *o*-Ph), 131.9 (*p*-Ph), 133.6 (d, $^3J_{C-P} = 8.3$ Hz, *m*-Ph). $^{31}P\{^1H\}$ NMR (C_6D_6): δ 236.2. IR (KBr, cm^{-1}): 3052 (w), 2961 (m), 2900 (br-vs), 2854 (s), 1482 (m), 1436 (vs), 1376 (m), 1100 (vs), 1022 (m), 997 (w), 940 (vs), 802 (w), 747 (s), 708 (s), 695 (vs), 527 (vs), 518 (vs). Anal. Calcd for $C_{39}H_{46}U_1Cl_1P_1$: C, 57.18; H, 5.66. Found: C, 57.48; H, 5.65.

Synthesis of $(C_5Me_5)_2U(Br)[CHPPh_3]$, 3. To a stirring suspension of copper (I) bromide (31 mg, 0.22 mmol) in THF, $(C_5Me_5)_2U(CH_3)_2$ (145 mg, 0.21 mmol) in THF was added. After an overnight stir at room temperature, the solution was filtered to remove Cu metal

and dried *in vacuo* to yield $(C_5Me_5)_2U(CH_3)(Br)$ (125 mg, 97%). 1H NMR (300 MHz, C_6D_6): δ -156.6 (s, 3H, -CH₃), 10.06 (s, 30H, C_5Me_5). The product from the previous step was used without any further purification. A sealed bomb flask was charged with $(C_5Me_5)_2U(CH_3)(Br)$ (113 mg, 0.19 mmol), $CH_2=PPh_3$ (52 mg, 0.19 mmol), and THF was heated to 60-62 °C while stirring overnight. The resulting deep red solution was dried *in vacuo* to yield the product as deep red microcrystalline powder (158 mg, 98%). 1H NMR (500 MHz, C_6D_6): δ -1.43 (s, 1H, $CHPPh_3$), 5.10 (s, 30H, C_5Me_5), 6.64 (t, 6H, $^3J_{H-H} = 7.4$ Hz, *o*-Ph), 6.92 (t, 3H, $^3J_{H-H} = 7.6$ Hz, *p*-Ph), 7.87 (br-t, 6H, $^3J_{H-H} = 8.85$ Hz, *m*-Ph). ^{13}C DEPT135 (C_6D_6): -37.0 ($C_5(CH_3)_5$), 130.7 (d, $^2J_{C-P} = 10.0$ Hz, *o*-Ph), 133.1 (*p*-Ph), 137.0 (d, $^3J_{C-P} = 8.5$ Hz, *m*-Ph). $^{31}P\{^1H\}$ NMR (C_6D_6): δ 248.8. IR (KBr, cm^{-1}): 2962 (m), 2898 (s), 2853 (s), 1481 (w), 1437 (vs), 1376 (w), 1100 (vs), 1023 (m), 999 (w), 938 (vs), 800 (w), 749 (m), 710 (m), 694 (s), 528 (m), 518 (m). Anal. Calcd for $C_{39}H_{46}U_1Br_1P_1$: C, 54.32; H, 5.37. Found: C, 53.66; H, 5.42.

Synthesis of $(C_5Me_5)_2U(I)[CHPPh_3]$, 4. To a stirring suspension of copper (I) iodide (79 mg, 0.41 mmol) in THF, $(C_5Me_5)_2U(CH_3)_2$ (223 mg, 0.41 mmol) in THF was added. After an overnight stir at room temperature, the solution was filtered to remove Cu metal and dried *in vacuo* to yield $(C_5Me_5)_2U(CH_3)(I)$ (239 mg, 89%). 1H NMR (300 MHz, C_6D_6): δ -146.1 (s, 3H, -CH₃), 11.01 (s, 30H, C_5Me_5). The product from the previous step was used without any further purification. A sealed bomb flask was charged with $(C_5Me_5)_2U(CH_3)(I)$ (238 mg, 0.37 mmol), $CH_2=PPh_3$ (101 mg, 0.37 mmol), and THF was heated to 60-62 °C while stirring overnight. The resulting deep red solution was dried *in vacuo* to yield the product as deep red microcrystalline powder (329 mg, 99%). 1H NMR (500 MHz, C_6D_6): δ 5.03 (s, 30H, C_5Me_5), 7.48 (t, 3H, $^3J_{H-H} = 7.45$ Hz, *p*-Ph), 7.56 (t,

6H, $^3J_{\text{H-H}} = 7.3$ Hz, *o*-Ph), 11.85 (br-t, 6H, $^3J_{\text{H-H}} = 8.55$ Hz, *m*-Ph), 30.02 (s, 1H, *CHPPH*₃). ¹³C DEPT135 (C₆D₆): -39.2 (C₅(CH₃)₅), 132.3 (d, $^2J_{\text{C-P}} = 10.0$ Hz, *o*-Ph), 134.8 (*p*-Ph), 141.9 (br-s, *m*-Ph). ³¹P{¹H} NMR (C₆D₆): δ 258.0. IR (KBr, cm⁻¹): 2962 (m), 2922 (m), 2860 (w), 1483 (w), 1438 (s), 1413 (w), 1380 (w), 1262 (s), 1114 (vs), 1021 (vs), 938 (w), 908 (w), 801 (s), 748 (m), 719 (w), 690 (m), 501 (m). Anal. Calcd for C₃₉H₄₆U₁I₁P₁: C, 51.44; H, 5.09. Found: C, 51.36; H, 5.29.

Crystal structure determination and refinement. The selected single crystals of **1-4** were mounted on a nylon cryoloop using viscous hydrocarbon oil. X-ray data collection was performed at 100(2) or 150(2) K. The X-ray data were collected on a Bruker CCD diffractometer with monochromated Mo-K α radiation ($\lambda = 0.71073$ Å). The data collection and processing utilized Bruker Apex2 suite of programs.⁵⁸ The structures were solved using direct methods and refined by full-matrix least-squares methods on F^2 using Bruker SHELX-97 program.⁵⁹ All non-hydrogen atoms were refined with anisotropic displacement parameters. All hydrogen atoms were placed at calculated positions and included in the refinement using a riding model. Thermal ellipsoid plots were prepared by using Olex2⁶⁰ with 50% of probability displacements for non-hydrogen atoms. Crystal data and details for data collection for complexes **1-4** are provided in Table 2-1.

Table 2-1. X-ray crystallographic data shown for complexes **1-4**.

	1	2	3	4
CCDC deposit number	1826639	1826640	1826641	1826638
Empirical formula	C ₃₉ H ₄₆ ClPTh	C ₃₉ H ₄₆ ClPU	C ₃₉ H ₄₆ BrPU	C ₃₉ H ₄₆ IPU

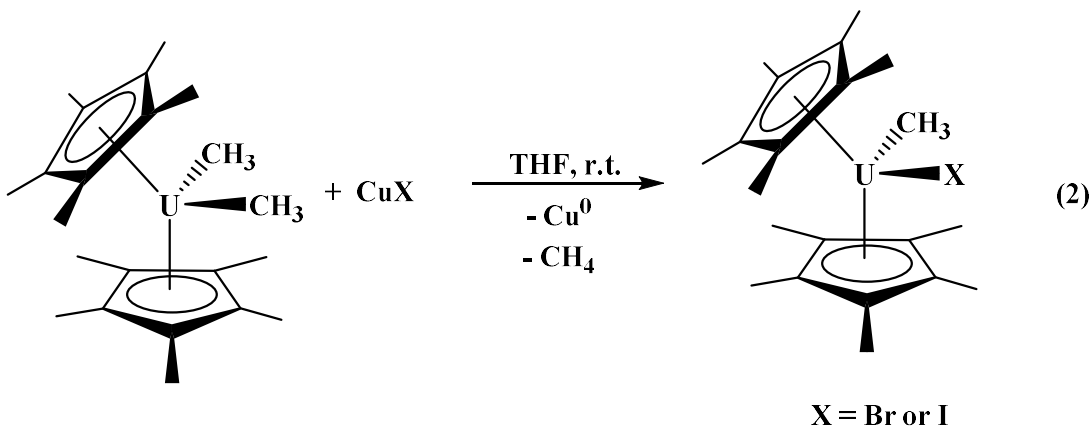
Formula weight (g/mol)	813.22	819.21	863.67	910.66
Crystal habit, color	Needle, Yellow	Needle, Dark Red	Prism, Dark Red	Plate, Brown-Black
Temperature (K)	160(2)	100	100	100
Space group	P2 ₁ /n	P12 ₁ /n1	P12 ₁ /n1	P12 ₁ /n1
Crystal system	Monoclinic	Monoclinic	Monoclinic	Monoclinic
Volume (Å ³)	3500.2(4)	3421.0(6)	3447.2(4)	3493.2(7)
a (Å)	12.6319(8)	12.4968(14)	12.3828(7)	12.2069(14)
b (Å)	17.2434(11)	17.2000(18)	17.2508(10)	17.4166(19)
c (Å)	16.0803(10)	15.9248(17)	16.1499(10)	16.4468(18)
α (°)	90	90	90	90
β (°)	92.107(2)	91.9576(17)	92.239(2)	92.555(2)
γ (°)	90	90	90	90
Z	4	4	4	4
Calculated density (Mg/m ³)	1.543	1.591	1.664	1.732
Absorption coefficient (mm ⁻¹)	4.407	4.895	5.940	5.601
Final R indices [I > 2 σ (I)]	R1 = 0.0361, wR2 = 0.0574	R ₁ = 0.0216, wR ₂ = 0.0403	R1 = 0.0300, wR2 = 0.0512	R ₁ = 0.0221, wR ₂ = 0.0554

Computational Details. The electronic structures of the series of the uranium complexes were studied using density functional theory (DFT) with the PBE0 approximation for exchange-correlation, as implemented in the Amsterdam Density Functional (ADF) code package.^{13, 108} Relativistic effects were incorporated using the scalar-relativistic zeroth order regular approximation (ZORA).¹⁰⁹⁻¹¹¹ The spin-polarized, frozen-core, all-electron wavefunctions were expanded in a basis of Slater-type orbitals

(STOs) optimized for use in molecular DFT-ZORA calculations.¹¹² Specifically, we employed the following atomic STOs: double-zeta (DZ) for H; double-zeta with polarization (DZP) for C, P, Cl; triple-zeta with polarization (TZP) for Br, I, U. The basis functions^{20, 113} associated with the atomic cores were frozen. In all calculations, the triplet state ($S = 1$) was selected.

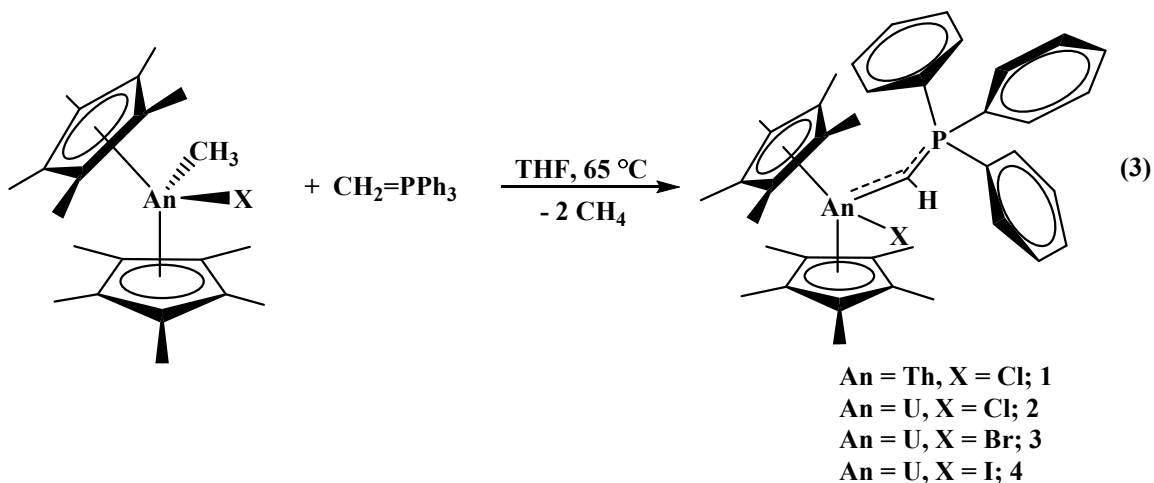
Results and Discussion

Syntheses. The production of $(C_5Me_5)_2AnX(CH_3)$ has been previously reported from the reaction of $(C_5Me_5)_2An(CH_3)_2$ with $(C_5Me_5)_2AnX_2$.¹² This was carried out to synthesize the chloride species, $(C_5Me_5)_2ThCl(CH_3)$ and $(C_5Me_5)_2UCl(CH_3)$. However, we found that the reaction of $(C_5Me_5)_2U(CH_3)_2$ with CuBr or CuI cleanly afforded $(C_5Me_5)_2UBr(CH_3)$ and $(C_5Me_5)_2UI(CH_3)$, respectively, in quantitative yield, eq 2. The use of copper(I) salts for transmetalation reactions at uranium metal centers has been previously reported.¹¹⁴⁻¹¹⁵



The reaction of $(C_5Me_5)_2An(X)(CH_3)$, An = Th, U, X = Cl, Br, I, with $CH_2=PPh_3$ makes the corresponding phosphorano-stabilized carbene complexes, $(C_5Me_5)_2An(X)(CHPPh_3)$; An = Th, X = Cl, **1**; An = U, X = Cl, **2**; An = U, X = Br, **3**; An

= U, X = I, **4**, eq 3, in moderate to excellent yields. All of the uranium complexes are deep red in color, while all the thorium complexes are yellow.



Spectroscopy. The ^1H , ^{13}C , and ^{31}P NMR spectra of **1** are similar to the bromide and iodide complexes, Table 2-2. For the diamagnetic thorium complexes, the ^1H and ^{13}C NMR resonances show a downfield shift while the ^{31}P NMR resonance has an upfield shift with decreasing electronegativity of the halide. This trend in the ^1H NMR spectra of the uranium analogs is maintained, but the ^{31}P NMR resonances also have a downfield shift. Despite multiple attempts, which included ^{13}C -labeling of the ylide, the ^{13}C NMR resonance of the carbene of the paramagnetic U(IV) complexes could not be found.

Table 2-2. ^1H , ^{13}C , and ^{31}P NMR resonances for the phosphorano-stabilized carbene ligand.

Carbene Resonances	1	$(\text{C}_5\text{Mes})_2\text{ThBr}(\text{C}(\text{HPPH}_3))$	$(\text{C}_5\text{Mes})_2\text{ThI}(\text{CH}(\text{PPh}_3))$	2	3	4
CHPPh_3	1.70	1.88 (${}^2J_{\text{H-P}} = 21$ Hz)	2.07 (${}^2J_{\text{H-P}} = 21$ Hz)	-17.3	-1.43	30.02
	(${}^2J_{\text{H-P}}$)					

	= 20 Hz)					
CHPPh ₃	104.1 (¹ J _{C-P} = 19.5 Hz)	107.6 (¹ J _{C-P} = 20 Hz)	113.7 (¹ J _{C-P} = 20 Hz)	--	--	--
CHPPh ₃	16.5	15.7	14.6	236.2	248.8	258.0

Structural Analysis. The solid-state crystal structures for complexes **1-4** were determined using single crystal X-ray diffraction analysis, Table 3. All four complexes are in a pseudo-tetrahedral arrangement about the metal center with short metal-carbon bonds. The thorium-carbon bond distance of 2.324(4) Å in **1**, Figure 2-1, is slightly longer than the 2.299(6) and 2.314(2) Å in the iodide and bromide analogs, respectively, but the third shortest thorium-carbon bond. The Hayton group reported the first thorium phosphorano-stabilized carbene with a thorium-carbon bond length of 2.362(2) Å. All of these complexes feature thorium-carbon bond distances shorter than the 2.436,²⁵ 2.492,¹¹⁶ and 2.475 Å⁴⁹ in other thorium methandiide complexes and significantly shorter than thorium-carbon bonds in alkyl complexes. For example, the thorium-C(methyl) bond in (C₅Me₅)₂Th(CH₃)₂ is 2.471(8) and 2.478(9) Å and (Ind*)₂Th(CH₃)₂ is 2.48(2) and 2.47(2) Å, Ind* = C₉Me₇.¹¹⁷ The thorium-chloride bond length of 2.70257(14) Å is ~0.1 Å longer than that in (C₅Me₅)₂ThCl₂,¹¹⁸ presumably due to the steric and donating properties of the carbene ligand.

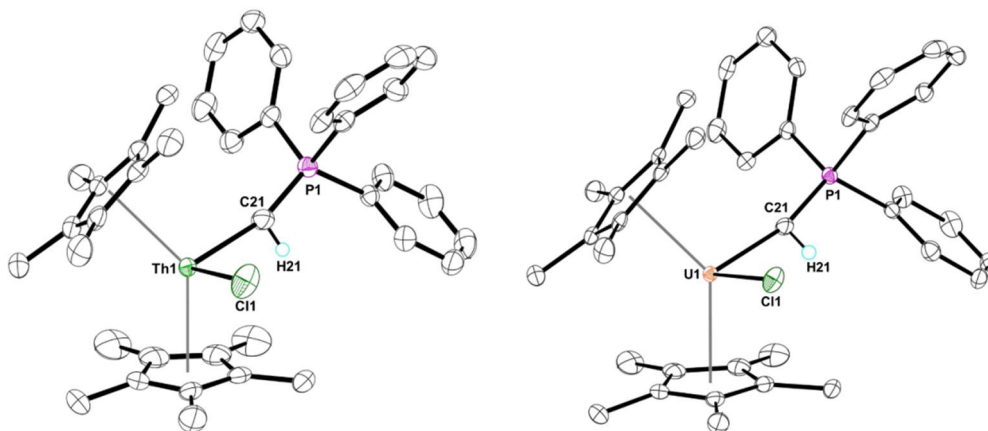


Figure 2-1. Thermal ellipsoid plots of **1** (left) and **2** (right) shown at the 50% probability level. The hydrogen atoms, except for H21, have been omitted for clarity.

Complexes **2**, **3**, and **4**, have uranium-carbon distances of 2.2454(2), 2.252(4), and 2.2428(2) Å, respectively, which are the shortest uranium(IV)-carbon bonds reported to date, Table 2-3. To compare, the phosphorano-stabilized carbene of Hayton is 2.278(8) Å. While a trend can be observed for the thorium complexes, none exists for the uranium analogs. However, this may also be due to the packing of **2-4** in the solid-state as we do find trends in the spectroscopy and electronic structure calculations of these complexes that are similar to the thorium analogs.

Table 2-3. Selected bond distances (Å) and angles (deg) for thorium and uranium carbene complexes.

Bond Distance (Å)/angle (deg)	X = Cl	X = Br	X = I
Th1-X1	2.70257(14)	2.86689(17) ^a	3.1052(4) ^a

Th1-C21	2.32351(13)	2.31369(15) ^a	2.2988(3) ^a
Th1-C21-P1	162.1662(14)	162.0454(16) ^a	163.098(3) ^a
U1-X1	2.6567(2)	2.8247(5)	3.0666(3)
U1-C21	2.2428(2)	2.252(4)	2.2454(2)
U1-C21-P1	166.0952(18)	166.1(3)	166.4890(18)
U1-C21-X	95.077(3)	94.26(10)	93.913 (4)

^a From reference ⁸⁵

Electronic Structure Calculations. The geometries of all three uranium-carbene complexes were optimized and the calculated. The agreement between theory and experiment for the uranium-carbene distances are within ~ 0.01 Å. Computationally, the uranium-carbon bonds have a similar trend to the thorium complexes in that the iodide complex, **4**, has the shortest uranium-carbon bond of 2.242 Å, followed by **3** and **2** at 2.252 and 2.256 Å, respectively. Additional insight into the nature of the uranium-carbene bond can be gained by transforming the Kohn-Sham orbitals into natural bond orbitals (NBOs).²⁰ Here we focus the discussion on the NBOs of the uranium-iodide complex, **4**, as no significant qualitative differences were seen in the chloride or bromide complexes. The uranium-carbene bond is made up of two α -spin NBOs and two β -spin NBOs; for each spin, there is one σ -type NBO and one π -type NBO (Figure 2-2). The NBO compositions are about 20% uranium and 80% carbon character except for the β -spin π -NBO, which has a lower uranium character of around 15%, likely the result of spin polarization by the paramagnetic uranium center. For both α - and β -spins, the π -NBOs have occupations of less than 0.9, which suggests that electrons in these NBOs are partially delocalized into nearby acceptor NBOs. A second-order perturbation theory

analysis of the Fock matrix in the NBO basis identifies the acceptor as a P–C antibonding σ -NBO (Figure 2-2).

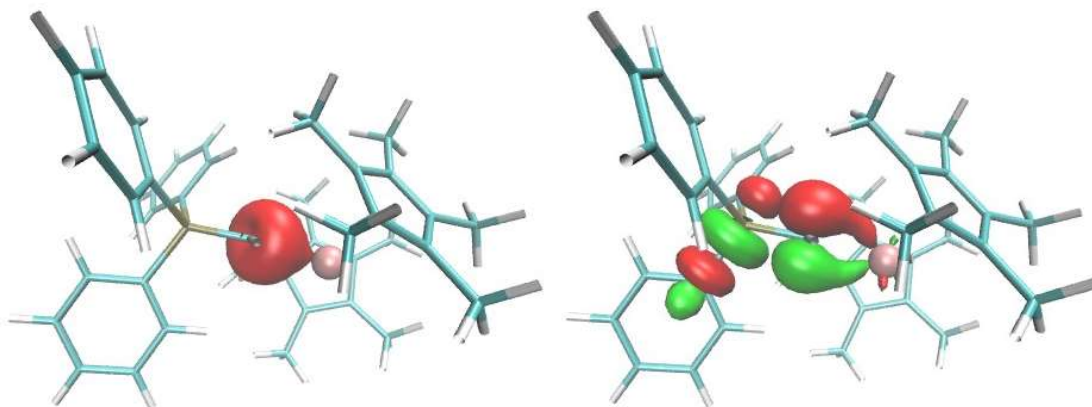


Figure 2-2. Natural bond orbitals (NBOs) in complex **4**. The uranium-carbene bond is composed of a σ -type (left) and π -type (right) NBO. The α - and β -spin NBOs are indistinguishable on this scale so only the α -spin NBOs are shown. The π -type NBO mixes with a P–C antibonding σ -NBO, thus extending the effects of spin polarization due to the paramagnetic uranium to the P–C centers.

The NBOs occupied by the two unpaired uranium $5f$ -electrons. We do not observe any appreciable mixing with NBOs on other atomic centers. Thus, the spin density is localized on the paramagnetic uranium center, and a natural population analysis yields a uranium spin density of about 2.2 electrons. The largest polarization effect is seen in the carbene carbon directly coordinated to the uranium (spin density of -0.06). This spin polarization extends to the P–C centers (spin density of -0.005) as a result of the delocalization of the π -component of the uranium-carbene bond (Figure 2-2).

Further analysis of the uranium-carbene bonding was carried out within the quantum theory of atoms in molecules (QTAIM) framework,¹⁰⁵ focusing on the critical point in the

total density along the uranium-carbene bond. At this bond critical point, the density ρ , Laplacian of the density $\nabla^2\rho$, total energy density, H , and bond ellipticity, ε , were evaluated, and the results are summarized in Table 2-4. In addition, two bond index measures are also included in Table 2-4: the Wiberg bond index evaluated in the natural atomic orbital (NAO) basis, and the QTAIM delocalization index, which is related to the density integrated over the uranium and carbene atomic basins. In general, covalent bonds between light elements have $\rho > 0.2$ while $\rho < 0.1$ is indicative of closed-shell interactions; our values of $\rho \sim 0.1$ suggest weak covalency, and is comparable to the ρ values for similar complexes reported by Hayton and Hroborik.²⁶ In comparison, methandiide complexes, when treated with sufficient basis functions, have ρ values that are less than 0.1.⁵⁰ However, we point out that most uranium methandiide complexes have been treated with local density approximation (LDA), an inadequate method for f electron systems.¹¹⁹ When uranium methandiide complexes are examined using high-level calculations (CASSCF/RASSCF or GGA), the delocalization indices for complexes 2-4 are approximately 25-50% larger at 0.943-0.979 as compared to 0.57-0.713 in U(IV) methandiides.^{50, 52} The positive values for the density Laplacian $\nabla^2\rho$, and the small values for the total energy density H , are also consistent with the characterization of weak covalency.

Table 2-4. Analysis of the uranium-carbene bond in $(C_5Me_5)_2U(X)(CHPh_3)$ complexes, X = Cl, **2**; Br, **3**; I, **4**, as derived from DFT-ZORA: percent uranium composition of natural bond orbitals (NBO), QTAIM bond critical point parameters (ρ , $\nabla^2\rho$, H , ε), and

bond index parameters (Wiberg index in the NAO basis and delocalization index over the U–C atomic basins).

	X = Cl, 2	X = Br, 3	X = I, 4
α -spin σ NBO %U	22%	22%	22%
α -spin π NBO %U	20%	20%	21%
β -spin σ NBO %U	20%	20%	20%
β -spin π NBO %U	15%	15%	15%
ρ	0.107	0.108	0.110
$\nabla^2\rho$	0.146	0.146	0.146
H	-0.0408	-0.0416	-0.0433
ε	0.328	0.326	0.327
Wiberg bond index	1.13	1.14	1.15
Delocalization index	0.943	0.955	0.979

The ^{13}C NMR resonances for the thorium carbene complexes are of interest as this provides spectroscopic evidence of the amount of covalent bonding in the thorium-carbon bond. Hayton and Hrobarik have correlated the resonance in the ^{13}C NMR spectrum of thorium methandiide and phosphorano-stabilized carbene complexes to the amount of covalent character in the thorium-carbon bond.⁵ The ^{13}C NMR resonance for the carbene carbon is located at 104.1 ppm for **1**. This is an upfield shift from the bromide and iodide with resonances at 107.6 and 113.7 ppm, respectively. This indicates a trend of more covalent character in the thorium-carbon bond of $\text{I} > \text{Br} > \text{Cl}$ in $(\text{C}_5\text{Me}_5)_2\text{ThX}(\text{CHPPh}_3)$ complexes. We rationalize this with respect to the steric and electronic properties of the

halides. Since iodide is the least electronegative, it will not provide as much electron donation to the highly electropositive thorium(IV) metal center. In addition, the iodide is larger and more removed from the thorium center, thus the carbene can be closer. These two factors, in concert, contribute to the short thorium-carbon bond distances.

The ^{13}C NMR resonances can be placed into a larger context with respect to terminal versus supported carbene and methandiide complexes of thorium. As shown by Hayton and Hrobarik, the ^{13}C NMR resonance can be correlated to the amount of covalent character in the thorium-carbon bond. With a significant downfield shift (>100 ppm), terminal carbene complexes show a degree of multiple bonding character. Further, we can compare these complexes to $(\text{C}_5\text{H}_5)_2\text{Zr}(\text{C}_6\text{H}_5)(\text{CHPPh}_3)$, a zirconium phosphorano-stabilized carbene complex with no f orbital contribution.¹²⁰ This complex also has a short Zr-C(carbene) bond distance of 2.157(4) Å and ^{13}C NMR resonance at 106.2 ppm. Therefore, our metallocene complexes are similar to a zirconium analog, which contains some multiple bond character if compared to other zirconium alkyl complexes. For example, $(\text{C}_5\text{H}_5)_2\text{Zr}(\text{CH}_3)_2$ has a Zr-C(methyl) bond distance of 2.273(5) and 2.280(5) Å,¹²¹ hence there is a consistency of ~ 0.1 Å contraction in the metal-carbon bond with phosphorano-stabilized carbene complexes compared to their alkyl counterparts. As illustrated in Figure 2-3, this is in stark contrast to methandiide complexes, which show little spectroscopic evidence of multiple bonding. Again, comparing thorium-alkyl complexes to methandiides, the Th-C_{methyl} bond distance in $(\text{Ind}^*)_2\text{Th}(\text{CH}_3)_2$ is 2.48(2) and 2.47(2) Å with a ^{13}C NMR resonance at 68.4 ppm. These values parallel with methandiide complexes, $[\text{Th}(\text{BIPM}^{\text{TMS}})\{\text{N}(\text{SiMe}_3)_2\}(\mu\text{-Cl})]_2$, $\text{Th}(\text{BIPM}^{\text{TMS}})\{\text{N}(\text{SiMe}_3)_2\}(\text{NCPh}_2)$, $\text{Th}(\text{BIPM}^{\text{TMS}})\{\text{N}(\text{SiMe}_3)_2\}(\text{OC}(\text{H})(\text{NCPh}_2)(\text{C}_{14}\text{H}_9))$,

Th(BIPM^{TMS}){N(SiMe₃)₂}{OC(N^tBu)NCPH₂} with reported ¹³C NMR shifts of 80.95, 77.95, 67.25, and 83.05 ppm, respectively, and a bond distance of 2.410(8), 2.474(8), 2.453(4), and 2.463(5) Å,⁵⁴ respectively. In fact, in the bis(alkyl) thorium methandiide complex, Th(BIPM^{TMS})(CH₂SiMe₃)₂, the ¹³C NMR resonances of the CH₂SiMe₃ at 92.59 ppm are more downfield than the deprotonated carbon at 73.75 ppm.⁵⁰ Hence, Hayton's phosphorano-stabilized carbene complex was the first molecular complex isolated with thorium-carbon multiple bonding character. We come to this conclusion even based on Cavell's thorium methandiide complexes, which have 5.7 and 7.0% thorium character in their thorium-carbon π-bond.²⁵ Additionally, in Zi and Fang's thorium methandiide, the thorium contribution in the π-bond could not be observed, indicating that it is less than the default of 5% orbital participation.¹¹⁶ In our opinion, without any spectroscopic data, since the ¹³C NMR resonance could not be found in any of those complexes, we cannot view that any more than a lone-pair donation from carbon to thorium, with the minimal, or any, contribution from thorium.

We note what would seem to be a counter point to our discussion is (C₅Me₅)₂Th(CH₂CMe₃)₂, which has thorium-carbon bond distances of 2.543(4) and 2.456(4) Å and a methylene ¹³C NMR resonance of 110.2 ppm.¹²² In addition, [Th(CH₂CMe₃)₅]¹⁻, has bond distances of 2.46(2)-2.56(2) Å and ¹³C NMR resonance of the methylene is located at 117.96 ppm.¹²³ This downfield shift is most likely due to the inductive effect of the *tert*-butyl group. Support for this can be observed in comparing the ¹³C NMR spectrum of LiCH₂Me₃ and LiCH₃ which are observed at ~38 ppm¹²⁴ and ~-15 ppm, respectively, depending on solvent and coordinating ligand to lithium.

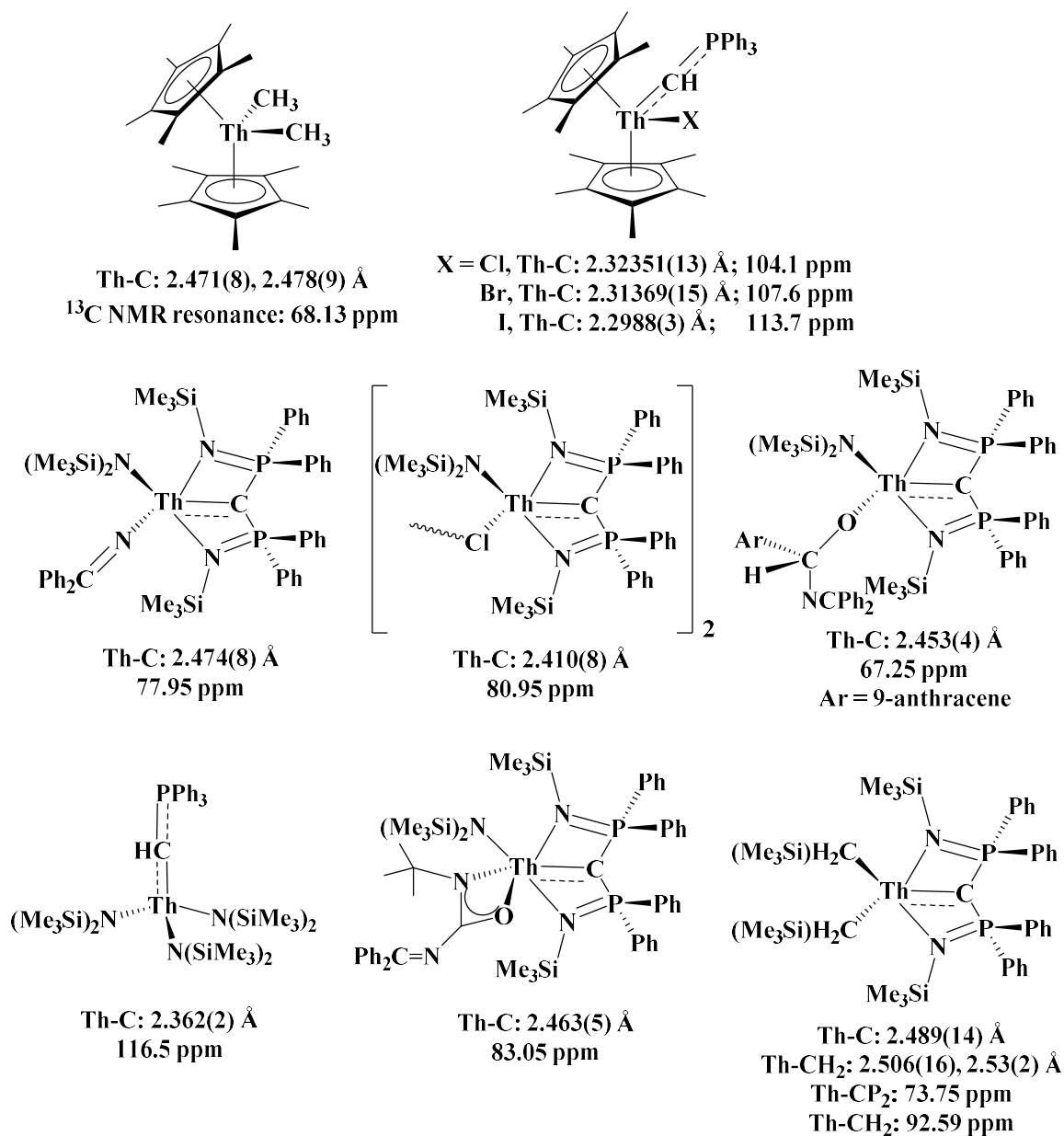


Figure 2-3. Summary of relevant reported ^{13}C NMR resonances and thorium-carbon bond distances. Those with only one of the two characteristics have been omitted.

While no spectroscopic evidence can be elucidated from U(IV) complexes, to our knowledge, no U(VI) methandiide or carbene complexes have reported ^{13}C NMR resonances. This makes judging the relative covalent character of paramagnetic uranium

carbene or methandiide complexes difficult, but the same crystallographic evidence holds for U(IV) methandiide complexes: the U(IV)-carbon bond in most methandiide complexes remain similar to a U(IV)-carbon of an alkyl, while phosphorano-stabilized carbenes are far shorter. A review of uranium(IV) methandiide complexes has been reported and a range of 2.274(8)-2.393(15) Å was found.⁵⁴ Most of these complexes are only slightly shorter than typical U(IV)-C_{alkyl} bond distances of 2.4-2.5 Å.¹²⁵ Since there are examples of methandiide complexes with shorter uranium-carbon bonds, then we submit that these compounds contain multiple bonding character, however that character is less than phosphorano-stabilized carbene complexes based on QTAIM calculations, which is, admittedly, low.

Conclusion

Four new actinide(IV) complexes of the form, (C₅Me₅)₂An(X)(CHPPh₃), with short metal-carbon bonds have been synthesized featuring terminal phosphorano-stabilized carbene ligands. The ¹³C NMR resonances of the thorium complexes have been contextualized with other thorium carbene complexes as well as those methandiide complexes having reported ¹³C NMR spectra. The results show that phosphorano-stabilized carbenes show a degree of multiple bonding character which exceeds those of reported thorium methandiide complexes. Spectroscopically, thorium methandiides contain very little to no multiple bonding characters as the ¹³C NMR spectra and crystallographic data resemble alkyl compounds rather than carbenes. Further analysis of the U(IV) complexes is needed to truly understand the extent of multiple bonding character. We present these findings to demonstrate that density functional theory can be

used as a tool, but further evidence, if possible, should be gathered to gain more conclusive evidence of actinide structure and bonding.

Chapter 3: Four Electron Reduction Chemistry Using an Uranium(III)

Phosphido Complex

Introduction

The reductive chemistry of U(III) complexes has produced impressive small molecule activation¹²⁶ with substrates such as azides in the formation of the imido functional group¹²⁷⁻¹²⁹. Imido ligands, in addition to other moieties,^{82, 130-134} have furthered our understanding of actinide-ligand bonding, which promotes the concept of involvement of f- and d-orbitals when constructing a multiple bond¹³⁵⁻¹³⁹.

Reductive chemistry with uranium has been done in a variety of ways including redox-active ligands¹⁴⁰, an uranium(III) precursor¹⁴¹, or a combination of both the ligand and U(III) metal center¹⁴². Uranium(IV) can also be the starting oxidation state but this requires a redox-active ligand¹²⁷, a reducing agent¹⁴¹, or the reaction with a primary amide to form the imido species¹⁴³⁻¹⁴⁸. There are also examples with, what we will term, pseudo redox-active ligands. These ligands are typically not redox-active but undergo reductive coupling in the process of actinide-mediated redox chemistry. These would include tetraphenylborate¹⁴⁹, benzyl¹⁵⁰, pentamethylcyclopentadienyl¹⁵¹, and, recently, phosphido ligands¹⁵².

Our interest has been investigating the chemistry of the actinides, hard Lewis acids, with soft Lewis bases such as phosphorus. This is because the coordination chemistry of the actinides is dominated by hard donor ligands, with the number of U(III) complexes with the heavier congeners of the chalcogen group being limited^{90-91, 153-161}, and no U(III)

complexes have been reported with any element other than nitrogen in the pnictogen series. However, thorium(IV)^{80, 130, 152, 162} and uranium(IV)¹⁶³⁻¹⁶⁵ complexes of phosphorus, arsenic, antimony¹⁶⁶, and bismuth¹⁶⁶ are known, but also rare.

Here, we report the first U(III) phosphido complex, $(C_5Me_5)_2U[P(2,4,6-Me_3C_6H_2)(SiMe_3)](THF)$, as well as show that reductive coupling of the phosphido ligand produces four-electron reduction chemistry of Me_3SiN_3 to yield the bis(imido) complex, $(C_5Me_5)_2U(=NSiMe_3)_2$. Our overall goal for this complex was to exploit the weak uranium-phosphorus bond as well as the reducing power of U(III) to perform both insertion and reduction chemistry. We chose substrates, namely organic azides and isocyanide, which have been known to undergo both types of reactions.

Experimental

General Considerations. All compounds were handled under an inert atmosphere of N_2 inside a glovebox. $HP(C_6H_2Me_3-2,4,6)(SiMe_3)$,¹⁶⁷ benzyl potassium,¹⁶⁸ $(C_5Me_5)_2UI(THF)$,¹⁶⁹ $(C_5Me_5)_2UCl_2$,¹² and $(C_5Me_5)_2U(CH_3)I$ prepared according to the procedure previously reported. Toluene and THF were dried by passing through solvent purification system, MBRAUN, USA. Azidotrimethylsilane, 1-azidoadamantane, and tert-butyl isocyanide were purchased from Aldrich and used without further purification. C_6D_6 obtained from Cambridge Isotope Laboratories was subjected to 3 cycles of Freeze-Pump-Thaw and dried over 4Å molecular sieves prior to use. All 1H and $^{13}C\{^1H\}$ NMR experiments were performed on 500 or 600 MHz Bruker spectrometers. All $^{31}P\{^1H\}$ and ^{29}Si INEPT experiments were performed on a 300 MHz Bruker spectrometer. All chemical shifts and coupling constant are reported in ppm and Hz, respectively. All 1H and $^{13}C\{^1H\}$ chemical shifts were reported with respect to residue C_6D_5H at 7.16 ppm

and $^{13}\text{C}_6\text{D}_6$ at 128.06 ppm. All $^{31}\text{P}\{^1\text{H}\}$ spectra were calibrated externally to 85% H_3PO_4 . All ^{29}Si spectra were calibrated externally to TMS. Infrared spectra were recorded as KBr pellets on Perkin-Elmer Spectrum One FT-IR spectrometer.

Synthesis of $(\text{C}_5\text{Me}_5)_2\text{U}[\text{P}(\text{C}_6\text{H}_2\text{Me}_3-2,4,6)(\text{SiMe}_3)](\text{THF})$, **1.** To a scintillation vial charged with $(\text{C}_5\text{Me}_5)_2\text{UI}(\text{THF})$ (356 mg, 0.5 mmol), THF (5 mL), and a magnetic stir bar, $\text{KP}(\text{C}_6\text{H}_2\text{Me}_3-2,4,6)(\text{SiMe}_3)$ (132 mg, 0.5 mmol) in THF (5 mL) was added at room temperature. The solution was stirred at room temperature overnight, after which THF was removed *in vacuo*. The solid was then extracted with toluene and filtered through Celite to yield a dark brown solution, after which, toluene was removed *in vacuo* to yield $(\text{C}_5\text{Me}_5)_2\text{U}[\text{P}(\text{C}_6\text{H}_2\text{Me}_3-2,4,6)(\text{SiMe}_3)](\text{THF})$ as a dark brown powder (384 mg, 95%). X-ray quality crystals of $(\text{C}_5\text{Me}_5)_2\text{U}[\text{P}(\text{C}_6\text{H}_2\text{Me}_3-2,4,6)(\text{SiMe}_3)](\text{THF})$ were obtained by concentrated the solution of $(\text{C}_5\text{Me}_5)_2\text{U}[\text{P}(\text{C}_6\text{H}_2\text{Me}_3-2,4,6)(\text{SiMe}_3)](\text{THF})$ in diethyl ether and placed in the freezer for several days. IR (KBr, cm^{-1}): 2962 (s), 2905 (vs), 2857 (s), 1439 (m), 1377 (w), 1261 (w), 1246 (m), 1095 (br-m), 1021 (m), 906 (w), 838 (vs), 668 (w), 628 (w), 606 (w), 551 (w). Anal. Calcd for $\text{C}_{36}\text{H}_{58}\text{OPSiU}$: C, 53.78; H, 7.27. Found: C, 53.76; H, 7.05.

Synthesis of $(\text{C}_5\text{Me}_5)_2\text{U}[\text{N}(\text{SiMe}_3)]_2$, **2.** Method A: To a scintillation vial charged with KC_8 (58 mg, 0.42 mmol), THF (2.5 mL), and a magnetic stir bar, $(\text{C}_5\text{Me}_5)_2\text{UCl}_2$ (124 mg, 0.21 mmol) in THF (2.5 mL) was added at room temperature. The solution was stirred for 1 hour at room temperature. Excess amount of azidotrimethylsilane (ca. 0.1 mL, 0.76 mmol) was added via syringe. Gas evolution from the solution was observed immediately follow by a color change from green to brown. The solution was let to stir at room temperature overnight followed by filtration over Celite to yield a dark green solution.

THF and excess azidotrimethylsilane were removed *in vacuo* to yield $(C_5Me_5)_2U[N(TMS)]_2$ as a dark green powder (100mg, 68%). Method B: To a scintillation vial charged with $(C_5Me_5)_2U[P(C_6H_2Me_3-2,4,6)(SiMe_3)](THF)$ (206 mg, 0.26 mmol), toluene (3 mL), and a magnetic stir bar, an excess amount of azidotrimethylsilane (ca. 0.1 mL, 0.76 mmol) was added via syringe. Gas evolution from the solution was observed immediately. The solution was left to stir at room temperature overnight. X-ray quality of $(C_5Me_5)_2U[N(TMS)]_2$ was obtained by concentrated this solution to ca. 1 mL and placed in the freezer for several days (48 mg, 27%). 1H NMR (C_6D_6 , 500 MHz, 298 K): δ 4.40 (s, 30H, $C_5(CH_3)_5$), 0.34 (s, 18H, $=N(Si(CH_3)_3)$). $^{13}C\{^1H\}$ NMR (C_6D_6 , 125 MHz): δ 138.9 ($C_5(CH_3)_5$), 16.9 ($=N(Si(CH_3)_3)$), 9.4 ($C_5(CH_3)_5$). ^{29}Si INEPT NMR (C_6D_6 , 60 MHz): δ -52.9 ($=N(Si(CH_3)_3)$). IR (KBr, cm^{-1}): 2952 (m), 2904 (m), 2858 (m), 1437 (w), 1377 (w), 1258 (w), 1240 (m), 1084 (w), 1065 (w), 1020 (w), 977 (s), 929 (s), 889 (m), 832 (m), 749 (w). Anal. Calcd for $C_{26}H_{48}N_2Si_2U$: C, 45.73; H, 7.08; N, 4.10. Found: C, 45.93; H, 7.11; N, 3.92.

Synthesis of $(C_5Me_5)_2U[=N(Ad)]_2$ from $(C_5Me_5)_2U[P(C_6H_2Me_3-2,4,6)(SiMe_3)](THF)$,

3. To a a scintillation vial charged with $(C_5Me_5)_2U[P(C_6H_2Me_3-2,4,6)(SiMe_3)](THF)$ (49 mg, 0.06 mmol), toluene (3 mL) and a magnetic stir bar, 1-azidoadamantane (22 mg, 0.12 mmol) was added at room temperature. The resulting dark brown solution was let to stir at room temperature overnight, after which it was concentrated to ca. 1 mL and placed in freezer for several days to yield $(C_5Me_5)_2U[N(Ad)]_2$ as dark brown powder (10 mg, 20%). 1H NMR matches with data previously reported.¹⁷⁰

Synthesis of $[(C_5Me_5)_2U(CNC(CH_3)_3)(\mu-CN)]_3$, 4. A scintillation vial charged with $(C_5Me_5)_2U[P(C_6H_2Me_3-2,4,6)(SiMe_3)](THF)$ (127 mg, 0.16 mmol), pentane (5 mL), and

a magnetic stir bar was chilled in -45°C freezer for 30 min prior to use. The vial was removed from the freezer and an excess amount of tert-butyl isocyanide (ca. 0.1 mL, 0.88 mmol) was added via syringe. The solution was let to stir at room temperature overnight and the excess tert-butyl isocyanide and solvent were removed. The residue was then dissolved in pentane and placed in the freezer for several days to yield $[(C_5Me_5)_2U(CNC(CH_3)_3)(\mu-CN)]_3$ black crystalline powder (56 mg, 57%). Signals corresponding to C_5Me_5 and $CNC(CH_3)_3$ were not observed in 1H NMR. IR (KBr, cm^{-1}): 2963 (m), 2909 (s), 2855 (m), 2142 (m), 2087 (w), 1442 (m), 1374 (m), 1260 (m), 1244 (m), 1199 (m), 1084 (vs), 1022 (s), 935 (m), 908 (m), 885 (m), 837 (m), 801 (m). Anal. Calcd for $C_{78}H_{117}N_6U_3$: C, 50.56; H, 6.36; N, 4.54. Found: C, 51.14; H, 6.73; N, 4.29.

Crystallographic data collection and structure determination

The structures of compound **1**, **2**, and **4** were solved by iterative dual space phasing as implemented in SHELXT¹⁷¹ and refined by full matrix least squares refinement against F^2 using SHELXL.¹⁷² The models were modified with the aid of the visualization/interface program Olex2.⁶⁰ Full-occupancy non-hydrogen atoms were located from the difference map and refined anisotropically. For compound **4**, after locating all non-hydrogen atoms associated with the main moiety, significant difference map peaks indicated the presence of disorder affecting one of the Cp* ligands bonded to U2 and the presence of a disordered solvent molecule occupying void space in the lattice. A second conformation of the disordered Cp* ring, related to the first by an approximate 36° rotation about the center of the ring, was located from difference map peaks. The relative occupancies of the two conformations were manually adjusted to minimize the least squares goodness-of-fit and R factors, with relative occupancies of 67% to 33% ultimately producing the

most satisfactory fit. Five of the largest difference map peaks located in lattice void space were modeled as carbon atoms belonging to a pentane molecule of crystallization. Based on the comparatively low value of the difference map peak heights and the large isotropic thermal ellipsoids observed when refining these as carbon atoms, it was apparent that the total occupancy of the solvent molecule would be less than 1. Fixing the occupancies at 50% and refining anisotropically produced a model which accounted for the electron density in a satisfactory way and can be interpreted as a pentane molecule for which the terminal carbon atoms are relatively well ordered while the propylene group is highly disordered about a cylinder containing all reasonable conformations. Hydrogen atoms for all full occupancy carbon atoms were placed in calculated positions. Their thermal parameters were constrained to ride on the carrier atom, while their coordinates were allowed to rotate about the C-C bond axis of rotation. Hydrogen atoms bonded to disordered methyl groups were placed in idealized staggered geometries. A rigid group restraint was applied to the anisotropic thermal parameters of all atoms.¹⁷³

The disordered pentane molecule was able to be refined anisotropically but reached a point where they oscillated indefinitely from cycle to cycle rather than converged. These values were then fixed for the rest of the refinement. An unsuccessful attempt was made to remove the contribution of the disordered pentane from the structure using PLATON SQUEEZE,¹⁷⁴ which estimated a solvent contribution of 265 electrons per cell, compared to an expected 168 electrons for a full occupancy pentane molecule. Refinement against modified data caused the disordered Cp* ligands to refine to unrealistic bond distances. Together these indicated that the reflections being modified by SQUEEZE were impacting refinement of the main moiety in an unrealistic way. The half-occupancy

pentane molecule does not correspond to any realistic geometry for any single conformation of that molecule but is an acceptable approximation for the space and electron density occupied by a number of randomly disordered conformations. Hydrogen atoms positions were not calculated for this reason.

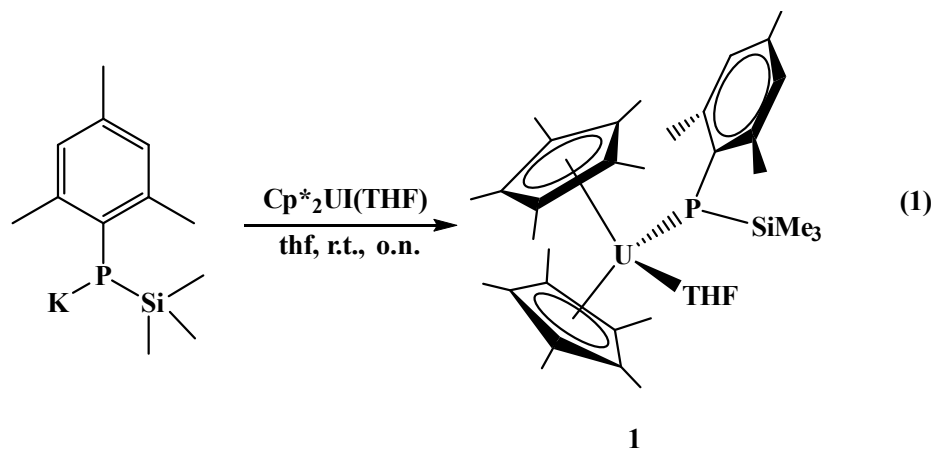
The final model has prolate thermal ellipsoids for the other Cp* ligand bonded to U2, and for one of the tert-butylisonitrile ligands. For the Cp* ligand this most likely indicates unresolved disorder, however there was insufficient information from the difference map to locate a second conformation and refine it. The structure contains unusually short methyl-to-methyl intramolecular contacts for the two ligands bonded to U2, which is likely a consequence of both the unresolved disorder in the second Cp* ligand and the constraint of hydrogen atoms to idealized geometries.

Table 3-1. Crystallography data for complexes **1**, **2**, and **4**.

	1	2	4
CCDC deposit number	1828732	1828736	1829165
Empirical formula	C ₃₆ H ₅₈ OPSiU	C ₂₆ H ₄₈ N ₂ Si ₂ U	C _{80.50} H ₁₁₇ N ₆ U ₃
Formula weight (g/mol)	803.91	682.87	1882.88
Crystal habit, color	Needle, Red	Prism, Green	Plate, Brown
Temperature (K)	150(2)	100(2)	100(2)
Space group	P2 ₁ /n	P2 ₁ 2 ₁ 2 ₁	Pca2 ₁
Crystal system	Monoclinic	Orthorhombic	Orthorhombic
Volume (Å ³)	3566.8(4)	3038.3(6)	8241.7(7)
a (Å)	9.6794(5)	13.2573(14)	18.8226(9)
b (Å)	20.3019(12)	14.8359(16)	23.0418(10)
c (Å)	18.3009(11)	15.4478(17)	19.0030(9)
α (°)	90	90	90
β (°)	97.346(2)	90	90
γ (°)	90	90	90
Z	4	4	4
Calculated density (Mg/m ³)	1.497	1.493	1.517
Absorption coefficient (mm ⁻¹)	4.654	5.436	5.922
Final R indices [I > 2σ(I)]	R1 = 0.0282, wR2 = 0.0465	R1 = 0.0250, wR2 = 0.0628	R1 = 0.0388, wR2 = 0.0714

Result and discussion.

The synthesis of (C₅Me₅)₂U[P(C₆H₂Me₃-2,4,6)(SiMe₃)](THF), **1**, was done by reacting (C₅Me₅)₂UI(THF) with the bulky phosphido ligand, KP(C₆H₂Me₃-2,4,6)(SiMe₃), eq. 1, which resulted in an immediate color change from green to brown. The product was isolated as a dark brown powder. No resonances could be definitively assigned in ¹H NMR spectrum of **1** and the ³¹P NMR signal could not be located.



The structure of **1** was determined by X-ray crystallographic analysis. The U-P bond distance of 2.8903(9) Å is similar to the U(IV)-P bond distance of 2.883(2) Å in U(Tren^{TIPS})(PH₂), Tren^{TIPS} = N{CH₂CH₂NSi(ⁱPr)₃}₃. This is a result of the lack of steric crowding in the equatorial plane of **1**.

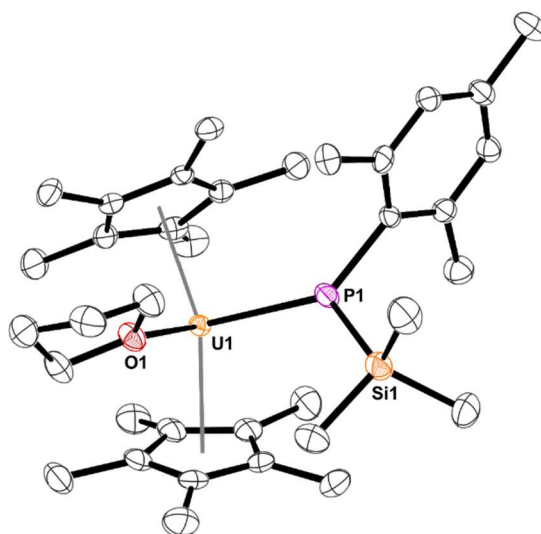
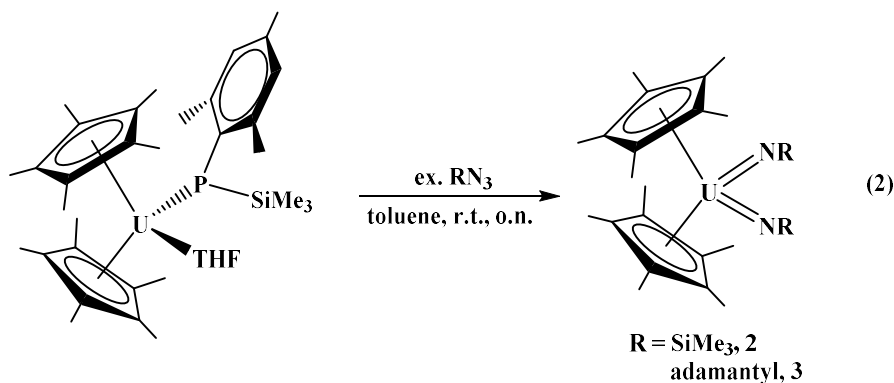


Figure 3-1. Thermal ellipsoid plots of **1** shown at the 50% probability level. The hydrogen atoms have been omitted for clarity.

The reactivity of **1** was examined with organic azides and *tert*-butyl isocyanide, which are known to undergo both insertion and reduction chemistry. Since U(III) is highly

reducing, coupled with the weak uranium-phosphorus bond, we explored the possibility of both reaction types occurring with **1**. This was not the case. Organic azides such as 1-azidoadamantane (N_3Ad) and azidotrimethylsilane (Me_3SiN_3) react with **1** to form bis(imido) complexes, eq. 2. Both uranium(VI) products, $(C_5Me_5)_2U[=N(SiMe_3)]_2$, **2**, and $(C_5Me_5)_2U[=N(Ad)]_2$, **3**, can be isolated after recrystallization in low yield, eq. 2. While no color change occurred, gas evolution was observed. Complex **3** has been previously reported by Burns and co-workers from $(C_5Me_5)_2UCl_2$ with two equivalents of N_3Ad in the presence of excess potassium graphite. Complex **2** can be made from this route as well.



The 1H NMR spectrum of **2** indicated a diamagnetic species with $(C_5Me_5)^{1-}$ resonance at 4.40 ppm and the $SiMe_3$ group at 0.34 ppm. The resonance at -53 ppm for $SiMe_3$ in the ^{29}Si NMR spectrum is shifted considerably to higher frequency compared to other U(VI) complexes containing a silyl group previously reported¹⁷⁵. For example, $(BIPM)UOCl_2$ and $(BIPM)U(NMe_3)(O)(DMAP)_2$ have ^{29}Si chemical shifts at -0.69 and -8.28 ppm, respectively²³. However, there are no uranium(VI) complexes with the $(=NSiMe_3)^{2-}$ functional group to compare directly. When compared to diamagnetic transition metal imido complexes, the ^{29}Si NMR chemical shift is also quite upfield shifted.

The structure of **2** was determined by X-ray crystallographic analysis. The U-N bond distances in **2** are 1.948(5) and 1.957(5) Å. These bond lengths are similar to other metallocene bis(imido) complexes. For example, $(C_5Me_5)_2U(=NAd)_2$, **3**, has U-N bond distances of 1.94(2) and 1.96(2) Å, while $(C_5Me_5)_2U(=NPh)_2$ are 1.952(7) Å.

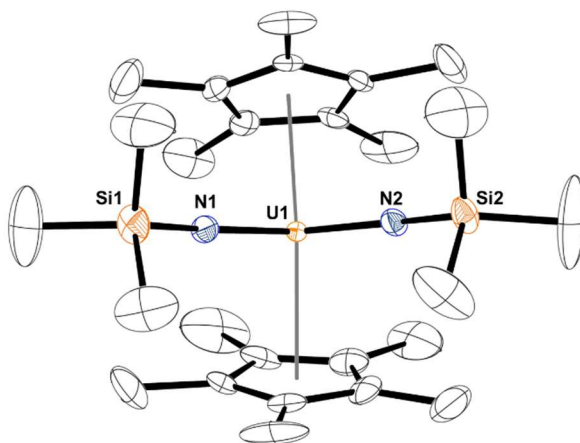
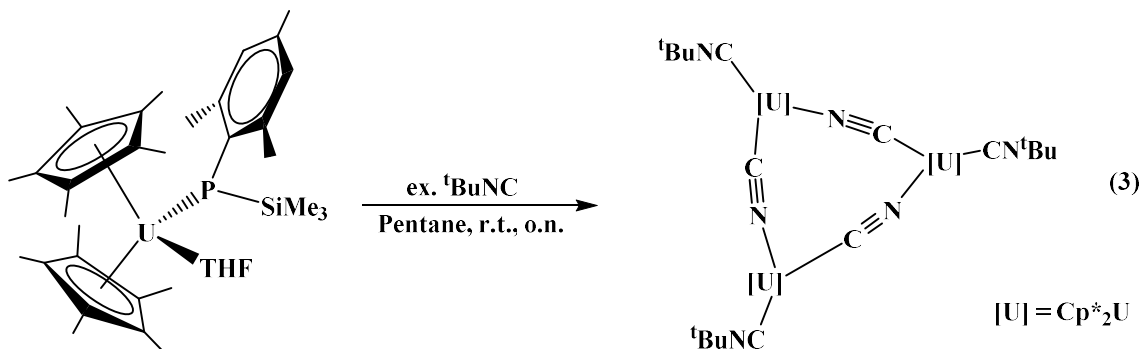


Figure 3-2. Thermal ellipsoid plots of **2** shown at the 50% probability level. The hydrogen atoms have been omitted for clarity.

The reaction of **1** with two equivalents of an organic azide is a four-electron reduction. Three electrons from metal-based oxidation of U(III) to U(VI) and one-electron from the reductive coupling of the phosphido ligand to form half an equivalent of $(Me_3Si)PP(SiMe_3)(Me)$. This type of reactivity has been observed previously with $(C_5Me_5)_2U(BPh_4)$ and azobenzene¹⁴⁹.

Reaction of **1** with ^tBuNC forms the previously known bridging cyanide product, $[(C_5Me_5)_2U(CNC(CH_3)_3)(\mu-CN)]_3$, **4**, eq 3. This complex was previously synthesized from the reaction of $(C_5Me_5)_3U$ with an excess of ^tBuNC¹⁷⁶. In this case, the ligand-based redox chemistry of the phosphido acts as in a similar manner to the $(C_5Me_5)^{1-}$ ligand in the sterically crowded $(C_5Me_5)_3U$. Complex **4** maintains the +3 oxidation state

and the byproduct of this reaction could not be determined, but no evidence of coupled phosphido product was found.



Conclusions

The synthesis and reactivity of the first U(III) phosphido complex has been conducted. With organic azides or ${}^t\text{BuNC}$, the reactivity involves the elimination of the phosphido ligand either by reductive coupling or some other means. Unfortunately, our overall goal of combining functionalization and redox chemistry was not achieved; however, **1** can be used as a reducing agent through metal- and ligand-based reactivity.

Chapter 4: Influence of Substituents on Electronic Structure of Mono- and Bis(Phosphido) Thorium(IV) Complexes

Introduction

While actinides prefer the harder Lewis bases such as oxygen and nitrogen, the lower congeners of these elements, like phosphorus, have been understudied. Interest in the heavier main group elements stems from the observation that covalent bonding in the actinide-ligand bond increases going down a group.^{90-91, 177} Hence, while the actinides prefer 2p elements, the energy between the 5f and *np* orbitals decreases with increasing *n*,^{98, 101, 178} thus presenting the paradox that covalent bonding does not translate into strong bonds. This concept is not shared in transition metal and main group elements³ because the overlap between *nd* orbitals and *np* orbitals is significantly greater than the overlap between 5f and *np* orbitals.

In the report of the first actinide-phosphorus bonds, the reaction of $(C_5Me_5)_2ThCl_2$ with two equivalents of $KPPh_2$ produced the dark purple complex, $(C_5Me_5)_2Th(PPh_2)_2$.³⁰ A similar result was obtained for $(C_5Me_5)_2ThEt_2$, $Et = CH_2CH_3$. While purple is an expected color for a paramagnetic species such as $Th(III)$ ¹⁷⁹ or radical-based ligand,^{74, 180} the ¹H NMR spectrum of this complex was diamagnetic, suggesting a ligand to metal charge transfer. Previously, we have reported bis(phosphido) complexes of thorium, $(C_5Me_5)_2Th[PH(C_6H_2R_{3-2,4,6})]_2$, $R = CH_3$,¹⁶² ⁱPr,⁸⁰ but these complexes were pale yellow, similar to $(C_5Me_5)_2Th(Cl)[P(SiMe_3)_2]$.¹⁸¹ This indicates that the ligand to metal charge transfer can be manipulated with respect to secondary versus primary phosphido ligands as well as changing the substituents in secondary phosphidos. Additionally, the zirconium analog, $(C_5Me_5)_2Zr[PH(C_6H_2Me_{3-2,4,6})]_2$,¹⁸² is described as a red wine color,

so not all metallocene bis(phosphido) metal complexes are the same. Finally, metallocene complexes of thorium bis(amides) are pale in color. For example, $(C_5Me_5)_2Th(NMe_2)_2$ is light yellow.¹⁸³ Again, phosphorus plays a role in the electronic structure of organothorium complexes.

Herein, we report a series of thorium phosphido complexes with the metallocene ligand framework. The colors of these complexes range from pale yellow to dark purple depending on the phosphorus substituents. The electronic structure has been investigated using UV-vis spectroscopy as well as time-dependent density functional theory calculations to show the ligand to metal charge transfer band originates from the energy associated with the donating properties of the phosphorus substituents. Hence, more donating substituents lead to larger band gaps and, thus, light colored complexes.

Experimental

General considerations.

All syntheses were carried out under N_2 atmosphere using glovebox and Schlenk techniques. All solvents used were dried by passing through solvent purification system, MBRAUN, USA. AgOTf and $KN(SiMe_3)_2$ were obtained from Sigma Aldrich. $HP(C_6H_2Me_3-2,4,6)_2$,¹⁸⁴ $HP(C_6H_2Me_3-2,4,6)(SiMe_3)$,¹⁶⁷ $HP(C_6H_2Me_3-2,4,6)(CH_3)$,¹⁸⁵ $(C_5Me_5)_2ThCl_2$,¹² $(C_5Me_5)_2ThMe_2$,¹² and $(C_5Me_5)_2Th[PH(C_6H_2Me_3-2,4,6)]_2$ ¹⁶² were synthesized as previously described. $K[P(C_6H_2Me_3-2,4,6)_2]$ was prepared from $HP(C_6H_2Me_3-2,4,6)_2$ and $KN(SiMe_3)_2$ in toluene. $KP(C_6H_2Me_3-2,4,6)(SiMe_3)$ was prepared from $HP(C_6H_2Me_3-2,4,6)(SiMe_3)$ and potassium benzyl¹⁶⁸ in toluene. $KP(C_6H_2Me_3-2,4,6)(CH_3)$ was prepared from $HP(C_6H_2Me_3-2,4,6)(CH_3)$ and $KN(SiMe_3)_2$ in toluene. Benzene-*d*₆ (Cambridge Isotope Laboratories) was degassed by three freeze-

pump-thaw cycles and stored over activated 4 Å molecular sieves. All ^1H and $^{13}\text{C}\{^1\text{H}\}$ spectra were taken on either 500 or 600 MHz Bruker spectrometers. All $^{31}\text{P}\{^1\text{H}\}$, ^{29}Si INEPT, and ^{19}F spectra were taken on a 300 MHz Bruker spectrometer. All NMR chemical shifts were reported in ppm. ^1H NMR shifts were referenced internally to the residual solvent peak, $\text{C}_6\text{D}_5\text{H}$, at 7.16 ppm. ^{13}C NMR shifts were referenced internally to $^{13}\text{C}_6\text{D}_6$ at 128.06 ppm. $^{31}\text{P}\{^1\text{H}\}$ NMR shifts were referenced externally to 85% H_3PO_4 at 0 ppm. ^{29}Si NMR shifts were reported by referenced externally to TMS at 0 ppm. ^{19}F NMR shifts were referenced externally to hexafluorobenzene at -164.9 ppm. All infrared spectra were taken on Perkin-Elmer Spectrum One FT-IR spectrometer recorded as KBr pellets. Elemental analyses were performed at the University of California, Berkeley Microanalytical Facility using a Perkin-Elmer Series II 2400 CHNS analyzer.

Synthesis of $\text{KP}(\text{C}_6\text{H}_2\text{Me}_3\text{-2,4,6})(\text{SiMe}_3)$. To a scintillation vial charged with benzyl potassium (182 mg, 1.4 mmol), toluene (5 mL), and a magnetic stir bar, $\text{HP}(\text{C}_6\text{H}_2\text{Me}_3\text{-2,4,6})(\text{SiMe}_3)$ (313 mg, 1.4 mmol) was added neat at room temperature. The suspension was stirred at room temperature for 48 hours. The solution was then filtered through Celite to yield a yellow solution. Solvent and remaining starting material were removed *in vacuo* to yield $\text{KP}(\text{C}_6\text{H}_2\text{Me}_3\text{-2,4,6})(\text{SiMe}_3)$ as a yellow powder (196 mg, 54%). ^1H NMR (C_6D_6 , 600 MHz, 298 K): δ 6.92 (s, 2H, *m*-Mes), 2.57 (s, 6H, $\text{CH}_3\text{-}o\text{-Mes}$), 2.14 (s, 3H, $\text{CH}_3\text{-}p\text{-Mes}$), 0.29 (d, 9H, $^3J_{\text{H-P}} = 4.2$ Hz, $-\text{Si}(\text{CH}_3)_3$). $^{13}\text{C}\{^1\text{H}\}$ NMR (C_6D_6 , 150 MHz): δ 145.1 (d, $^2J_{\text{C-P}} = 4.5$ Hz, *o*-Mes), 143.0 (d, $^2J_{\text{C-P}} = 45$ Hz, *ipso*-Mes), 132.9 (*p*-Mes), 128.8 (*m*-Mes), 27.9 (d, $^2J_{\text{C-P}} = 10.5$ Hz, $\text{CH}_3\text{-}o\text{-Mes}$), 20.9 (*p*-Mes), 5.5 (d, $^2J_{\text{C-P}} = 12$ Hz, $-\text{Si}(\text{CH}_3)_3$). $^{31}\text{P}\{^1\text{H}\}$ NMR (C_6D_6 , 121 MHz): δ -180.2. ^{29}Si INEPT NMR (C_6D_6 , 60 MHz): δ 2.14 (d, $^1J_{\text{Si-P}} = 47.9$ Hz, $-\text{Si}(\text{CH}_3)_3$).

Caution! Thorium-232 is an alpha-emitting radiometal with a half-life of 1.4×10^{10} years. It was used in a radiological laboratory with appropriate personal protective and counting equipment.

Synthesis of $(C_5Me_5)_2Th(Cl)[P(C_6H_2Me_3-2,4,6)_2]$, 1. $K[P(C_6H_2Me_3-2,4,6)_2]$ (118 mg, 0.38 mmol) in Et_2O (10 mL) was added to $(C_5Me_5)_2ThCl_2$ (220 mg, 0.38 mmol) in Et_2O (10 mL) and stirred for 2 hours. The resulting purple solution was filtered over a plug of Celite and the volatiles removed *in vacuo* to yield a purple solid (172 mg, 56%). X-ray quality crystals were grown from a concentrated diethyl ether solution at -35 °C. 1H NMR (C_6D_6 , 500 MHz, 298 K): δ 6.93 (s, 4H, *m*-Mes), 2.63 (s, 12H, *o*-Mes), 2.18 (s, 6H, *p*-Mes), 2.01 (s, 30H, C_5Me_5). $^{13}C\{^1H\}$ NMR (C_6D_6 , 125 Hz, 298 K): 144.1 (d, $^2J_{P-C} = 7.9$ Hz), 139.7, 136.1, 129.3 (d, $^3J_{P-C} = 5.2$ Hz), 128.7, 25.8 (d, $^3J_{P-C} = 10.4$ Hz), 21.0, 11.9. $^{31}P\{^1H\}$ NMR (C_6D_6 , 120 MHz): δ 114.8. IR (KBr, cm^{-1}): 2965 (s), 2917 (s), 2856 (s), 1606 (m), 1445 (s), 1378 (m), 1262 (m), 1085 (s), 1031 (s), 952 (w), 848 (s), 802 (m), 654 (w). UV-vis (0.25 mM, Toluene): 534 nm, $\epsilon = 375$ $M^{-1} cm^{-1}$. Despite multiple attempts, a satisfactory elemental analysis could not be obtained due to similar solubility of **1** and $HPMe_2$.

Synthesis of $(C_5Me_5)_2Th[P(C_6H_2Me_3-2,4,6)(CH_3)]_2$, 2. $(C_5Me_5)_2ThCl_2$ (140 mg, 0.24 mmol) in toluene was added to $KP(C_6H_2Me_3-2,4,6)(CH_3)$ (100 mg, 0.49 mmol) in toluene and stirred overnight. The formation of a precipitate was observed immediately followed the addition. The resulting deep red solution was filtered over a plug of Celite and the volatiles removed *in vacuo* to yield a red solid (168 mg, 83%). X-ray quality crystals were grown from a concentrated diethyl ether solution at -35 °C. 1H NMR (C_6D_6 , 600 MHz, 298 K): δ 7.08 (s, 4H, *m*-Mes), 2.86 (s, 12H, *o*-Mes), 2.33 (d, 6H, $^2J_{H-P} = 5.4$ Hz,

P-Me), 2.24 (s, 6H, *p*-Mes), 2.07 (s, 30H, *C*₅*Me*₅). ¹³C{¹H} NMR (C₆D₆, 150 Hz, 298 K): 144.1, 142.8, 129.0, 126.0, 25.0 (dd, *J*_{P-C} = 4.0 Hz, *J*_{P-C} = 5.2 Hz), 21.2, 15.2 (d, ¹*J*_{P-C} = 6 Hz), 11.6. ³¹P{¹H} NMR (C₆D₆, 120 MHz): δ 117.5. IR (KBr, cm⁻¹): 2972 (m), 2954 (s), 2893 (vs), 2856 (s), 1599 (w), 1484 (w), 1448 (s), 1347 (s), 1289 (w), 1262 (w), 1118 (w), 1053 (w), 1021 (m), 886 (m), 844 (s), 821 (w), 716 (w), 683 (w), 616 (w), 608 (w), 552 (w). UV-vis (0.25 mM, Toluene): 533 nm, ε = 260 M⁻¹ cm⁻¹. Anal. Calcd for C₄₀H₅₈P₂Th₁: C, 57.68; H, 7.02. Found: C, 57.32; H, 7.13.

Synthesis of (C₅Me₅)₂Th(CH₃)OTf, 3. In an absence of light, AgOTf (117 mg, 0.46 mmol) in THF (5 mL) was added to (C₅Me₅)₂Th(CH₃)₂ (243 mg, 0.46 mmol) in THF (5 mL) and stirred overnight. The resulting dark grey suspension was filtered over a plug of Celite and the volatiles removed *in vacuo* to yield a white solid (264 mg, 87%). X-ray quality crystals were grown from a concentrated toluene solution at -35 °C. ¹H NMR (C₆D₆, 600 MHz, 300K): δ 2.05 (s, 30H, *C*₅*Me*₅), 0.52 (s, 3H, Th-*Me*). ¹³C{¹H} NMR (C₆D₆, 150 MHz, 300 K): δ 125.9, 68.6, 11.6, CF₃ resonance could not be located. ¹⁹F NMR (C₆D₆, 283 MHz, 300 K): δ -71.2. IR (KBr, cm⁻¹): 2917 (m), 2867 (m), 1440 (w), 1382 (w), 1314 (m), 1252 (s), 1217 (vs), 1122 (w), 1020 (vs), 805 (w), 629 (m). This compound has been previously reported but using triflic acid.¹⁸⁶⁻¹⁸⁷

Synthesis of (C₅Me₅)₂Th(CH₃)[P(C₆H₂Me₃-2,4,6)₂], 4. A 20 mL scintillation vial was charged with (C₅Me₅)₂Th(CH₃)Cl (330 mg, 59.8 mmol) and toluene (3 mL), and placed in a -25 °C freezer to cool for 30 minutes. A second vial was charged with KPMe₂ (184 mg, 59.8 mmol). The KPMe₂ was then transferred to the cooled solution of (C₅Me₅)₂Th(CH₃)Cl, with about 5 mL of toluene. The reaction was stirred for about 1.5 hours, resulting in a cloudy red solution. The volatiles were removed under reduced

pressure. The resulting red-purple crude solid was triturated in diethyl ether and filtered over Celite to remove any free phosphine generated. The remaining solid was then washed through the filter using toluene, until the red-purple solution ran clear, leaving a yellow solid behind (KPMes₂). The toluene solution was concentrated and layered with pentane. From the layered solution, a red-purple solid (127 mg, 47% yield) deposited out overnight. Through subsequent recrystallizations, more material was able to be isolated. ¹H NMR (600 MHz, C₆D₆): δ 6.92 (s, 4H, *m*-Mes), 2.54 (s, 12H, *o*-Mes), 2.18 (s, 6H, *p*-Mes), 1.93 (s, 30H, C₅(CH₃)₅), 0.41 (s, 3H, Th-CH₃). ¹³C{¹H} (C₆D₆, 150 MHz): δ 143.54 (d, ¹J_{C-P} = 9 Hz, P-C-Mes), 140.88 (d, ²J_{C-P} = 1.5 Hz, ArC-ortho), 135.43 (s, ArC-para), 129.18 (d, ³J_{C-P} = 4.5 Hz, ArC-meta) 125.13 (s, C₅(CH₃)₅), 72.77 (s, Th-CH₃), 25.68 (d, ³J_{C-P} = 10.5 Hz, Mes-CH₃-ortho), 21.04 (s, Mes-CH₃-para), 11.59 (s, C₅(CH₃)₅). ³¹P{¹H} (C₆D₆, 120 MHz): δ 105.3. IR (KBr, cm⁻¹): 2971 (s), 2909 (vs), 2861 (s), 1601 (w), 1546 (w), 1462 (w), 1446 (vs), 1396 (w), 1396 (w), 1373 (m), 1290 (w), 1260 (w), 1176 (w), 1108 (m), 1087 (w), 1050 (w), 1030 (m), 1018 (w), 950 (w), 847 (vs), 801 (w), 711 (w), 618 (w), 556 (m), 545 (w), 517 (w). UV-vis (0.6 mM, Toluene): 525 nm, ε = 640 M⁻¹cm⁻¹. Anal. Calcd for C₃₉H₅₅P₁Th₁: C, 59.53; H, 7.05. Found: C, 59.40; H, 7.11.

Synthesis of (C₅Me₅)₂Th(CH₃)[P(C₆H₂Me₃-2,4,6)(SiMe₃)], 5. KP(C₆H₂Me₃-2,4,6)(SiMe₃) (79 mg, 0.3 mmol) in toluene (5 mL) was added to (C₅Me₅)₂Th(CH₃)OTf (201 mg, 0.3 mmol) in toluene (5 mL) and stirred overnight. The resulting orange solution was filtered over a plug of Celite and the volatiles removed *in vacuo* to yield an orange solid (169 mg, 76%). X-ray quality crystals were grown from a concentrated diethyl ether solution at -35 °C. ¹H NMR (C₆D₆, 600 MHz, 300 K): δ 7.04 (s, 2H, *m*-Mes), 2.80 (s, 6H, *o*-Mes), 2.22 (s, 3H, *p*-Mes), 1.99 (s, 30H, C₅Me₅), 0.43 (s, 3H, Th-

Me), 0.39 (d, 9H, $^2J_{H-P} = 4.8$ Hz, SiMe₃). $^{13}\text{C}\{^1\text{H}\}$ NMR (C₆D₆, 150 MHz, 300 K): 144.9 (d, $^2J_{C-P} = 5.1$ Hz), 137.3 (d, $^1J_{C-P} = 9.45$ Hz), 135.3, 128.5 (d, $^3J_{P-C} = 4.2$ Hz), 125.2, 71.3, 27.5 (d, $^3J_{P-C} = 9.15$ Hz), 21.1, 11.7, 4.57 (d, $^2J_{P-C} = 11.4$ Hz). $^{31}\text{P}\{^1\text{H}\}$ NMR (C₆D₆, 120 MHz): δ 11.9. ^{29}Si INEPT NMR (C₆D₆, 60 MHz): δ 6.44 (d, $^1J_{\text{Si-P}} = 7.8$ Hz). IR (KBr, cm⁻¹): 2968 (s), 2944 (s), 2909 (vs), 2859 (s), 1488 (w), 1437 (m), 1377 (m), 1237 (s), 1106 (m), 1044 (m), 1022 (m), 948 (w), 836 (vs), 747 (w), 677 (w), 629 (m). UV-vis (0.10 mM, Toluene): 495 nm, $\epsilon = 285 \text{ M}^{-1} \text{ cm}^{-1}$. Anal. Calcd for C₃₂H₅₀Cl₁P₁Si₁Th₁: C, 53.50; H, 7.21. Found: C, 52.56; H, 7.05.

Synthesis of (C₅Me₅)₂Th[P(C₆H₂Me₃-2,4,6)(SiMe₃)]₂, 6, and (C₅Me₅)₂Th(Cl)[P(C₆H₂Me₃-2,4,6)(SiMe₃)], 7. KP(C₆H₂Me₃-2,4,6)(SiMe₃) (92 mg, 0.35 mmol) in toluene (5 mL) was added to (C₅Me₅)₂ThCl₂ (100 mg, 0.17 mmol) in toluene (5 mL) and stirred overnight. The resulting orange solution was filtered over a plug of Celite and the volatiles removed *in vacuo* to yield a tacky orange solid (117 mg). ^{31}P NMR shows that the crude material contains both (C₅Me₅)₂Th(Cl)[P(C₆H₂Me₃-2,4,6)(SiMe₃)] and (C₅Me₅)₂Th[P(C₆H₂Me₃-2,4,6)(SiMe₃)]₂ (9:1 ratio). Recrystallization from DME yielded a small quantity of x-ray quality crystals of (C₅Me₅)₂Th[P(C₆H₂Me₃-2,4,6)(SiMe₃)]₂, 6. ^1H NMR (C₆D₆, 600 MHz, 298 K): δ 7.11 (s, 4H, *m*-Mes), 2.86 (s, 12H, *o*-Mes), 2.25 (s, 6H, *p*-Mes), 2.09 (s, 30H, C₅Me₅), 0.51 (br-s, 18H). $^{13}\text{C}\{^1\text{H}\}$ NMR (C₆D₆, 150 Hz, 298 K): 145.4, 138.2 (d, $^1J_{C-P} = 7.5$ Hz), 135.8, 128.8, 128.1, 27.6, 21.1, 12.3, 4.37 (t, $^2J_{C-P} = 6$ Hz). $^{31}\text{P}\{^1\text{H}\}$ NMR (C₆D₆, 120 MHz): δ 48.5. ^{29}Si INEPT NMR (C₆D₆, 60 MHz): δ 7.14 (t, $^1J_{\text{Si-P}} = 1.9$ Hz). UV-vis (0.25 mM, Toluene): 455 nm, $\epsilon = 390 \text{ M}^{-1} \text{ cm}^{-1}$. Recrystallization from Et₂O yielded a small quantity of x-ray quality crystals of (C₅Me₅)₂Th(Cl)[P(C₆H₂Me₃-2,4,6)(SiMe₃)], 7. ^1H NMR (C₆D₆, 600 MHz, 298 K): δ 7.04

(s, 2H, *m*-Mes), 2.80 (s, 6H, *o*-Mes), 2.21 (s, 3H, *p*-Mes), 2.06 (s, 30H, *C*₅*Me*₅), 0.43 (d, 9H, ²*J*_{H-P} = 4.8 Hz). ¹³C{¹H} NMR (C₆D₆, 150 Hz, 298 K): 145.0 (d, ¹*J*_{C-P} = 4.5 Hz), 137.3 (d, ²*J*_{C-P} = 4.5 Hz), 135.69, 128.6 (d, ³*J*_{C-P} = 4.5 Hz), 128.2, 24.5, 21.1, 12.0, 4.6 (d, ²*J*_{C-P} = 10.5 Hz). ³¹P{¹H} NMR (C₆D₆, 120 MHz): δ 24.8. ²⁹Si INEPT NMR (C₆D₆, 60 MHz): δ 6.56 (d, ¹*J*_{Si-P} = 6 Hz). Despite multiple attempts, a satisfactory elemental analysis could not be obtained due to similar solubility of (C₅Me₅)₂Th(Cl)[P(C₆H₂Me₃-2,4,6)(SiMe₃)] and (C₅Me₅)₂Th[P(C₆H₂Me₃-2,4,6)(SiMe₃)]₂.

Computational Details. Theoretical calculations were carried out with Kohn-Sham density functional theory (KS-DFT) using the Amsterdam Density Functional (ADF2017) package.^{108, 188} The scalar relativistic zeroth order regular approximation (ZORA) relativistic Hamiltonian¹⁰⁹, along with the Perdew, Burke and Ernzerhof (PBE) functional¹⁸⁹ and TZP Slater-type basis sets¹¹² with small cores were used for geometry optimizations. Due to the charge transfer-like nature of valence excitations, the Coulomb attenuated method Becke 3-parameter Lee, Yang, Parr (CAM-B3LYP) functional¹⁹⁰ was employed for excitation spectra simulations using time-dependent DFT (TD-DFT) linear response calculations.

Crystal structure determination and refinement. The selected single crystal of **1-7** was mounted on a nylon cryoloop using viscous hydrocarbon oil. X-ray data collection was performed at 100(2) or 150(2) K. The X-ray data were collected on a Bruker CCD diffractometer with monochromated Mo-K α radiation ($\lambda = 0.71073 \text{ \AA}$). The data collection and processing utilized Bruker Apex2 suite of programs.⁵⁸ The structures were solved using direct methods and refined by full-matrix least-squares methods on *F*² using Bruker SHELX-97 program.⁵⁹ All non-hydrogen atoms were refined with anisotropic

displacement parameters. All hydrogen atoms were placed at calculated positions and included in the refinement using a riding model. Thermal ellipsoid plots were prepared by using Olex2⁶⁰ with 50% of probability displacements for non-hydrogen atoms. Crystal data and details for data collection for complexes **1-7** are provided in Table 4-1.

Table 4-1. X-ray crystallographic data shown for complexes **1-7**.

Complex	1	2	3
CCDC deposit number	1834568	1834569	1834570
Empirical formula	C ₃₈ H ₅₂ ClPTh	C ₄₀ H ₅₈ P ₂ Th	C ₅₁ H ₇₄ F ₆ O ₆ S ₂ Th ₂
Formula weight (g/mol)	807.25	832.84	1425.30
Crystal habit, color	Prism, Red	Prism, Red	Prism, Colorless
Temperature (K)	100(2)	100(2)	100(2)
Space group	P2 ₁ /n	C2/c	P2 ₁ /c
Crystal system	Monoclinic	Monoclinic	Monoclinic
Volume (Å ³)	3411.4(8)	4216.8(11)	5329.9(10)
a (Å)	11.7219(15)	17.321(3)	11.6583(12)
b (Å)	20.910(3)	13.840(2)	25.044(3)
c (Å)	14.0570(18)	17.800(3)	19.140(2)
α (°)	90°	90°	90°
β (°)	98.072(2)°	98.821(2)°	107.4960(10)°
γ (°)	90°	90°	90°
Z	4	4	4
Calculated density (Mg/m ³)	1.572	1.312	1.776

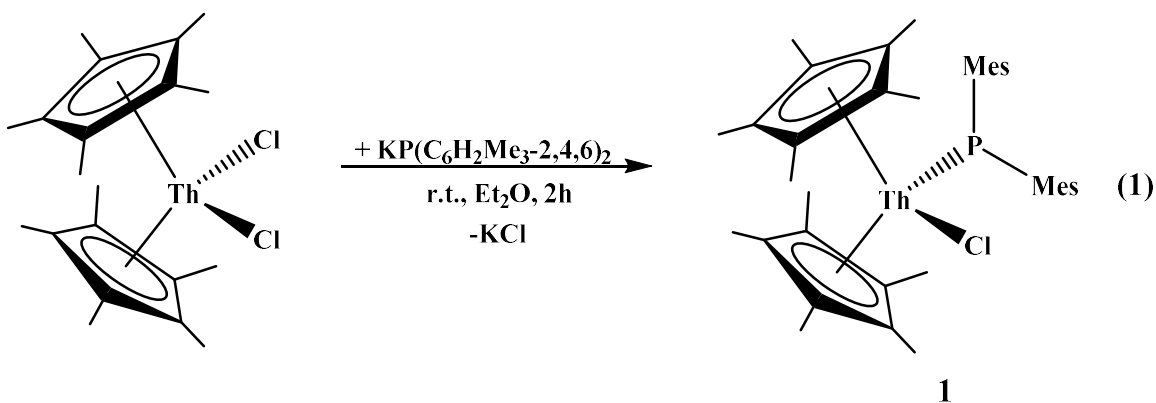
Absorption coefficient (mm^{-1})	4.521	3.635	5.719
Final R indices [$I > 2\sigma(I)$]	R1 = 0.0368, wR2 = 0.0840	R1 = 0.0439, wR2 = 0.1066	R1 = 0.0213, wR2 = 0.0454

4	5	6	7
1834571	1834572	1834574	1834573
$\text{C}_{39}\text{H}_{55}\text{PTh}$	$\text{C}_{33}\text{H}_{53}\text{PSiTh}$	$\text{C}_{44}\text{H}_{70}\text{P}_2\text{Si}_2\text{Th}$	$\text{C}_{32}\text{H}_{50}\text{CIPSiTh}$
786.84	740.85	949.16	761.27
Plate, Pink	Prism, Yellow	Prism, Orange	Plate, Orange
100(2)	100(2)	100(2)	100(2)
$\text{P12}_1/\text{n1}$	P-1	C2/c	P-1
Monoclinic	Triclinic	Monoclinic	Triclinic
3441.3(6)	3274.8(5)	4506.8(2)	3239.3(6)
11.6978(11)	9.4091(8)	15.4033(4)	9.4027(9)
20.919(2)	14.9346(13)	18.6254(5)	14.8838(15)
14.2090(13)	23.706(2)	15.7119(4)	23.531(2)
90°	89.868(2)°	90°	90.122(2)°
98.2090(10)°	87.257(2)°	91.091(2)°	93.183(2)°
90°	79.804(2)°	90°	99.858(2)°
4	4	4	4
1.519	1.503	1.399	1.561
4.404	4.658	12.044	4.791
R1 = 0.0204,	R1 = 0.0369,	R1 = 0.0226,	R1 = 0.0173,

wR2 = 0.0451	wR2 = 0.0545	wR2 = 0.0570	wR2 = 0.0444
--------------	--------------	--------------	--------------

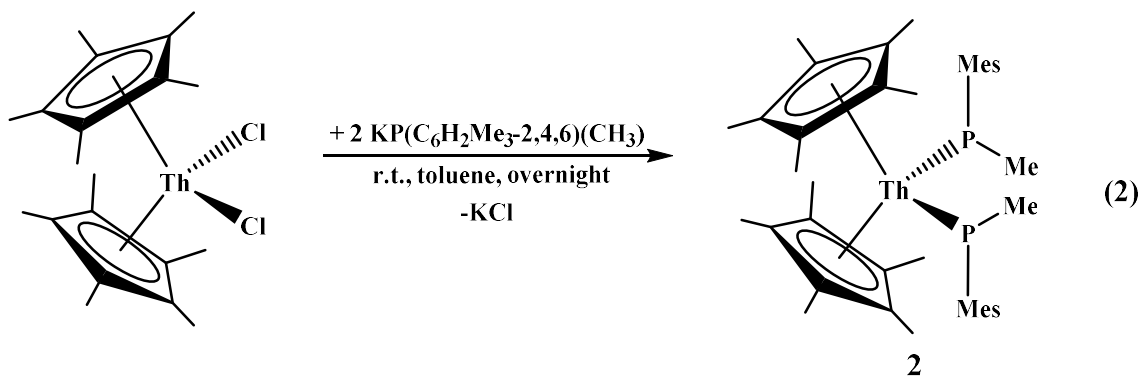
Results and Discussion

Syntheses. Reaction of $(C_5Me_5)_2ThCl_2$ with $KP(C_6H_2Me_3-2,4,6)_2$ results in an immediate color change from colorless to a dark purple. The 1H NMR spectrum of the reaction indicated the product as, $(C_5Me_5)_2Th(Cl)[P(C_6H_2Me_3-2,4,6)_2]$, **1**, eq 1, with only coordination of only one phosphido ligand. Allowing the reaction to proceed for more than 2-3 hours produces large amounts of phosphine and coupled phosphido, Mes_2PPMes_2 ,¹⁹¹ as observed in the ^{31}P NMR spectrum. The reaction with two equivalents of $KP(C_6H_2Me_3-2,4,6)_2$ does not yield the bis(phosphido) complex, presumably due to the steric properties of the mesityl group.

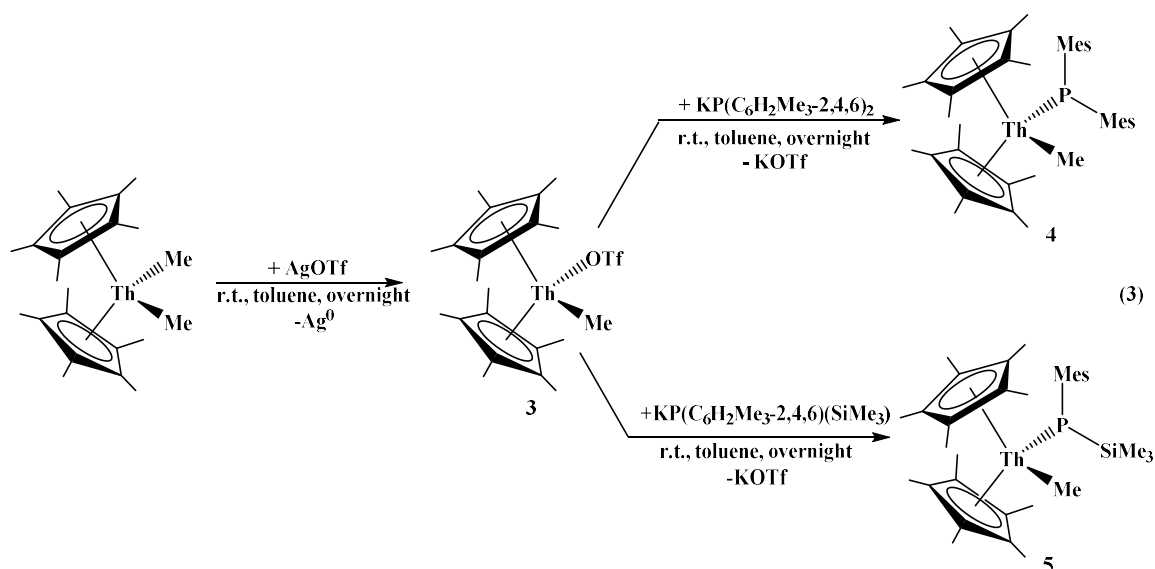


We note that $(C_5H_5)_2Zr(AsMes_2)_2$ is known,¹⁹² but this could be due to the use of $(C_5H_5)^{1-}$ instead of $(C_5Me_5)^{1-}$ as well as arsenic being much larger than phosphorus, producing longer Zr-As bonds. When the steric properties are decreased using $KP[(C_6H_2Me_3-2,4,6)(CH_3)]$, the bis(phosphido) complex, $(C_5Me_5)_2Th[P(C_6H_2Me_3-2,4,6)(CH_3)]_2$, **2**, can be isolated, eq 2. Complex **2** is also dark purple in color. This is in contrast to our

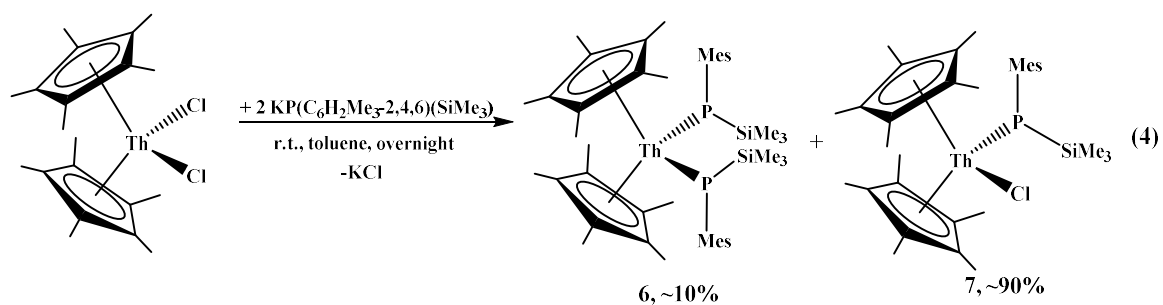
previously reported bis(phosphido) complex, $(C_5Me_5)_2Th[PH(C_6H_2Me_3-2,4,6)]_2$, which has a pale-yellow color.



Hence, the substituents on phosphorus make a large difference in the electronic structure of the thorium complex. To test that the effect takes place from the phosphido ligand and not the chloride, the methyl analog was synthesized. For this, $[(C_5Me_5)_2Th(CH_3)(OTf)]_2$, **3**, $OTf = OSO_2CF_3$, was used. Complex **3** can be made in an analogous way to the uranium complex through the reaction of $(C_5Me_5)_2Th(CH_3)_2$ with $AgOTf$.¹¹⁴ Reaction of **3** or $(C_5Me_5)_2Th(CH_3)Cl$ with $KP(C_6H_2Me_3-2,4,6)_2$ produced a dark red-purple solution for which the product was identified as $(C_5Me_5)_2Th(CH_3)[P(C_6H_2Me_3-2,4,6)]_2$, **4**. Interestingly, the reaction of **3** with $KP[(SiMe_3)(C_6H_2Me_3-2,4,6)]$ produces an orange colored solution, $(C_5Me_5)_2Th(CH_3)[P(SiMe_3)(C_6H_2Me_3-2,4,6)]$, **5**, not dark purple.



To probe this further, $(C_5Me_5)_2Th[P(C_6H_2Me_3-2,4,6)(SiMe_3)]_2$, **6**, and $(C_5Me_5)_2Th(Cl)[P(C_6H_2Me_3-2,4,6)(SiMe_3)]$, **7**, were both made upon reaction of $(C_5Me_5)_2ThCl_2$ with two equivalents of $K[P(C_6H_2Me_3-2,4,6)(SiMe_3)]$. Both of these complexes are orange. We found that the reaction favors **7**, however, approximately 10% of the product is **6** and could not be separated besides crystallization. Using one equivalent or slightly less than one equivalent produces **7**, however, remaining $(C_5Me_5)_2ThCl_2$ is observed which was not easily removed due to similar solubility with **7**.



Structural Analysis. Complexes **1**, Figure 4-1; **2**, Figure 4-2; **4**, Figure 4-1; **6**, Figure 4-3; and **7**, Figure 4-4, were structurally characterized using single crystal X-ray diffraction analysis. All phosphido complexes are monomeric with pseudo-tetrahedral geometry

featuring two $(C_5Me_5)^{1-}$ ligands and one or two phosphido groups. Selected bond distances and angles can be found in Table 1. All thorium-phosphorus bond distances are in the range of 2.7872(15)-2.8713(12) Å and most are within the sum of the ionic radii for a thorium-phosphorus single bond of 2.86 Å.¹⁹³ These bond lengths are typical in metallocene complexes as 2.861(7) and 2.887(8) Å are observed in $(C_5Me_5)_2Th(PPh_2)_2$ ³⁰ and 2.888(4) Å in $(C_5Me_5)_2Th(CH_3)[P(SiMe_3)_2]$.¹⁸¹ Complex **3** is isostructural with the uranium analog, $[(C_5Me_5)_2U(CH_3)(OSO_2CF_3)]_2$.¹⁹⁴

Table 4-2. Selected bond distances (Å) and angle (deg) for complexes **1**, **2**, **4-7**.

Bond distance/ angle	1, E = Cl	2, E = P	4, E = CH₃	5, E = CH₃	6, E = Cl	7, E = P
Th-P	2.8525(14)	2.7872(15)	2.8682(8)	2.8713(12)	2.8472(8)	2.8377(8)
Th-E	2.6295(14)	2.7872(15)	2.472(3)	2.473(4)	2.6297(7)	2.8376(8)
P-Th-E	104.45(4)	84.88(6)	101.81(8)	90.94(10)	91.69(2)	91.45(4)

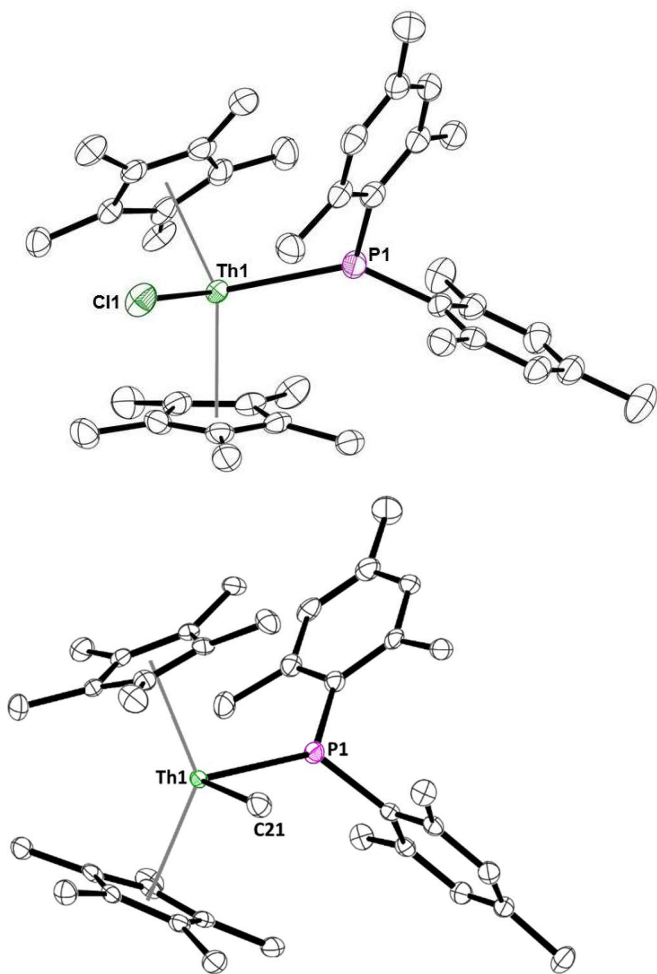


Figure 4-1. Thermal ellipsoid plots of **1** (left) and **4** (right) shown at the 50% probability level. The hydrogen atoms have been omitted for clarity.

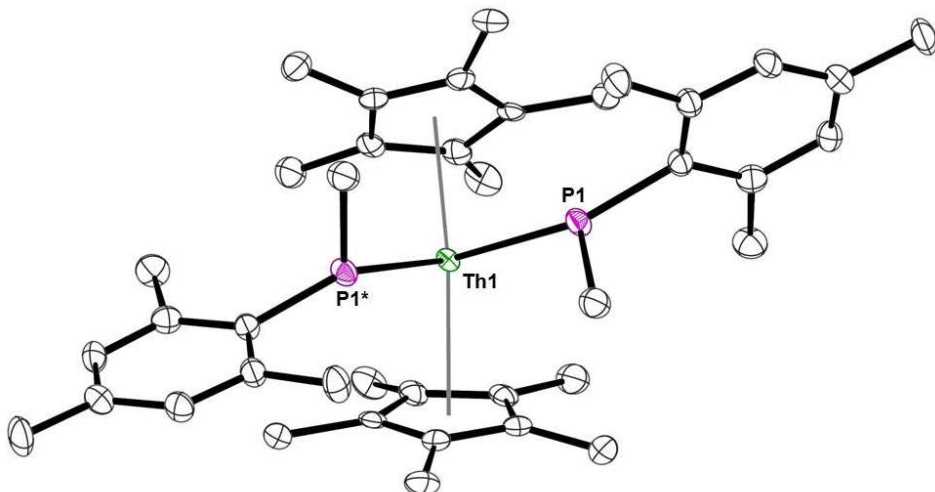


Figure 4-2. Thermal ellipsoid plot of **2** shown at the 50% probability level. The hydrogen atoms have been omitted for clarity.

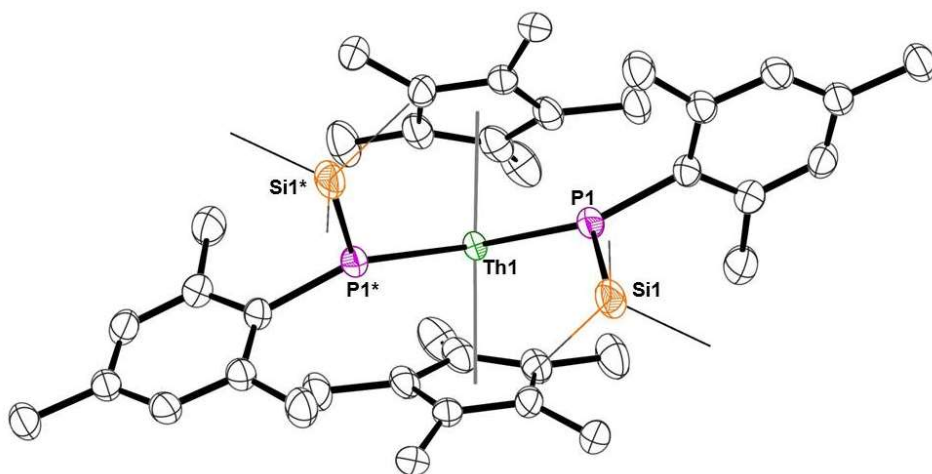


Figure 4-3. Thermal ellipsoid plot of **6** shown at the 50% probability level. The hydrogen atoms have been omitted for clarity.

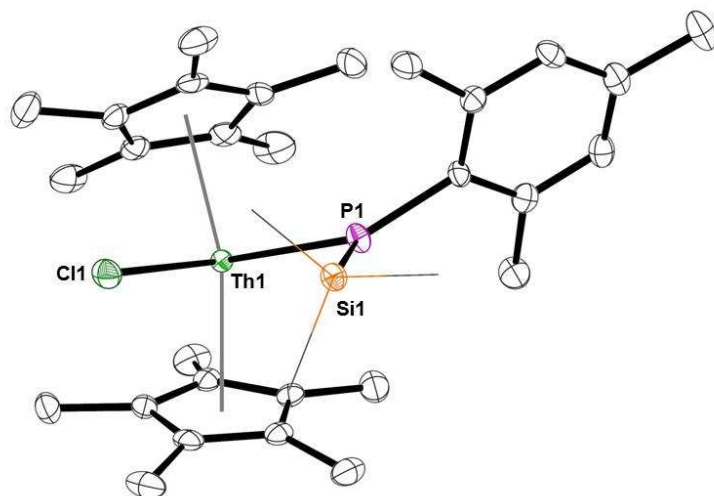


Figure 4-4. Thermal ellipsoid plot of **7** shown at the 50% probability level. The hydrogen atoms have been omitted for clarity.

Spectroscopy and TD-DFT Calculations. The ^{31}P NMR spectrum of each complex is shown in Table 2. A trend emerges from the data with more electron donating groups having shifts at lower frequency ('upfield') while the more withdrawing group are shifted to higher frequency ('downfield'). Given this trend, the ^{31}P NMR spectra of $(\text{C}_5\text{Me}_5)_2\text{Th}(\text{X})[\text{P}(\text{SiMe}_3)_2]$, $\text{X} = \text{Cl}$ and CH_3 , were reported at +109.0 and +115.2 ppm, respectively.¹⁴ We found that these resonances are -109.0 and -115.2 ppm and have been corrected in Table 2. This aligns nicely with the recently reported $(\text{Tren}^{\text{R}})\text{Th}[\text{P}(\text{SiMe}_3)_2]$, $\text{Tren} = \text{N}(\text{CH}_2\text{CH}_2\text{NR})_3$, $\text{R} = \text{DMBS} = \text{Si}^i\text{Pr}_3$, which displays a ^{31}P NMR signal at -100.09 ppm, and $\text{R} = \text{TIPS} = \text{SiMe}_2^t\text{Bu}$, at -66.45 ppm.¹⁹⁵ As the substituent on phosphorus gets more donating, from mesityl to SiMe_3 to H , then the shift is to lower frequency. For example, in comparing $(\text{C}_5\text{Me}_5)_2\text{Th}(\text{Cl})(\text{PMes}_2)$, **1**, $(\text{C}_5\text{Me}_5)_2\text{Th}(\text{Cl})[\text{P}(\text{SiMe}_3)(\text{Mes})]$, **7**, and $(\text{C}_5\text{Me}_5)_2\text{Th}(\text{Cl})[\text{P}(\text{SiMe}_3)_2]$, the ^{31}P NMR resonances move from +114.8 to +24.8 to -109.0 ppm, respectively, by changing from two to one to zero aryl groups on the

phosphido phosphorus and from zero to one to two silyl groups. This is also true of non-metallocene complexes as $(\text{Tren}^{\text{TIPS}})\text{ThPH}_2$ shows a ^{31}P NMR resonance at -144.08 ppm,¹³⁰ further upfield from the -66.45 ppm for $(\text{Tren}^{\text{TIPS}})\text{Th}[\text{P}(\text{SiMe}_3)_2]$. Additionally, $\text{Th}[\text{P}(\text{CH}_2\text{CH}_2\text{PMe}_2)]_4$ has a ^{31}P NMR resonance at 83 ppm for the phosphido phosphorus,¹⁹⁶ which fits into our general scheme of phosphido phosphorus with alkyl or aryl substituents being >75 ppm. When the phosphido phosphorus has one aryl or alkyl substituent with a more donating group such as silyl or proton, then a shift to lower frequency is observed between -50 to 50 ppm. Two silyl groups on the phosphido are typically located < -50 ppm. These trends fit with the current literature without regard to the ancillary ligand, however the ligand framework cannot be ignored. For example, $\text{bis}(\text{NHC})\text{borateTh}(\text{PHMe}_2)_2$ has a ^{31}P NMR resonance at 21.7 ppm,¹⁵² while $(\text{C}_5\text{Me}_5)_2\text{Th}(\text{PHMe}_2)_2$ is located at 15.4 ppm.

This is also reflected in the observed colors of aryl versus silyl or hydrogen-substituted phosphido ligands, Table 4-2. The electronic absorption spectroscopies of complexes 1, 2, and 4 have absorption maxima of 525-535 nm, indicating a red to violet color is observed. However, when the substituent is a hydrogen or a silyl, then absorption maxima are found 440-500 nm. This corresponds to yellow to yellow-orange coloring. Again, this fits with other substituted phosphido ligands with non-metallocene frameworks. For example, $(\text{Tren}^{\text{TIPS}})\text{ThPH}_2$ is colorless,¹³⁰ $\text{Th}[\text{P}(\text{CH}_2\text{CH}_2\text{PMe}_2)]_4$ is an intense red,¹⁹⁶ and $(\text{BIMA})_3\text{Th}(\text{PHMe}_2)$ is yellow, whilst $(\text{BIMA})_3\text{Th}(\text{PPh}_2)$, BIMA = $\text{MeC}(\text{N}^i\text{Pr})_2$, is bright orange.¹⁹⁷

Table 4-3. ^{31}P NMR resonances for metallocene thorium phosphido complexes, Mes = $\text{C}_6\text{H}_2\text{Me}_3$ -2,4,6.

Complex	^{31}P NMR Resonance (ppm)	Color	Visible Absorbance (nm)
$(\text{C}_5\text{Me}_5)_2\text{Th}(\text{Cl})[\text{P}(\text{Mes})_2]$, 1	114.8	Purple	534
$(\text{C}_5\text{Me}_5)_2\text{Th}[\text{P}(\text{Mes})(\text{CH}_3)]_2$, 2	117.5	Purple	540
$(\text{C}_5\text{Me}_5)_2\text{Th}(\text{CH}_3)[\text{P}(\text{Mes})_2]$, 4	105.3	Red-Purple	523
$(\text{C}_5\text{Me}_5)_2\text{Th}(\text{CH}_3)[\text{P}(\text{Mes})(\text{SiMe}_3)]$, 5	11.9	Orange	456
$(\text{C}_5\text{Me}_5)_2\text{Th}[\text{P}(\text{Mes})(\text{SiMe}_3)]_2$, 6	48.5	Orange	490
$(\text{C}_5\text{Me}_5)_2\text{Th}(\text{Cl})[\text{P}(\text{Mes})(\text{SiMe}_3)]$, 7	24.8	Orange	---
$(\text{C}_5\text{Me}_5)_2\text{Th}[\text{PH}(\text{Mes})_2]$	15.4	Yellow	445
$(\text{C}_5\text{Me}_5)_2\text{Th}(\text{PPh}_2)_2$	144	Purple	570, 498
$(\text{C}_5\text{Me}_5)_2\text{Th}[\text{P}(\text{CH}_2\text{CH}_3)]_2$	136	Purple	---
$(\text{C}_5\text{Me}_5)_2\text{Th}(\text{Cl})[\text{P}(\text{SiMe}_3)_2]$	-109.0*	Yellow	---
$(\text{C}_5\text{Me}_5)_2\text{Th}(\text{CH}_3)[\text{P}(\text{SiMe}_3)_2]$	-115.2*	Yellow	---

*Corrected from reference ¹⁸¹

Time-Dependent DFT calculations were performed on the complexes, $(\text{C}_5\text{Me}_5)_2\text{Th}[\text{PH}(\text{Mes})_2]$, (referred to as $\text{Th}[\text{PH}(\text{Mes})_2]$), $(\text{C}_5\text{Me}_5)_2\text{Th}(\text{Cl})(\text{PMes}_2)$, **1**, $(\text{C}_5\text{Me}_5)_2\text{Th}[\text{P}(\text{CH}_3)(\text{Mes})_2]$, **2**, $(\text{C}_5\text{Me}_5)_2\text{Th}(\text{CH}_3)[\text{P}(\text{Mes})(\text{SiMe}_3)]$, **5**, and $(\text{C}_5\text{Me}_5)_2\text{Th}[\text{P}(\text{SiMe}_3)(\text{Mes})_2]$, **6**, to explore their electronic structure. The thorium-ligand bond lengths, as well as nearest neighbor atom bond lengths, and Cp – Cp plane angles are reproduced well in the optimized geometries. An overview of the electronic structure of the complexes is detailed in the molecular orbital (MO) diagram of Figure 4-5. The MO levels correspond to the energy scale on the left and inlaid for all complexes are

isosurfaces (± 0.03 atomic units) of the highest occupied MO (HOMO) and lowest unoccupied MO (LUMO).

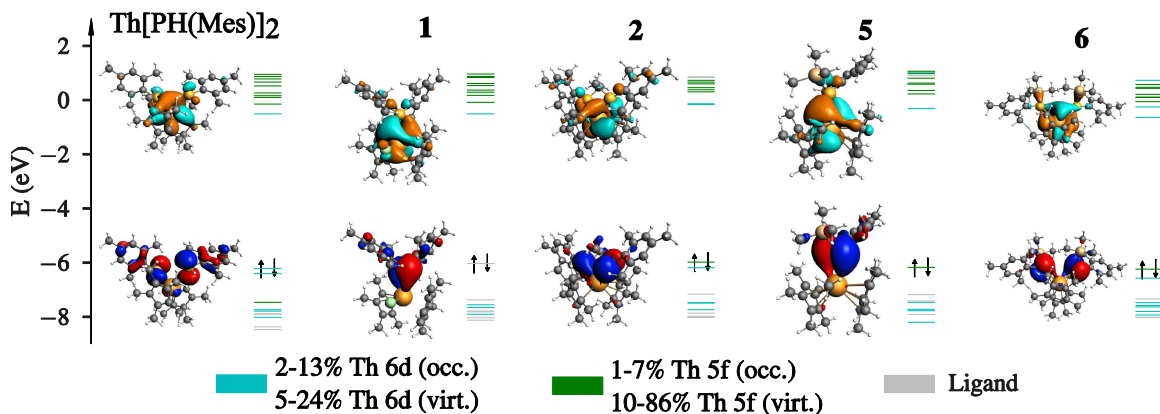


Figure 4-5. Molecular orbital (MO) diagram of related thorium complexes. 6d and 5f indicate at least 5% total thorium character in the molecular orbital with the larger contribution taking precedent in the coloring scheme. Ligand denotes less than 5% thorium character. Isosurfaces (± 0.03 au) of LUMO (above) and HOMO (below).

The HOMO for all complexes is dominantly phosphorus 3p with very little Th mixing. In the case of all the phosphido complexes, the HOMO-1 is of similar character. The doubly substituted phosphidos exhibit larger 5f contribution in the HOMO whereas the primary substituted phosphido shows larger 6d contribution in the HOMO. In the case of direct Cl ligation, Th mixing is negligible. Below the HOMO, there are numerous delocalized Cp and mesityl π orbitals. For all complexes, the LUMO is primarily Th 6d in character, with orbitals above the LUMO consisting heavily of significant mixes of Th 5f, 6d and 7s.

Absorption spectra were simulated with a range-separated exchange functional due to the significant charge transfer character of the transitions of interest. Theoretical spectra were generated by Gaussian broadening (full-width-half-max of 0.06 eV) of excitation energies weighted by their corresponding oscillator strengths. A comparison of experimental and theoretical absorption spectra of $(C_5Me_5)_2Th[PH(Mes)]_2$ and **2** can be seen in Figure 4-6. The overall agreement of energies and peak intensities between the experimental and theoretical spectra is good. To inspect further the nature of the features seen in the experimental spectra, natural transition orbitals (NTOs) were computed and analyzed for all complexes. Given the similarity of the complexes, it is not surprising to see the same theme across the series. The shape of all occupied NTOs is that of phosphorus 3p orbitals. For the virtual NTOs, the lowest energy excitations are identifiable as 6d in nature. For the higher energy excitations, there is subtle competition between 6d and 5f character, making a clear identification in some cases difficult. The picture that emerges is that the absorbance spectra of these Th complexes are largely dominated by ligand-to-metal charge transfer (LMCT) excitations from P to Th. Substitution on P with electron donating (withdrawing) groups destabilizes (stabilizes) the phosphorus 3p orbitals, lowering (rising) the energy difference for LMCT transitions, resulting in a red-shift (blue-shift) of the absorbance spectrum. The observation that stronger electron-donating substituents on phosphorus lead to downfield ^{31}P NMR signals, i.e. these P nuclei are *less* shielded, is not in contradiction with this analysis. Most likely, the electron donation leads to an increase of negative paramagnetic contributions to the ^{31}P isotropic nuclear magnetic shielding, similar to organic molecules that were analyzed recently.¹⁹⁸

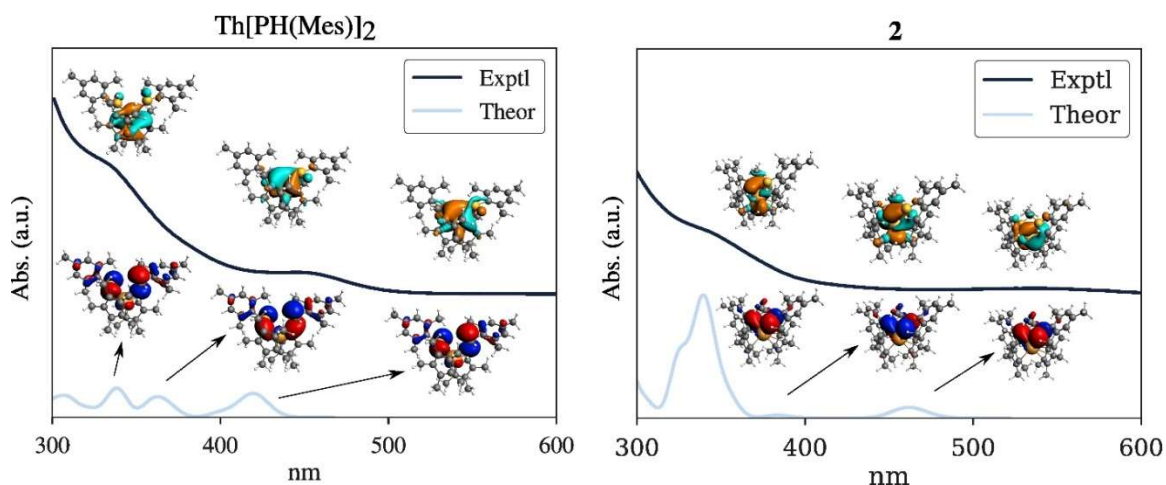


Figure 4-6. Comparison of experimental and theoretical absorption spectra for $(C_5Me_5)_2Th[PH(Mes)]_2$ and $(C_5Me_5)_2Th[P(Mes)(CH_3)]_2$, **2**. Observable features of the experimental spectra are reproduced well by the calculations. Inlaid on the spectra are isosurfaces (± 0.03 au) of natural transition orbitals (NTOs) positioned to correspond to the spectral features observed.

Conclusion

The synthesis of new thorium-phosphido complexes, $(C_5Me_5)_2ThX[P(Mes)R]$, has been conducted to understand the origin of colors which are produced when the other substituent on phosphorus, $R = H, Me, Mes,$ and $SiMe_3$, is varied. Whether $X =$ another phosphido ligand or chloride or methyl, does not change the electronic structure significantly, and the phosphido ligand seems to control that aspect of the molecule. A ligand to metal charge transfer (LMCT) from the 3p of phosphorus to the thorium, either 5f or 6d or a hybrid, is responsible for the different hues based on the time-dependent density functional theory calculations. Due to the similar energetics of the 5f and 6d orbitals, the exact orbital cannot be definitively determined. The differences in structure

and bonding are supported by the ^{31}P NMR and UV-vis spectra which indicate the trend of increasing donating strength of $\text{Mes} < \text{Me} < \text{SiMe}_3 < \text{H}$, which leads to increasing frequency in the UV-vis and ^{31}P NMR spectra. Resonances at 114.8, 117.5, 48.5 and 15.4 ppm were observed for the mesityl, methyl, silyl, and proton substituents, respectively. The difference in mesityl and methyl is likely due to a mono(phosphido) versus bis(phosphido) ligated complex as a direct comparison could not be made since we were unsuccessful in making $(\text{C}_5\text{Me}_5)_2\text{Th}[\text{P}(\text{Mes}_2)]_2$. We have further correlated our data with other phosphido complexes, showing that trend exists beyond metallocene compounds. Overall, we have shown that organothorium phosphido complexes can have unique electronic structures based simply on the thorium-phosphorus bond and the substituents coordinated to phosphorus.

Appendix A: Copper(I) Clusters with Bulky Dithiocarboxylate, Thiolate, and Selenolate Ligands²

Introduction

Copper has attracted attention due to its photochemical,¹⁹⁹ catalytic,²⁰⁰⁻²⁰¹ and anti-microbial properties,²⁰² as well as cytotoxicity.²⁰³ In nature, copper mainly occurs in the +1 and +2 oxidation states, and it is well known that copper(I) prefers to coordinate to soft donor ligands. Thus, the coordination chemistry of copper in nature is mainly dominated by amino acids such as histidine, cysteine, and methionine or ligands containing soft donor atoms such as sulfur.²⁰⁴ A variety of coordination numbers exist, ranging from two to five, and are predominantly linear, trigonal planar or tetrahedral geometries are observed. Copper-transporting proteins, such as eukaryote Atx1, are flexible in nature and feature copper in coordination numbers of two or three,²⁰⁵ while CusA a protein that is essential in bacteria for copper resistance,²⁰⁶ was found to contain one Cu(I) in a trigonal planar geometry, Figure A-1.

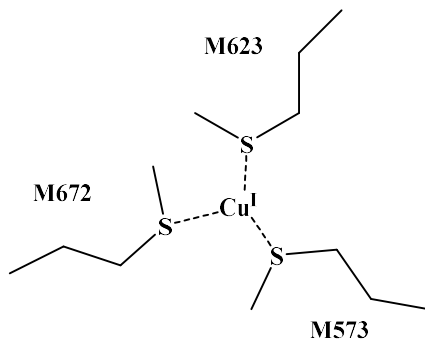


Figure A-1. Active site of CusA is shown.

² A version of this chapter has been published: Dalton Trans., 2016, 45, 14265-14276.

The enforcement of low coordination numbers can be achieved by having a ligand with large steric demand. The terphenyl-based ligand frameworks, Figure A-2, can provide such steric properties. Several derivatives of terphenyl ligands with nearly every main group element have been synthesized. Our interest was to use dithiocarboxylate, thiolate, and selenolate derivatives to produce copper(I) complexes to model the active site of copper-containing enzymes with linear, trigonal planar, or tetrahedral coordination geometries. We have previously used amidinate ligands to examine the dinuclear copper Cu_A site²⁰⁷ and used the insertion of carbon disulfide into copper-nitrogen bonds to produce polymetallic clusters and control the number of metal ions using the steric properties of the amidinate ligand. Herein, we report the synthesis and characterization of a series of copper complexes with coordination numbers of two, three, and four with linear, trigonal planar and tetrahedral geometries using sulfur and selenium-based terphenyl ligands.

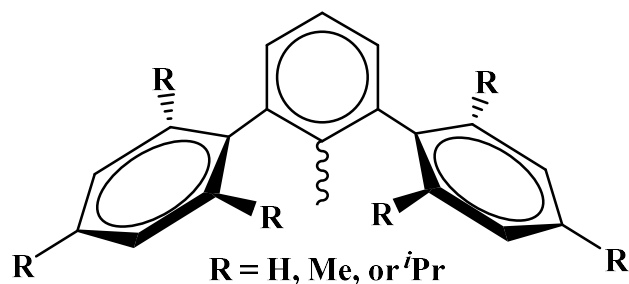


Figure A-2. General drawing of the terphenyl ligands used in this manuscript.

Experimental

General Considerations. All syntheses were carried out under a dry N_2 atmosphere using standard glovebox and Schlenk line techniques. Organic solvents were obtained from Acros and Sigma Aldrich and dried by standard procedures. Potassium *tert*-butoxide

(Fisher), $[\text{Cu}(\text{NCCH}_3)_4]\text{PF}_6$ and 10% wt. triethylphosphine (PEt_3) in hexane (Strem), potassium *bis*(trimethylsilyl)amide, carbon disulfide, and 2.5 M *n*-butyllithium (Aldrich) were purchased. $\text{Cu}_2[(2,6\text{-}(\text{Mes})_2\text{C}_6\text{H}_3)]_2$,²⁰⁸ $(\text{Et}_2\text{O})_2\text{Li}[\text{CS}_2(2,6\text{-}(\text{Mes})_2\text{C}_6\text{H}_3)]$,²⁰⁹ $(\text{THF})_2\text{Li}[\text{CS}_2(2,6\text{-}(\text{Trip})_2\text{C}_6\text{H}_3)]$,²⁰⁹ $\text{HS}(2,6\text{-}(\text{Mes})_2\text{C}_6\text{H}_3)$,²¹⁰ $\text{HSe}(2,6\text{-}(\text{Mes})_2\text{C}_6\text{H}_3)$,²¹¹ $[\text{CuI}(\text{PEt}_3)]_4$,²¹² $\text{K}[\text{S}(2,6\text{-}(\text{Trip})_2\text{C}_6\text{H}_3)]$,²¹⁰ $\text{K}[\text{Se}(2,6\text{-}(\text{Trip})_2\text{C}_6\text{H}_3)]$,²¹³ 2,6-(Ph)₂C₆H₃I (Ph = C₆H₅),²¹⁴ and $\text{Cu}_3[(2,6\text{-}(\text{Ph})_2\text{C}_6\text{H}_3)]_3$ ²⁰⁸ were prepared as previously described. $\text{K}[\text{Se}(2,6\text{-}(\text{Mes})_2\text{C}_6\text{H}_3)]$ and $\text{K}[\text{S}(2,6\text{-}(\text{Mes})_2\text{C}_6\text{H}_3)]$ were made from the following procedure: $\text{K}[\text{S}(2,6\text{-}(\text{Mes})_2\text{C}_6\text{H}_3)]$ was generated from $\text{HS}(2,6\text{-}(\text{Mes})_2\text{C}_6\text{H}_3)$ and potassium *tert*-butoxide. The reaction was done in THF at room temperature for 1 hour, followed by removal of solvent *in vacuo* to yield solid $\text{K}[\text{S}(2,6\text{-}(\text{Mes})_2\text{C}_6\text{H}_3)]$. $\text{K}[\text{Se}(2,6\text{-}(\text{Mes})_2\text{C}_6\text{H}_3)]$ was generated from $\text{HSe}(2,6\text{-}(\text{Mes})_2\text{C}_6\text{H}_3)$ and potassium *bis*(trimethylsilyl)amide in toluene. Solid $\text{K}[\text{Se}(2,6\text{-}(\text{Mes})_2\text{C}_6\text{H}_3)]$ was separated from solution by centrifugation and dried *in vacuo*. Acetonitrile-*d*₃ and benzene-*d*₆ (Cambridge Isotope Laboratories) were dried over molecular sieves and degassed with three freeze–evacuate–thaw cycles. All ¹H and ¹³C NMR data were obtained from 500 MHz and 600 MHz DRX Bruker spectrometer. All ⁷⁷Se and ⁷Li NMR data were obtained from 300 MHz DRX Bruker spectrometer. All ³¹P NMR data were obtained from 250 MHz and 300 MHz DRX Bruker spectrometer. ¹H NMR shifts given were referenced internally to the residual solvent peaks at δ 7.16 ppm for C₆D₅H and 7.26 ppm for CHCl₃. All ³¹P NMR shifts given were referenced externally to 85% H₃PO₄ at 0 ppm. All ⁷⁷Se NMR shifts given were referenced externally to diphenyldiselenide in CDCl₃ at 463 ppm. All ⁷Li NMR shifts given were referenced externally to 1 M solution of LiCl in D₂O at 0 ppm. Infrared spectra were recorded as KBr pellets on Perkin-Elmer Spectrum One FT-

IR spectrometer. UV-Vis spectra were recorded on a Varian CARY 100 Bio spectrophotometer. Elemental analyses were performed by Atlantic Microlabs, Inc. (Norcross, GA).

Synthesis of $\text{Cu}_4[\text{S}_2\text{C}(\text{2,6-(Mes)}_2\text{C}_6\text{H}_3)]_4$, **1.** In a 20 mL scintillation vial, 2.5 mL of THF was added to $[\text{Cu}(\text{CH}_3\text{CN})_4]\text{PF}_6$ (68 mg, 0.18 mmol) followed by 7.5 mL of $(\text{Et}_2\text{O})_2\text{Li}[\text{CS}_2(\text{2,6-(Mes)}_2\text{C}_6\text{H}_3)]$ (100 mg, 0.18 mmol) in THF to yield a dark brown colored solution. The mixture was stirred at room temperature overnight after which the solvent was removed *in vacuo*. The brown solid was extracted with toluene then filtered through Celite and the solvent was removed *in vacuo* to yield a brown powder (60 mg, 72%). X-ray quality crystals were obtained from a concentrated THF solution at $-24\text{ }^\circ\text{C}$. ^1H NMR (600 MHz, C_6D_6): δ 2.16 (s, 24H, *p*-Mes), 2.21 (s, 48H, *o*-Mes), 6.83 (s, 16H, *m*-Mes), 6.89 (d, 8H, $^3J_{\text{H-H}} = 7.2\text{ Hz}$, *m*- C_6H_3), 7.07 (t, 4H, $^3J_{\text{H-H}} = 7.2\text{ Hz}$, *p*- C_6H_3). $^{13}\text{C}\{^1\text{H}\}$ NMR (C_6D_6): δ 21.4, 21.5, 128.3, 129.3, 129.6, 136.5, 137.1, 137.2, 137.9, 145.5, 229.2. IR (KBr, cm^{-1}): 2956 (m), 2917 (s), 2855 (w), 1611 (w), 1567 (w), 1449 (s), 1376 (w), 1263 (w), 1099 (s), 1018 (vs), 885 (w), 849 (s), 806 (w), 758 (w), 737 (w), 580 (w), 470 (w). Anal. Calcd for $\text{C}_{104}\text{H}_{110}\text{Cu}_4\text{S}_8$: C, 66.77; H, 5.93. Found: C, 66.73; H, 5.87.

Synthesis of $\text{Cu}_2[\text{S}_2\text{C}(\text{2,6-(Trip)}_2\text{C}_6\text{H}_3)]_2(\text{NCCH}_3)$, **2.** The synthesis was carried out in a similar manner to $\text{Cu}_4[\text{S}_2\text{C}(\text{2,6-(Mes)}_2\text{C}_6\text{H}_3)]_4$ with $[\text{Cu}(\text{CH}_3\text{CN})_4]\text{PF}_6$ (65 mg, 0.17 mmol) and $(\text{THF})_2\text{Li}[\text{CS}_2(\text{2,6-(Trip)}_2\text{C}_6\text{H}_3)]$ (100 mg, 0.14 mmol) to yield an orange solid. The crude product was dissolved in acetonitrile, filtered through Celite, and allowed to evaporate at room temperature outside of the glovebox to yield a small amount of $\text{Cu}_2[\text{S}_2\text{C}(\text{2,6-(Trip)}_2\text{C}_6\text{H}_3)]_2(\text{NCCH}_3)$ crystals.

Synthesis of $\text{Cu}_2[\text{S}_2\text{C}(2,6\text{-(Mes)}_2\text{C}_6\text{H}_3)]_2(\text{PEt}_3)_2$, **3.** In a 20 mL scintillation vial, 5 mL of THF was added to of $(\text{Et}_2\text{O})_2\text{Li}[\text{CS}_2(2,6\text{-(Mes)}_2\text{C}_6\text{H}_3)]$ (100 mg, 0.18 mmol) followed by 5 mL of $[\text{CuI}(\text{PEt}_3)]_4$ (57 mg, 0.046 mmol) in THF to yield a deep red solution. The mixture was stirred at room temperature overnight, after which the solvent was removed *in vacuo*. The deep red solid was extracted with hexanes the filtered through Celite and the solvent was removed *in vacuo* to yield deep red powder (101 mg, 96%). X-ray quality crystals were obtained from a concentrated hexanes solution at $-24\text{ }^\circ\text{C}$. ^1H NMR (500 MHz, C_6D_6): 0.83 - 0.9 (m, 18H, $\text{P}(\text{CH}_2\text{CH}_3)_3$), 1.02 - 1.05 (m, 12H, $\text{P}(\text{CH}_2\text{CH}_3)_3$), 2.29 (s, 12H, *p*-Mes), 2.43 (s, 24H, *o*-Mes), 6.85 (s, 8H, *m*-Mes), 6.92 (d, 4H, $^3J_{\text{H-H}} = 7.5\text{ Hz}$, *m*- C_6H_3), 7.11 (t, 2H, $^3J_{\text{H-H}} = 7.5\text{ Hz}$, *p*- C_6H_3). $^{13}\text{C}\{^1\text{H}\}$ NMR (C_6D_6): 8.7, 17.1 (d, $^1J_{\text{C-P}} = 15\text{ Hz}$), 21.5, 22.2, 127.5, 128.4, 129.3, 135.8, 137.1, 137.8, 139.5, 149.8, 246.8. $^{31}\text{P}\{^1\text{H}\}$ NMR (C_6D_6 , 300 K): δ -8.97. IR (KBr, cm^{-1}): 2962 (vs), 2913 (vs), 2877 (s), 2729 (w), 1610 (w), 1570 (w), 1453 (s), 1376 (m), 1260 (w), 1220 (w), 1180 (w), 1158 (w), 1095 (w), 1019 (vs), 907 (m), 848 (m), 805 (w), 753 (m), 694 (w), 622 (w), 581 (w). Anal. Calcd for $\text{C}_{62}\text{H}_{80}\text{Cu}_2\text{P}_2\text{S}_4$: C, 65.17; H, 7.06. Found: C, 65.26; H, 7.33.

Synthesis of $\text{Cu}[\text{S}_2\text{C}(2,6\text{-(Mes)}_2\text{C}_6\text{H}_3)](\text{PEt}_3)_2$, **4.** In a 20 mL scintillation vial, 5 mL of toluene was added to $[\text{CuI}(\text{PEt}_3)]_4$ (57 mg, 0.046 mmol) followed by 10% wt. PEt_3 in hexane (217 mg, 0.18 mmol). The solution was then added to a suspension of $(\text{Et}_2\text{O})_2\text{Li}[\text{CS}_2(2,6\text{-(Mes)}_2\text{C}_6\text{H}_3)]$ (100 mg, 0.18 mmol) in toluene. The mixture was stirred at room temperature overnight after which the solution was filtered through Celite and the solvent was removed *in vacuo* to yield orange powder (61 mg, 48%). X-ray quality crystals were obtained from a concentrated toluene solution at $-24\text{ }^\circ\text{C}$. ^1H NMR (600 MHz, C_6D_6): δ 0.81 - 0.86 (m, 18H, $\text{P}(\text{CH}_2\text{CH}_3)_3$), 1.07 - 1.11 (m, 12H,

P(CH₂CH₃)₃), 2.26 (s, 6H, *p*-Mes), 2.54 (s, 12H, *o*-Mes), 6.88 (s, 4H, *m*-Mes), 6.98 (d, 2H, ³J_{H-H} = 7.2Hz, *m*-C₆H₃), 7.15 (t, 1H, ³J_{H-H} = 7.2Hz, *p*-C₆H₃). ¹³C{¹H} NMR (C₆D₆): 8.6, 17.2 (t, ¹J_{C-P} = 8.4 Hz), 21.4, 22.2, 127.1, 127.9, 129.1 135.5, 137.4, 137.7, 139.8, 150.8, 251.7. ³¹P{¹H} NMR (C₆D₆, 300 K): δ -7.01. IR (KBr, cm⁻¹): 3035 (m), 3005 (m), 2957 (vs), 2911 (vs), 2877 (vs), 2727 (w), 1607 (w), 1568 (w), 1483 (w), 1452 (s), 1411 (m), 1374 (s), 1247 (w), 1219 (w), 1180 (w), 1096 (w), 1013 (br-vs), 923 (m), 854 (m), 804 (w), 773 (vs), 749 (vs), 703 (m), 675 (m), 636 (m), 582 (w), 526 (w). Anal. Calcd for C₃₇H₅₅Cu₁P₂S₂: C, 64.46; H, 8.04. Found: C, 64.70; H, 7.92.

Synthesis of Cu[S₂C(2,6-(Trip)₂C₆H₃)](PEt₃)₂, 5. The synthesis was carried out in a similar manner to Cu[S₂C(2,6-(Mes)₂C₆H₃)](PEt₃)₂ with (THF)₂Li[CS₂(2,6-(Trip)₂C₆H₃)] (100 mg, 0.14 mmol), [CuI(PEt₃)₄] (43 mg, 0.04 mmol), and 10% wt. PEt₃ in hexane (166.5 mg, 0.14 mmol) to yield an orange powder of Cu[S₂C(2,6-(Trip)₂C₆H₃)](PEt₃)₂ (53 mg, 44%). X-ray quality crystals were obtained from a concentrated hexanes solution at -24 °C. ¹H NMR (600 MHz, C₆D₆): δ 0.8 - 0.9 (m, 18H, P(CH₂CH₃)₃), 1.06 - 1.12 (m, 12H, P(CH₂CH₃)₃), 1.21 (d, 12H, ³J_{H-H} = 7.2 Hz, *o*-CH(CH₃)₂), 1.34 (d, 12H, ³J_{H-H} = 7.2 Hz, *p*-CH(CH₃)₂), 1.59 (d, 12H, ³J_{H-H} = 7.2 Hz, *o*-CH(CH₃)₂), 2.92 (sept, 2H, ³J_{H-H} = 7.2 Hz, *p*-CH(CH₃)₂), 3.44 (sept, 4H, ³J_{H-H} = 7.2 Hz, *o*-CH(CH₃)₂), 7.08 (t, 1H, ³J_{H-H} = 7.5 Hz, *p*-C₆H₃), 7.19 (d, 2H, ³J_{H-H} = 7.5 Hz, *m*-C₆H₃), 7.21 (s, 4H, *m*-Trip). ¹³C{¹H} NMR (C₆D₆): δ 8.7, 17.3 (dd, ¹J_{C-P} = 8.6 Hz, ²J_{C-P} = 8.4 Hz), 23.4, 23.5, 26.6, 31.6, 34.7, 120.4, 124.6, 130.8, 135.8, 137.6, 147.3, 148.1, 150.1, 251.4. ³¹P{¹H} NMR (C₆D₆, 300 K): δ -7.61. IR (KBr, cm⁻¹): 3050 (m), 2929 (vs), 2962 (vs), 2869 (vs), 1604 (m), 1566 (w), 1458 (s), 1419 (m), 1479 (m), 1360 (m), 1316 (w), 1258 (w), 1166 (w), 1101 (m), 1026

(s), 931 (w), 874 (m), 802 (w), 764 (s), 712 (w), 651 (w), 627 (w), 464 (w), 432 (w), 408 (w). Anal. Calcd for $C_{49}H_{79}Cu_1P_2S_2$: C, 68.61; H, 9.28. Found: C, 68.32; H, 9.30.

Synthesis of $(Et_2O)_2Li[CS_2(2,6-(Ph)_2C_6H_3)]$, 6. In a Schlenk flask, 20 mL of *n*-hexane and 20 mL of diethylether was added to 2,6-(Ph)₂C₆H₃I (1.0 g, 2.8 mmol). On the Schlenk line, the flask was cooled to 0 °C in an ice bath. 2.5 M *n*-butyllithium (1.2 mL, 3 mmol) was added via syringe. Formation of white precipitate was observed immediately. The flask was allowed to stir at 0 °C for an hour. Ice bath was removed and replaced with a dry ice acetone bath. Once the solution reached -70 °C, carbon disulfide (0.2 mL, 3.3 mmol) was added via syringe. The flask was then allowed to stir in dry ice/ acetone bath overnight. The resulting orange suspension in light orange liquid was dried under vacuum and brought into N₂ glovebox. The residue was partially dissolved in a 1:1 ratio of *n*-hexane and diethyl ether and transferred a 20 mL scintillation vial. The content in the scintillation vial was concentrated and cooled to -24°C overnight. The product was isolated as an orange powder which was with *n*-hexane and dried under vacuum (859 mg, 66% yield). X-ray quality crystals were obtained from concentrated a *n*-hexane/ diethyl ether solution at -24 °C. ¹H NMR (600 MHz, C₆D₆): δ 0.92 (t, 12H, O(CH₂CH₃)₂), 3.12 (q, 8H, O(CH₂CH₃)₂), 7.10 (t, 1H, ³J_{H-H} = 7.8 Hz, *p*-C₆H₃), 7.10 - 7.13 (m, 2H, *p*-Ph), 7.17-7.20 (m, 4H, *m*-Ph), 7.24 (d, 2H, ³J_{H-H} = 7.8 Hz, *m*-C₆H₃), 7.94 - 7.95 (m, 4H, *o*-Ph). ¹³C{¹H} NMR (C₆D₆): δ 15.0, 65.9, 125.9, 126.3, 127.5, 130.0, 130.5, 136.7, 143.6, 154.9, 259.9. ⁷Li{¹H} NMR (C₆D₆, 297K): -0.17. IR (KBr, cm⁻¹): 3054 (m), 3027 (w), 2974 (s), 2931 (m), 2884 (m), 1597 (w), 1494 (m), 1439 (m), 1385 (m), 1221 (w), 1178 (w), 1154 (w), 1091 (s), 1065 (s), 1021 (vs), 999 (s), 967 (w), 914 (m), 776 (s), 759 (vs),

698 (vs), 613 (m), 530 (w). Anal. Calcd for C₂₇H₃₃LiO₁; C, 70.40; H, 7.22. Found: C, 70.42; H, 7.09.

Synthesis of Cu[S₂C(2,6-(Ph)₂C₆H₃)](PEt₃)₂, 7. The synthesis was carried out in a similar manner to Cu[S₂C(2,6-(Mes)₂C₆H₃)](PEt₃)₂ with (Et₂O)₂Li[CS₂(2,6-(Ph)₂C₆H₃)] (100 mg, 0.22 mmol), [CuI(PEt₃)₄] (67 mg, 0.05 mmol), and 10% wt. PEt₃ in hexane (257 mg, 0.22 mmol) to yield an orange powder of Cu[S₂C(2,6-(Ph)₂C₆H₃)](PEt₃)₂ (66 mg, 50%). X-ray quality crystals were obtained from a concentrated *n*-hexane solution at -24 °C. ¹H NMR (600 MHz, C₆D₆): δ 0.83 (s, 18H, P(CH₂CH₃)₃), 1.12 (q, 12H, P(CH₂CH₃)₃), 7.06 (t, 1H, ³J_{H-H} = 7.2 Hz, *p*-C₆H₃), 7.07-7.17 (m, 2H, *p*-Ph), 7.17 (d, 2H, ³J_{H-H} = 7.2 Hz, *m*-C₆H₃), 7.20 – 7.22 (m, 4H, *m*-Ph), 7.91 – 7.92 (m, 4H, *o*-Ph). ¹³C{¹H} NMR (C₆D₆): δ 8.5, 17.2, 125.9, 126.3, 127.4, 130.1, 130.9, 138.4, 143.8, 151.6, 251.9. ³¹P{¹H} NMR (C₆D₆, 300K): -7.73. IR (KBr, cm⁻¹): 3053 (w), 3025 (w), 2960 (s), 2978 (s), 2901 (s), 2872 (s), 2820 (w), 1598 (w), 1572 (w), 1492 (w), 1451 (s), 1416 (m), 1375 (m), 1251 (w), 1232(w), 1178 (w), 1153 (w), 1094 (w), 1024 (vs), 926 (m), 839 (w), 802 (w), 757 (vs), 694 (vs), 615 (m), 532 (m). Anal. Calcd for C₃₁H₄₃Cu₁S₂P₂; C, 61.51; H, 7.16. Found: C, 61.07; H, 7.10.

Synthesis of Cu[(2,6-(Mes)₂C₆H₃)](PEt₃)₂, 8. In a 20 mL scintillation vial, 5 mL of hexanes was added to Cu₂[(2,6-(Mes)₂C₆H₃)]₂ (43 mg, 0.057 mmol) followed by 0.1 mL of 10% wt. PEt₃ in hexane. The mixture was stirred at room temperature overnight, after which the solution was filtered through Celite and the solvent was removed *in vacuo* to yield a white powder (44 mg, 78%). X-ray quality crystals were obtained from a concentrated hexanes solution at -24 °C. ¹H NMR (600 MHz, C₆D₆): δ 0.48 (dt, 9H, ³J_{H-P} = 16.8 Hz, ³J_{H-H} = 7.8 Hz, P(CH₂CH₃)₃), 0.61 - 0.66 (m, 6H, P(CH₂CH₃)₃), 2.29 (s, 6H,

p-Mes), 2.40 (s, 12H, *o*-Mes), 6.93 (s, 4H, *m*-Mes), 7.22 (d, 2H, $^3J_{H-H} = 7.8$ Hz, *m*-C₆H₃), 7.42 (t, 1H, $^3J_{H-H} = 7.8$ Hz, *p*-C₆H₃). $^{13}\text{C}\{^1\text{H}\}$ NMR (C₆D₆, 298K): 8.7 (d, $^2J_{C-P} = 2.4$ Hz), 16.3 (d, $^1J_{C-P} = 21.9$ Hz), 21.2, 22.1, 124.3, 125.7, 128.0, 134.2, 136.2, 147.4, 151.0, 169.3. $^{31}\text{P}\{^1\text{H}\}$ NMR (C₆D₆, 300 K): δ -2.87. IR (KBr, cm⁻¹): 3027 (m), 2963 (vs), 2933 (vs), 2909 (vs), 2725 (w), 1607 (m), 1544 (m), 1446 (s), 1374 (m), 1233 (m), 1163 (w), 1077 (m), 1034 (s), 850 (m), 796 (m), 762 (m), 729 (m), 579 (w), 548 (w). Anal. Calcd for C₃₀H₄₀Cu₁P₂: C, 72.77; H, 8.14. Found: C, 72.10; H, 8.22.

Synthesis of Cu[(2,6-(Ph)₂C₆H₃)](PEt₃)₂, 9. The synthesis was carried out in a similar manner to Cu[(2,6-(Mes)₂C₆H₃)](PEt₃) with Cu₃[(2,6-(Ph)₂C₆H₃)]₃ (77 mg, 0.09 mmol) and 10% wt. PEt₃ in hexane (313 mg, 0.26 mmol) to yield a light yellow powder of Cu[(2,6-(Ph)₂C₆H₃)](PEt₃)₂ (82 mg, 59%). X-ray quality crystals were obtained from a concentrated *n*-hexane solution at -24 °C. ^1H NMR (600 MHz, C₆D₆): δ 0.74 (dt, 18H, P(CH₂CH₃)₃, $^3J_{H-P} = 15$ Hz, $^3J_{H-H} = 7.8$ Hz), 0.99-1.02 (m, 12H, P(CH₂CH₃)₃), 7.05-7.20 (m, 2H, *p*-Ph), 7.29-7.31 (m, 4H, *m*-Ph), 7.42 (t, 1H, $^3J_{H-H} = 7.8$ Hz, *p*-C₆H₃), 7.72 (d, 2H, $^3J_{H-H} = 7.8$ Hz, *m*-C₆H₃), 7.96-7.97 (m, 4H, *o*-Ph). $^{13}\text{C}\{^1\text{H}\}$ NMR (C₆D₆): 8.5 (d, $^2J_{C-P} = 4.5$ Hz), 17.4 (d, $^2J_{C-P} = 10.5$ Hz), 124.6, 125.0, 125.1, 128.4, 128.5, 150.9, 152.3, 177.4. $^{31}\text{P}\{^1\text{H}\}$ NMR (C₆D₆, 297K): -14.49. IR (KBr, cm⁻¹): 3073 (m), 3053 (m), 3018 (m), 2962 (s), 2932 (s), 2898 (s), 2873 (s), 2813 (w), 2726 (w), 1593 (m), 1573 (w), 1559 (w), 1490 (m), 1457 (s), 1442 (m), 1430 (m), 1412 (s), 1376 (m), 1285 (w), 1276 (w), 1236 (m), 1154 (w), 1089 (w), 1068 (w), 1026 (s), 903 (w), 798 (w), 751 (vs), 721 (s), 698 (vs), 613 (m), 554 (m), 500 (w), 419 (w). Anal. Calcd for C₃₀H₄₃Cu₁P₂: C, 68.09; H, 8.19. Found: C, 67.96; H, 8.04.

Synthesis of $\text{Cu}_3[\text{S}(\text{2,6-(Mes)}_2\text{C}_6\text{H}_3)]_3$, **10.** In a 20 mL scintillation vial, 5 mL of THF was added to $[\text{Cu}(\text{CH}_3\text{CN})_4]\text{PF}_6$ (81 mg, 0.22 mmol) followed by 5 mL of $\text{K}[\text{S}(\text{2,6-(Mes)}_2\text{C}_6\text{H}_3)]$ (84 mg, 0.22 mmol) in THF to yield a colorless solution. The mixture was stirred at room temperature overnight, after which the solvent was removed *in vacuo*. The white solid was extracted with toluene then filtered through Celite and the solvent was removed *in vacuo* to yield white powder in nearly quantitative yield. X-ray quality crystals were obtained from a concentrated toluene/acetonitrile solution at room temperature. ^1H NMR (500 MHz, C_6D_6): δ 2.06 (s, 36H, *o*-Mes), 2.24 (s, 18H, *p*-Mes), 6.74 (d, 6H, $^3J_{\text{H-H}} = 7.5$ Hz, *m*- C_6H_3), 6.82 (s, 12H, *m*-Mes), 6.91 (t, 3H, $^3J_{\text{H-H}} = 7.5$ Hz, *p*- C_6H_3). $^{13}\text{C}\{^1\text{H}\}$ NMR (C_6D_6): δ 21.3, 21.7, 125.9, 129.1, 129.7, 135.3, 135.9, 136.7, 139.8, 144.4. IR (KBr, cm^{-1}): 3031 (m), 2968 (s), 2913 (vs), 2853 (s), 2727 (w), 1609 (s), 1569 (m), 1481 (m), 1445 (vs), 1388 (s), 1375 (s), 1113 (w), 1090 (w), 1036 (s), 850 (vs), 798 (s), 771 (w), 741 (vs), 589 (m), 547 (w), 465 (w). Anal. Calcd for $\text{C}_{72}\text{H}_{75}\text{Cu}_3\text{S}_3$: C, 70.47; H, 6.16. Found: C, 70.42; H, 6.10.

Synthesis of $\text{Cu}_3[\text{Se}(\text{2,6-(Mes)}_2\text{C}_6\text{H}_3)]_3$, **11.** The synthesis was carried out in a similar manner to $\text{Cu}_3[\text{S}(\text{2,6-(2,4,6-Me}_3\text{C}_6\text{H}_3))]_3$ with $\text{K}[\text{Se}(\text{2,6-(Mes)}_2\text{C}_6\text{H}_3)]$ (100 mg, 0.25 mmol) and $[\text{Cu}(\text{CH}_3\text{CN})_4]\text{PF}_6$ (95 mg, 0.25 mmol) to yield a white solid of $\text{Cu}_3[\text{Se}(\text{2,6-(2,4,6-Me}_3\text{C}_6\text{H}_3))]_3$ (50 mg, 43%). X-ray quality crystals were obtained from concentrated toluene/acetonitrile solution at room temperature. ^1H NMR (600 MHz, C_6D_6): δ 2.07 (s, 36H, *o*-Mes), 2.26 (s, 18H, *p*-Mes), 6.71 (d, 6H, $^3J_{\text{H-H}} = 7.5$ Hz, *m*- C_6H_3), 6.80 (s, 12H, *m*-Mes), 6.94 (t, 3H, $^3J_{\text{H-H}} = 7.5$ Hz, *p*- C_6H_3). ^1H NMR (600 MHz, CDCl_3): δ 1.88 (s, 36H, *o*-Mes), 2.26 (s, 18H, *p*-Mes), 6.76 (d, 6H, $^3J_{\text{H-H}} = 7.8$ Hz, *m*- C_6H_3), 6.82 (s, 12H, *m*-Mes), 7.12 (t, 3H, $^3J_{\text{H-H}} = 7.8$ Hz, *p*- C_6H_3). $^{13}\text{C}\{^1\text{H}\}$ NMR (CDCl_3): δ 21.3,

21.4, 126.4, 128.5, 129.2, 130.9, 135.2, 136.7, 140.7, 145.4. $^{77}\text{Se}\{^1\text{H}\}$ NMR (THF, 297 K): δ -96.2. IR (KBr, cm^{-1}): 2912 (vs), 2854 (s), 2726 (w), 1605 (m), 1565 (m), 1443 (vs), 1379 (s), 1271 (w), 1228 (w), 1172 (w), 1093 (w), 1024 (s), 848 (s), 797 (s), 735 (s), 576 (m). Anal. Calcd for $\text{C}_{72}\text{H}_{75}\text{Cu}_3\text{Se}_3$: C, 63.22; H, 5.53. Found: C, 63.11; H, 5.64.

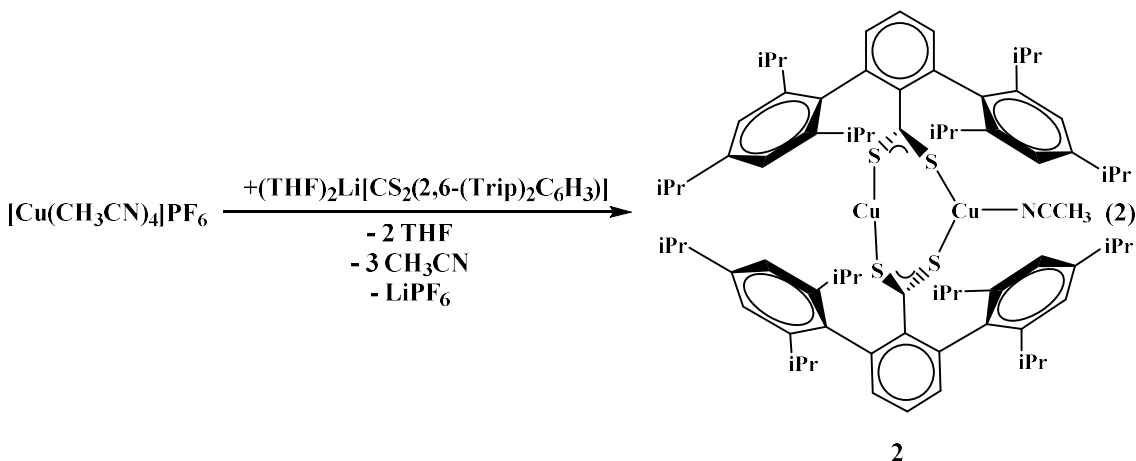
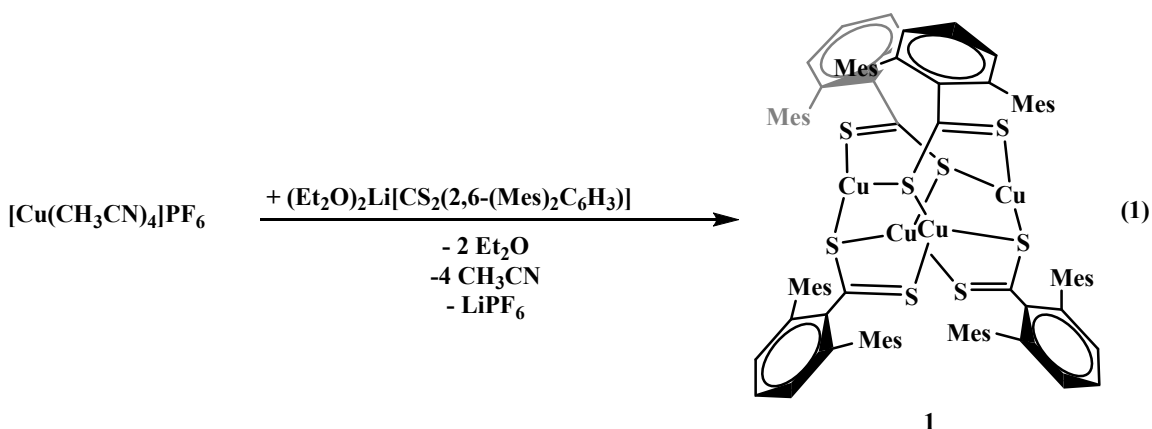
Synthesis of $\text{Cu}[\text{S}(2,6\text{-}(\text{Trip})_2\text{C}_6\text{H}_3)](\text{PEt}_3)$, **12.** In a 20 mL scintillation vial, 5 mL of THF was added to $[\text{CuI}(\text{PEt}_3)_4]$ (56 mg, 0.045 mmol) followed by 5 mL of $\text{K}[\text{S}(2,6\text{-}(\text{Trip})_2\text{C}_6\text{H}_3)]$ (100 mg, 0.18 mmol). The mixture was stirred at room temperature overnight yielding a cloudy white solution, after which the solvent was removed *in vacuo*. The white solid was extracted with hexane then filtered through Celite and the solvent was removed *in vacuo* to yield white powder (92 mg, 73%). X-ray quality crystals were obtained from a concentrated hexanes solution at $-24\text{ }^\circ\text{C}$. ^1H NMR (600 MHz, C_6D_6): δ 0.58 (dt, 9H, $^3J_{\text{H-P}} = 16.2\text{ Hz}$, $^3J_{\text{H-H}} = 7.2\text{ Hz}$, $\text{P}(\text{CH}_2\text{CH}_3)_3$), 0.78 - 0.83 (m, 6H, $\text{P}(\text{CH}_2\text{CH}_3)_3$), 1.23 (d, 12H, $^3J_{\text{H-H}} = 6.6\text{ Hz}$, *p*- $\text{CH}(\text{CH}_3)_2$), 1.27 (d, 12H, $^3J_{\text{H-H}} = 6.6\text{ Hz}$, *o*- $\text{CH}(\text{CH}_3)_2$), 1.60 (d, 12H, $^3J_{\text{H-H}} = 7.2\text{ Hz}$, *o*- $\text{CH}(\text{CH}_3)_2$), 2.80 (sept, 1H, $^3J_{\text{H-H}} = 7.2\text{ Hz}$, *p*- $\text{CH}(\text{CH}_3)_2$), 3.21 (sept, 2H, $^3J_{\text{H-H}} = 6.6\text{ Hz}$, *o*- $\text{CH}(\text{CH}_3)_2$), 6.94 (t, 1H, $^3J_{\text{H-H}} = 7.5\text{ Hz}$, *p*- C_6H_3), 7.01 (d, 2H, $^3J_{\text{H-H}} = 7.5\text{ Hz}$, *m*- C_6H_3), 7.31 (s, 4H, m-Trip). $^{13}\text{C}\{^1\text{H}\}$ NMR (C_6D_6): δ 8.0, 15.6 (d, $^1J_{\text{C-P}} = 21\text{ Hz}$), 24.1, 24.9, 25.0, 31.3, 34.3, 120.3, 122.4, 128.7, 139.2, 141.2, 146.2, 146.6, 153.6. $^{31}\text{P}\{^1\text{H}\}$ NMR (C_6D_6 , 297 K): δ -9.01. IR (KBr, cm^{-1}): 3040 (w), 2960 (vs), 2929 (vs), 2867 (s), 2750 (w), 1599 (w), 1565 (w), 1459 (s), 1413 (m), 1383 (s), 1359 (m), 1314 (m), 1254 (w), 1167 (w), 1107 (w), 1075 (w), 1044 (m), 1008 (w), 940 (w), 874 (m), 791 (w), 767 (m), 736 (m), 694 (w), 648 (w), 627 (w), 521 (w). Anal. Calcd for $\text{C}_{42}\text{H}_{64}\text{Cu}_1\text{P}_1\text{S}_1$: C, 72.53; H, 9.27. Found: C, 72.32; H, 9.47.

Synthesis of Cu[Se(2,6-(Trip)₂C₆H₃)](PEt₃), 13. The synthesis was carried out in a similar manner to Cu[S(2,6-(Trip)₂C₆H₃)](PEt₃) with K[Se(2,6-(Trip)₂C₆H₃)] (93 mg, 0.17 mmol) and [CuI(PEt₃)₄] (51.9 mg, 0.04 mmol) to yield a white solid of Cu[Se(2,6-(Trip)₂C₆H₃)](PEt₃) (71 mg, 42%). X-ray quality crystals were obtained from a concentrated hexanes solution at -24 °C. ¹H NMR (600 MHz, C₆D₆): δ 0.61 (br-s, 9H, P(CH₂CH₃)₃), 0.84 (br-s, 6H, P(CH₂CH₃)₃), 1.24 (d, 12H, ³J_{H-H} = 6.9 Hz, *p*-CH(CH₃)₂), 1.25 (d, 12H, ³J_{H-H} = 6.9 Hz, *o*-CH(CH₃)₂), 1.62 (d, 12H, ³J_{H-H} = 6.9 Hz, *o*-CH(CH₃)₂), 2.81 (sept, 1H, ³J_{H-H} = 6.9 Hz, *p*-CH(CH₃)₂), 3.18 (sept, 2H, ³J_{H-H} = 6.9 Hz, *o*-CH(CH₃)₂), 6.95 (d, 2H, ³J_{H-H} = 7.8 Hz, *m*-C₆H₃), 7.00 (t, 1H, ³J_{H-H} = 7.8 Hz, *p*-C₆H₃), 7.32 (s, 4H, *m*-Trip). ¹³C{¹H} NMR (C₆D₆): δ 8.02, 15.7 (d, ²J_{C-P} = 19.1 Hz), 24.1, 25.0, 25.1, 31.4, 34.3, 121.8, 122.6, 128.3, 140.2, 143.6, 145.7, 146.5, 147.7. ³¹P{¹H} NMR (C₆D₆, 300 K): δ -9.51. ⁷⁷Se{¹H} NMR (C₆D₆, 300K): δ 171.6 (d, ²J_{Se-P} = 49 Hz). IR (KBr, cm⁻¹): 3042 (w), 2958 (vs), 2929 (vs), 2866 (vs), 2748 (w), 1604 (w), 1594 (w), 1565 (m), 1536 (w), 1459 (s), 1412 (m), 1383 (vs), 1360 (s), 1336 (w), 1314 (m), 1255 (m), 1187 (w), 1167 (w), 1151 (w), 1106 (w), 1079 (w), 1068 (w), 1035 (s), 955 (w), 939 (m), 921 (w), 873 (s), 791 (m), 767 (s), 735 (s), 716 (m), 694 (w), 648 (w), 627 (w), 587 (w), 506 (w), 430 (w). Anal. Calcd for C₄₂H₆₄Cu₁P₁Se₁: C, 67.95; H, 8.69. Found: C, 67.65; H, 8.75.

Results and Discussion

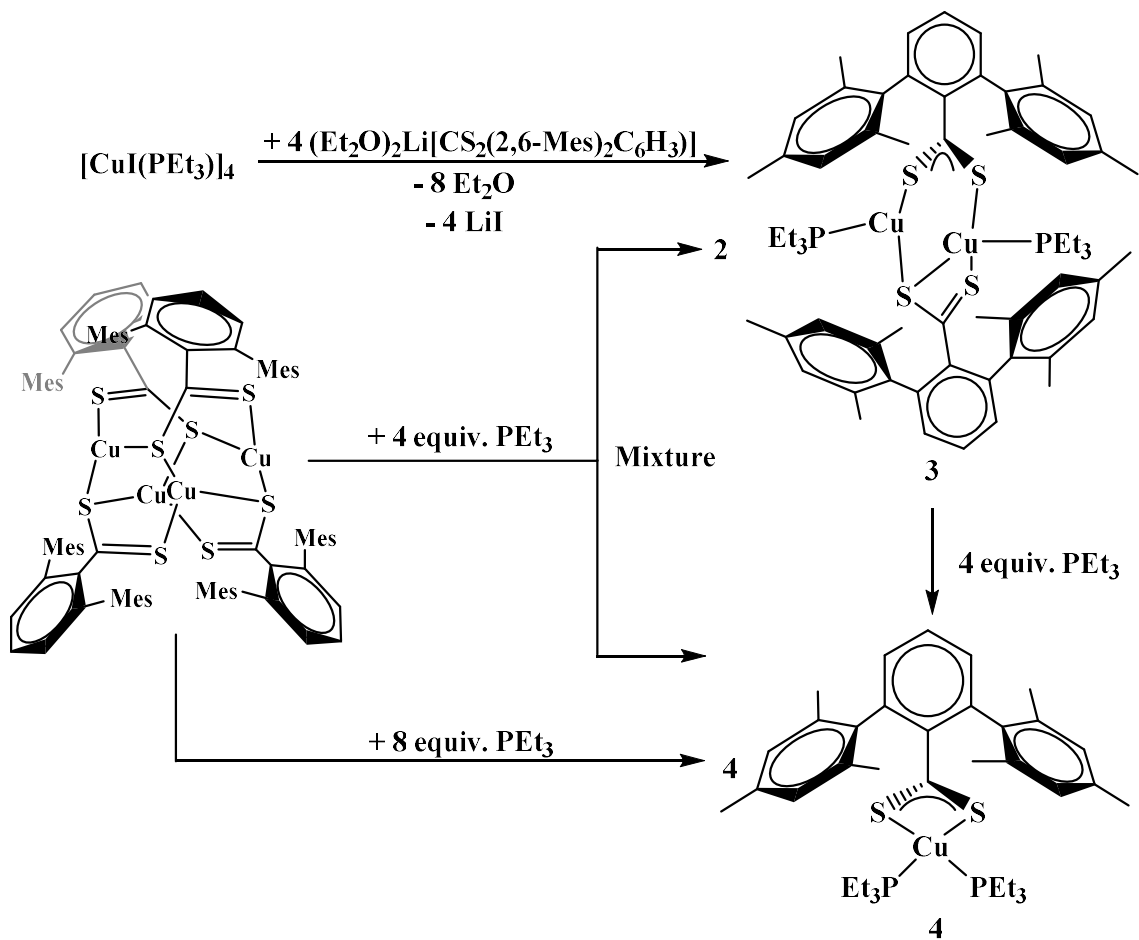
Dithiocarboxylate Complexes. To generate the dithiocarboxylate copper complexes, (Et₂O)₂Li[CS₂(2,6-(Mes)₂C₆H₃)] (Mes = 2,4,6-Me₃C₆H₂)²⁰⁹ and (THF)₂Li[CS₂(2,6-(Trip)₂C₆H₃)] (Trip = 2,4,6-iPr₃C₆H₂)²⁰⁹ were reacted with [Cu(NCCH₃)₄]PF₆. The reaction of (Et₂O)₂Li[CS₂(2,6-(Mes)₂C₆H₃)] with [Cu(NCCH₃)₄]PF₆ results in an

immediate color change from orange to dark brown. After workup, the product, $\text{Cu}_4[\text{S}_2\text{C}(2,6\text{-Mes})_2\text{C}_6\text{H}_3]_4$, **1**, could be isolated as a brown solid in moderate yield, eq 1. The reaction of $(\text{THF})_2\text{Li}[\text{CS}_2(2,6\text{-(Trip)}_2\text{C}_6\text{H}_3)]$ with $[\text{Cu}(\text{NCCH}_3)_4]\text{PF}_6$ also resulted in an immediate color change to dark brown, eq 2, and $\text{Cu}_2[\text{S}_2\text{C}(2,6\text{-Trip)}_2\text{C}_6\text{H}_3]_2(\text{NCCH}_3)$, **2**, was recovered as a brown solid. Unfortunately, **2** could not be obtained in acceptable purity for further characterization and we note that if a non-coordinating solvent such as toluene is used for recrystallization, a different product is obtained, but we have been unable to identify the resulting compound.



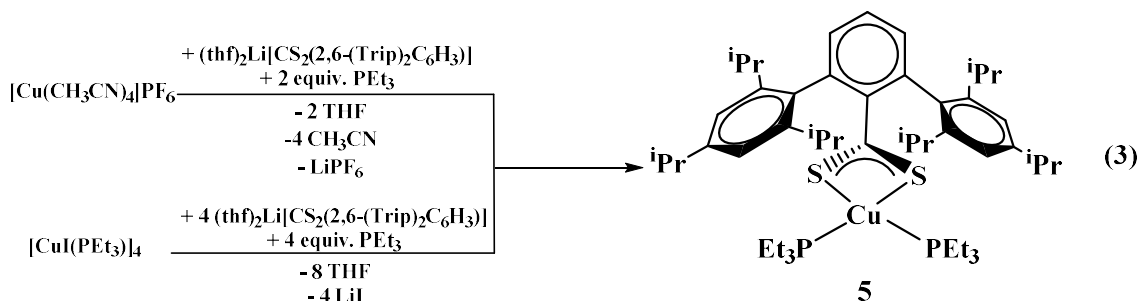
The reaction of complex **1** with four equivalents of triethylphosphine (PEt_3) yields two products: $\text{Cu}_2[\text{S}_2\text{C}(2,6\text{-Mes})_2\text{C}_6\text{H}_3]_2(\text{PEt}_3)_2$, **3**, and $\text{Cu}[\text{S}_2\text{C}(2,6\text{-Mes})_2\text{C}_6\text{H}_3](\text{PEt}_3)_2$, **4**,

Scheme 1. During the course of the reaction of **1** with PEt_3 , a color change from brown to orange could be observed. Complex **4** could also be synthesized from adding PEt_3 to **3**. To generate complex **3** with an acceptable purity, PEt_3 was preinstalled on the copper center by using $[\text{CuI}(\text{PEt}_3)_4]$, Scheme 1.

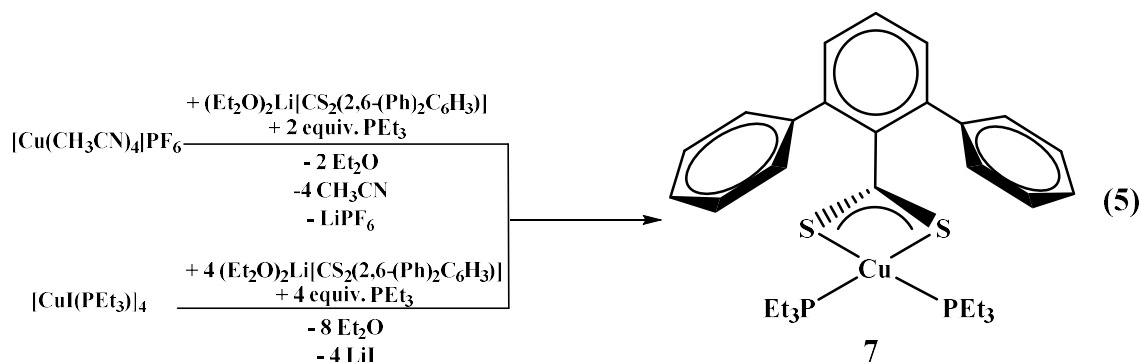
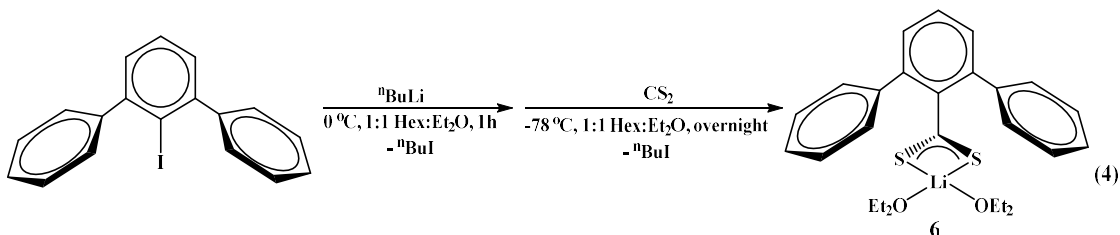


Scheme 1. Synthesis of **3** and **4**.

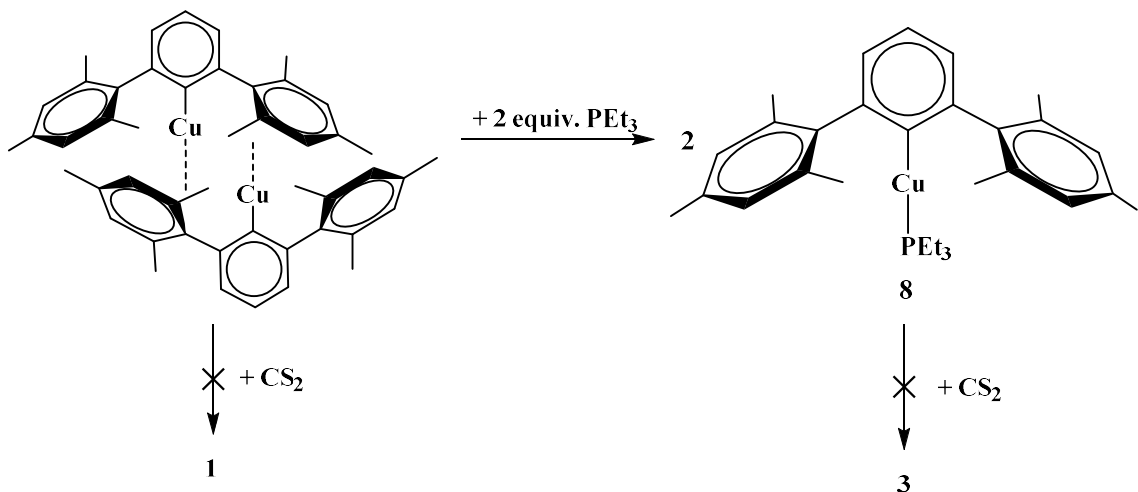
The reaction of $(\text{THF})_2\text{Li}[\text{CS}_2(2,6\text{-(Trip)}_2\text{C}_6\text{H}_3)]$ with $[\text{Cu}(\text{NCCH}_3)_4]\text{PF}_6$ in the presence of two equivalents of PEt_3 or $[\text{CuI}(\text{PEt}_3)_4]$ in the presence of one equivalent of PEt_3 both yielded $\text{Cu}[\text{S}_2\text{C}(2,6\text{-Trip})_2\text{C}_6\text{H}_3](\text{PEt}_3)_2$, **5**, in good yield, eq 3.



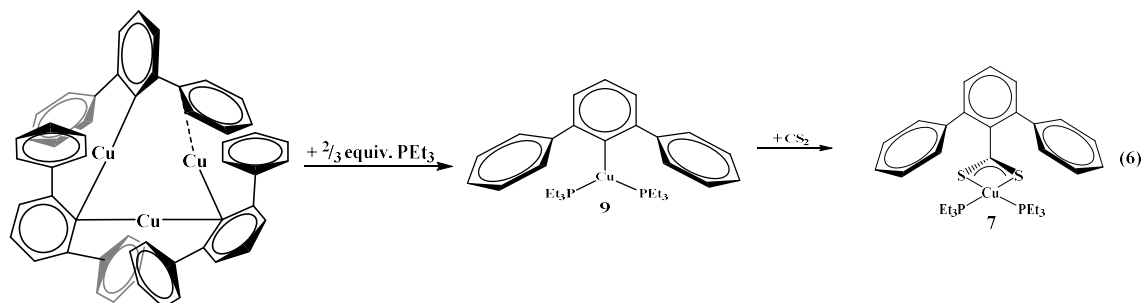
Finally, we wanted to examine an unsubstituted terphenyl ligand, which has not been examined as thoroughly as the mesityl and triisopropyl-derivatives. The reaction of 2,6-diphenyliodobenzene with ⁿBuLi followed by addition of CS₂ at -78 °C produced the dithiocarboxylate complex, (Et₂O)₂Li[S₂C(2,6-Ph)₂C₆H₃], **6**, eq 4. When **6** is reacted with [Cu(CH₃CN)₄]₂PF₆ in the presence of two equivalents of PEt₃, or [CuI(PEt₃)₄] in the presence of one equivalent of PEt₃, both yielded **8** in good yield (>75%), eq 5.



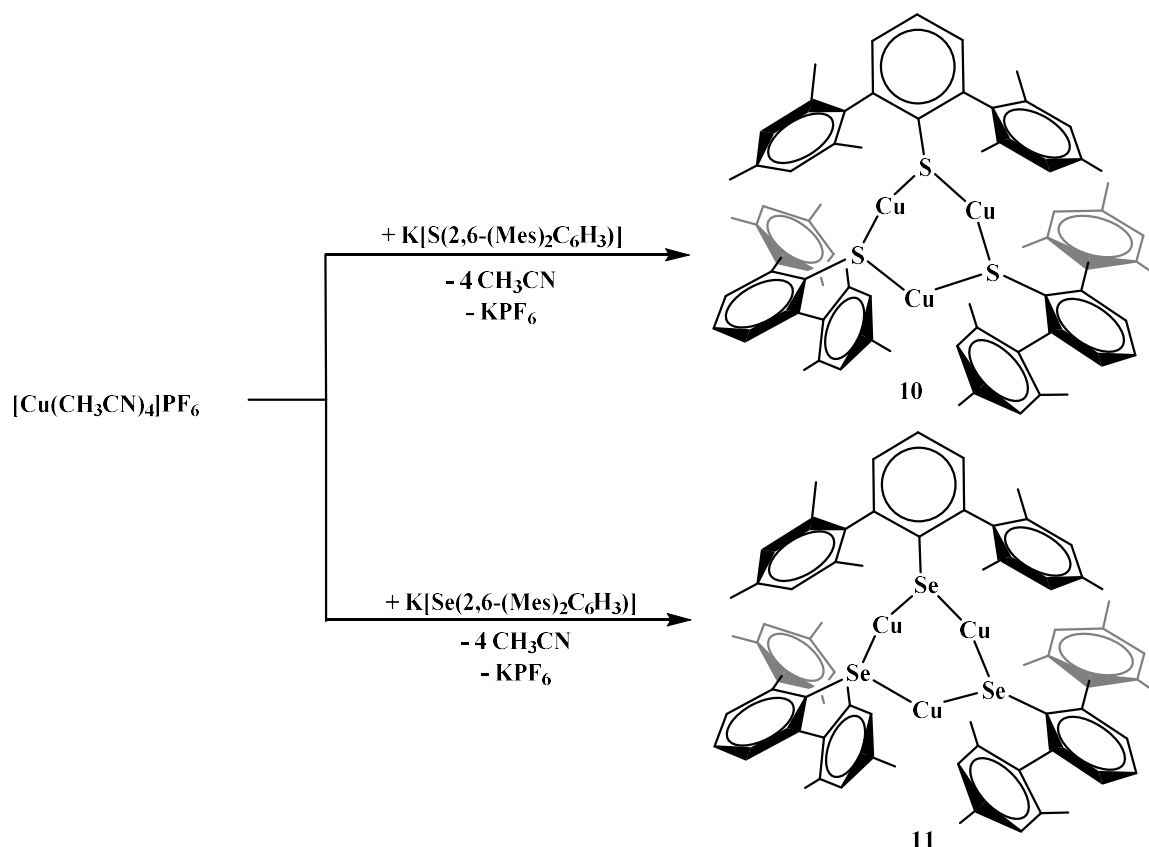
Given that complexes **1-5** and **7** could be made from metathesis with dithiocarboxylate salts, we investigated the possibility of producing the identical compounds by insertion of CS₂ into the copper-aryl bond of the corresponding terphenyl derivative. Complex **8** is made from Cu₂[(2,6-(Mes)₂C₆H₃)₂] with PEt₃. However, the reaction of Cu₂[(2,6-(Mes)₂C₆H₃)₂] or Cu[2,6-(Mes)₂C₆H₃](PEt₃), **8**, with CS₂ to generate copper-sulfur containing complexes did not yield the desired product, Scheme 2. In fact, no reaction was observed with either **8** or Cu₂[(2,6-(Mes)₂C₆H₃)₂] when reacted with CS₂. The steric bulk of the terphenyl ligand is believed to be the main contributor to the inertness of the complex. When two equivalents of PEt₃ are added to Cu₃[(2,6-(Ph)₂C₆H₃)₃]²⁰⁸ (Ph = phenyl) in hexanes, Cu[2,6-(Ph)₂C₆H₃](PEt₃)₂, **9**, is produced, eq 6. However, when **9** is reacted with CS₂, **7** was isolated, eq 6. This demonstrates the potential for enhanced reactivity with the unsubstituted terphenyl ligand over their more sterically encumbering counterparts.



Scheme 2. Synthesis of **8** from Cu₂[(2,6-(Mes)₂C₆H₃)₂] and reactivity toward carbon disulfide (CS₂) towards both complexes.

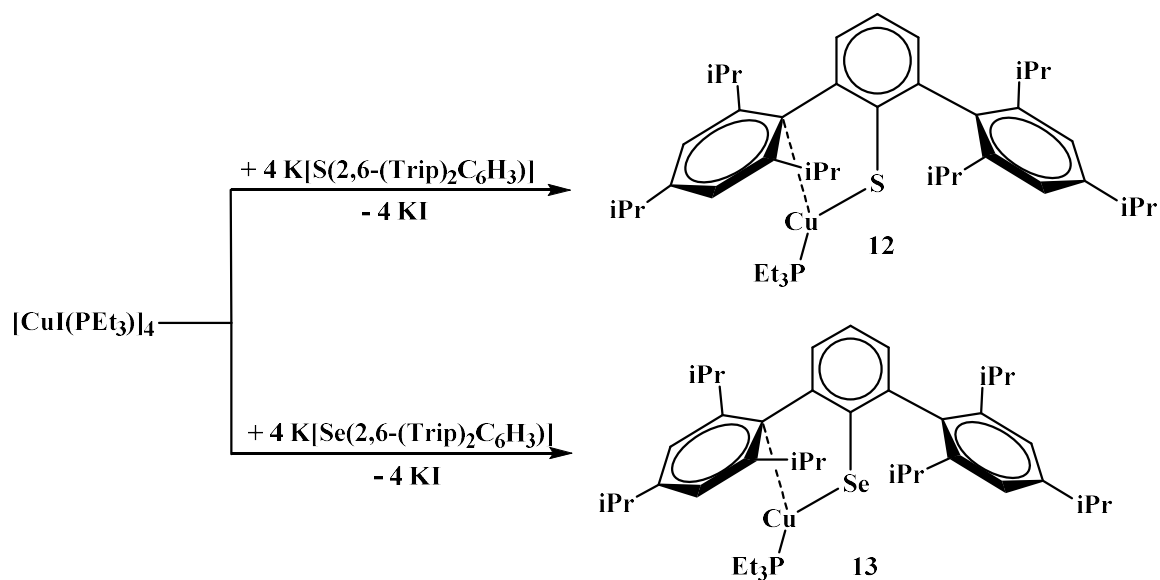


Chalcogenide complexes. To examine differences in dithiocarboxylate versus chalcogenide ligands, the thiolate and selenolate salts were synthesized. The reaction of $[\text{Cu}(\text{CH}_3\text{CN})_4]\text{PF}_6$ and $\text{K}[\text{S}(2,6\text{-(Mes)}_2\text{C}_6\text{H}_3)]$ proceeded with no color change and afforded $\text{Cu}_3[\text{S}(2,6\text{-(Mes)}_2\text{C}_6\text{H}_3)]_3$, **10**, Scheme 3. The product could be isolated in nearly quantitative yield (>98%). The reaction of $[\text{Cu}(\text{CH}_3\text{CN})_4]\text{PF}_6$ and $\text{K}[\text{Se}(2,6\text{-(Mes)}_2\text{C}_6\text{H}_3)]$ was carried out in a similar fashion to **10** yielding $\text{Cu}_3[\text{Se}(2,6\text{-(Mes)}_2\text{C}_6\text{H}_3)]_3$, **11**, Scheme 3.



Scheme 3. Synthesis of **10** and **11**.

With the triisopropyl derivatives, the reaction of $\text{K}[\text{E}(2,6\text{-(Trip)}_2\text{C}_6\text{H}_3)]$ with $[\text{CuI}(\text{PET}_3)]_4$ yielded mononuclear complexes, $\text{Cu}[\text{E}(2,6\text{-(Trip)}_2\text{C}_6\text{H}_3)](\text{PET}_3)$, $\text{E} = \text{S}$, **12**; Se , **13**, Scheme 4. Without PET_3 , no product could be readily isolated. Interestingly, all of the chalcogenide complexes, **10-13**, are colorless while the dithiocarboxylate complexes are brown or orange, presumably due to a ligand-to-metal charge transfer band from sulfur to an empty copper-based orbital which is not accessible within the visible region with the chalcogenide ligands. Reactivity with the unsubstituted terphenyl chalcogenide salts was attempted but yielded multiple products based on the ^1H NMR spectrum which could not be readily discriminated.



Scheme 4. Synthesis of **12** and **13**.

All complexes were characterized using 1H and ^{13}C NMR spectroscopy and, when appropriate, ^{31}P and ^{77}Se NMR spectroscopy, Table 1. The ^{77}Se NMR resonance for $Cu_3[Se(2,6-(Mes)_2C_6H_3)_3]$, **11**, was observed at -96.2 ppm while **13** showed a resonance at 171.6 ppm. This indicates that the donation from the selenium atom is far greater in **13** with a more downfield chemical shift.

Table A-1. Select ^1H , ^{13}C , and ^{31}P NMR resonances (in ppm) for complexes **1**, **3-13**.

Compound	^{13}C NMR CS:	^1H NMR						^{31}P NMR
		<i>o</i> -Mes	<i>p</i> -Mes	<i>o</i> -CH(CH ₃) ₂	<i>p</i> -CH(CH ₃) ₂	<i>o</i> -CH(CH ₃) ₂	<i>p</i> -CH(CH ₃) ₂	
$\text{Cu}_4[\text{S}_2\text{C}(2,6\text{-}(\text{Mes})_2\text{C}_6\text{H}_3)]_4$, 1	229.2	2.21	2.16					
$\text{Cu}_2[\text{S}_2\text{C}(2,6\text{-}(\text{Mes})_2\text{C}_6\text{H}_3)]_2(\text{PEt}_3)_2$, 3	246.8	2.43	2.29					-8.97
$\text{Cu}[\text{S}_2\text{C}(2,6\text{-}(\text{Mes})_2\text{C}_6\text{H}_3)](\text{PEt}_3)_2$, 4	251.7	2.54	2.26					-7.01
$\text{Cu}[\text{S}_2\text{C}(2,6\text{-}(\text{Trip})_2\text{C}_6\text{H}_3)](\text{PEt}_3)_2$, 5	251.4			1.21, 1.59	1.34	3.44	2.92	-7.61
$(\text{Et}_2\text{O})_2\text{Li}[\text{CS}_2(2,6\text{-}(\text{Ph})_2\text{C}_6\text{H}_3)]$, 6	251.4							
$\text{Cu}[\text{S}_2\text{C}(2,6\text{-}(\text{Ph})_2\text{C}_6\text{H}_3)](\text{PEt}_3)_2$, 7	251.9							-7.73
$\text{Cu}[(2,6\text{-}(\text{Mes})_2\text{C}_6\text{H}_3)](\text{PEt}_3)_2$, 8		2.40	2.29					-2.87
$\text{Cu}[(2,6\text{-}(\text{Ph})_2\text{C}_6\text{H}_3)](\text{PEt}_3)_2$, 9								-14.49
$\text{Cu}_3[\text{S}(2,6\text{-}(\text{Mes})_2\text{C}_6\text{H}_3)]_3$, 10		2.06	2.24					
$\text{Cu}_3[\text{Se}(2,6\text{-}(\text{Mes})_2\text{C}_6\text{H}_3)]_3$, 11		2.07	2.26					
$\text{Cu}[\text{S}(2,6\text{-}(\text{Trip})_2\text{C}_6\text{H}_3)](\text{PEt}_3)_2$, 12				1.27, 1.60	1.23	3.21	2.80	-9.01
$\text{Cu}[\text{Se}(2,6\text{-}(\text{Trip})_2\text{C}_6\text{H}_3)](\text{PEt}_3)_2$, 13				1.25, 1.62	1.24	3.18	2.81	-9.51

X-ray Crystallographic Analysis. X-ray structural analysis was used to determine the molecular structure of $\text{Cu}_4[\text{CS}_2(2,6\text{-}\text{Mes}_2\text{C}_6\text{H}_3)]_4$, **1**, shown in **Figure A-3**. All four ligands in the complex are $\mu_3:\eta^3$ featuring one bridging sulfur and one sulfur, which is directly coordinated to one copper atom. The geometry around each copper center could be described as trigonal planar. This is similar to the geometry and coordination environment for copper in the active site of CusA (see **Figure A-1**). Complex **1** also features two different types of C-S bonds. C(1)-S(1), C(26)-S(3), C(51)-S(6), and C(76)-S(7) all have relatively similar bond distances, 1.7313(18), 1.7404(18), 1.73820(4), and 1.739(2) Å, respectively. The average bond distance for all four bonds is 1.737 Å which

resembles that of a C-S single bond.²¹⁵ It should also be noted that all four sulfurs are bound to two copper atoms each in a bridging manner. On the other hand, C(1)-S(2), C(26)-S(4), C(51)-S(5), and C(76)-S(8) all have slightly shorter bond lengths of 1.6618(19), 1.6580(19), 1.6575(19), 1.660(2) Å, respectively, which resembles a C-S double bond.²¹⁵ This indicates that the anionic charge on the ligand is localized. Interestingly, **1** contains a striking feature in its quaternary carbon resonance on the thiocarboxylate group (229.2 ppm), which was significantly shifted downfield. This localization may be the reason for the observed shift since this is the only compound where localization is observed. The Cu-Cu interactions of 2.6-2.86 Å as well as the Cu-S bond lengths between 2.25-2.30 Å are similar to those observed in other tetranuclear dithiocarboxylate copper(I) clusters.^{216,217}

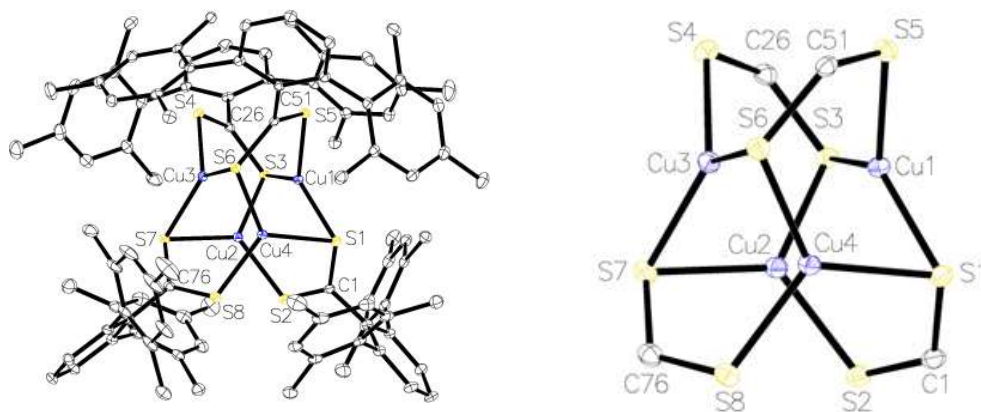


Figure A-3. Thermal ellipsoid plot of **1** shown at the 50% probability level. All hydrogen atoms and residual solvent molecule are omitted for clarity. The Cu₄S₈ core is shown on the right. Selected bond lengths: C1-S1: 1.7313(18) Å; C1-S2: 1.6618(19) Å; C26-S3: 1.7404(18) Å; C26-S4: 1.6580(19); C51-S5: 1.6575(19) Å; C51-S6: 1.73820(4) Å; C76-S7: 1.739(2) Å; C76-S8: 1.660(2) Å; Cu1-S5: 2.2500(5) Å; Cu1-S1: 2.2906(5) Å; Cu1-S3: 2.2907(5) Å; Cu1-Cu2: 2.6029(4) Å; Cu1-Cu4: 2.6113(4) Å; Cu1-Cu3: 2.8575(4) Å.

Figure A-4 shows the crystal structure of **2** obtained from acetonitrile by slow evaporation. The structure features a dinuclear species with a $\mu_2:\eta^2$ binding mode of the two dithiocarboxylate ligands. One copper, Cu2, is two-coordinate and has a near linear S2-Cu2-S3 bond angle of $169.01(3)^\circ$. The other copper ion, Cu1, is three-coordinate in a pseudo-trigonal planar geometry. The Cu1-S1 and Cu1-S4 bond distances of $2.2277(5)$ and $2.2205(5)$ Å, respectively, are slightly longer than Cu2-S2 and Cu2-S3 of $2.1543(5)$ and $2.1579(5)$ Å. This is due to the electron density siphoned by the nitrogen atom of acetonitrile bound to Cu1, which leads to longer copper-sulfur bond distances. The Cu-N(acetonitrile) bond distance is $2.004(2)$ Å.

The structures of **3** and **4** were determined by X-ray crystallography and revealed dinuclear and mononuclear complexes, respectively. In the solid-state, **3** forms a bimetallic core where the two ligands feature two different binding modes $\mu_2:\eta^3$ and $\mu_2:\eta^2$, **Figure A-5**. Within the $\mu_2:\eta^2$ unit, the two C-S bonds are essentially the same, indicating that the anionic charge of the ligand is delocalized along the S-C-S unit. The $\mu_2:\eta^3$ unit features two different C-S bonds. The longer C-S bond in C26-S4 resembles that of a single bond while C26-S3 is close to a double bond. Similar to **1**, the sulfur with the longer C-S bond distance is acting as a bridge between two copper centers. Since only one ^{13}C NMR resonance is found for the quaternary carbon, the two S-C-S units are the same on the NMR time scale. This type of bonding has been observed in dinuclear copper(I) complexes previously.²¹⁸

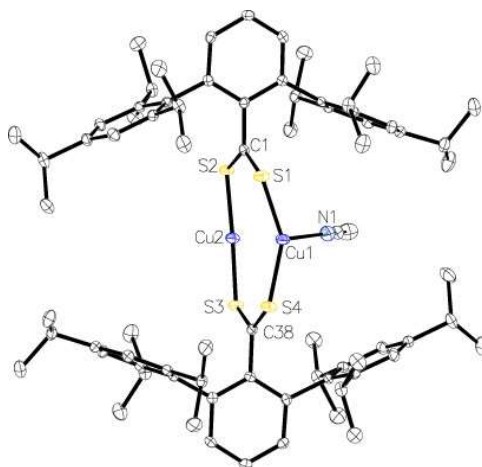


Figure A-4. Thermal ellipsoid plot of **2** shown at the 50% probability plot. All hydrogen atoms are omitted for clarity. Selected bond lengths: C1-S1: 1.6753(19) Å; C1-S2: 1.6912(19) Å; C38-S3: 1.6958(19) Å; C38-S4: 1.6677(19) Å; Cu1-S1: 2.2277(5) Å; Cu1-S4: 2.2205(5) Å; Cu2-S2: 2.1543(5) Å; Cu2-S3: 2.1579(5) Å; Cu1-N1: 2.004(2) Å.

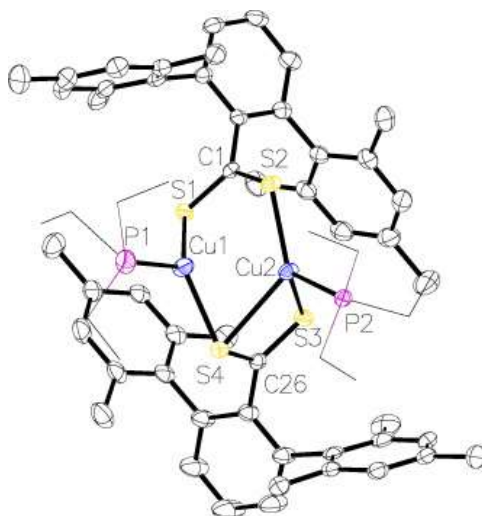


Figure A-5. Thermal ellipsoid plot of **3** shown at the 50% probability level. All hydrogen atoms, carbon atoms on PEt₃, and residue solvent molecule are omitted for clarity. Selected bond lengths: C1-S1: 1.6720(3) Å; C1-S2: 1.6720(3) Å; Cu1-S1: 2.2702(4) Å;

Cu2-S2: 2.2440(3) Å; C26-S3: 1.6648(2) Å; C26-S4: 1.7107(3) Å; Cu1-S4: 2.2635(3) Å;
Cu2-S4: 2.6307(4) Å; Cu2-S3: 2.3949(7) Å; Cu1-P1: 2.2201(8) Å; Cu2-P2: 2.2243(7) Å.

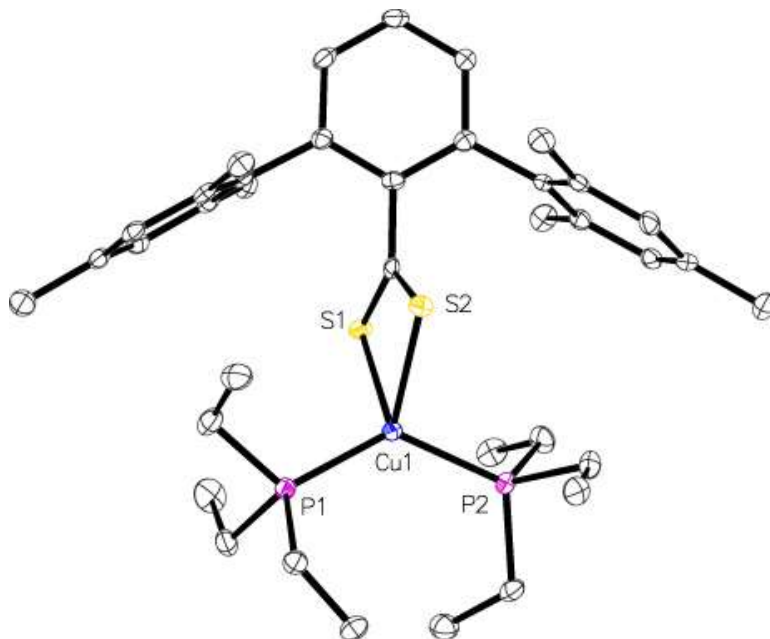


Figure A-6. Thermal ellipsoid plot of **4** shown at the 50% probability level. All hydrogen atoms and residue solvent molecule are omitted for clarity. Selected bond lengths: C1-S1: 1.6795(2) Å; C1-S2: 1.6851(4) Å; Cu1-P1: 2.2175(3) Å; Cu1-P2: 2.2360(3) Å; P1-Cu1-P2: 130.71(4)°; S1-Cu1-P1: 112.35(3)°; S2-Cu1-P1: 112.63(4)°; S1-Cu1-S2: 73.60(3)°.

The structures of **4**, **5**, and **7** are mononuclear copper(I) complexes with tetrahedral geometry with two sulfur and two phosphorus atoms coordinated. The data collection for **5** was done at 298 K due to a phase transition at low temperature. In all three compounds, the C-S bond lengths are nearly identical, which indicate that the anionic charge of the

ligand is delocalized. The copper-sulfur and –phosphorus bond distances and angles are similar to others reported.

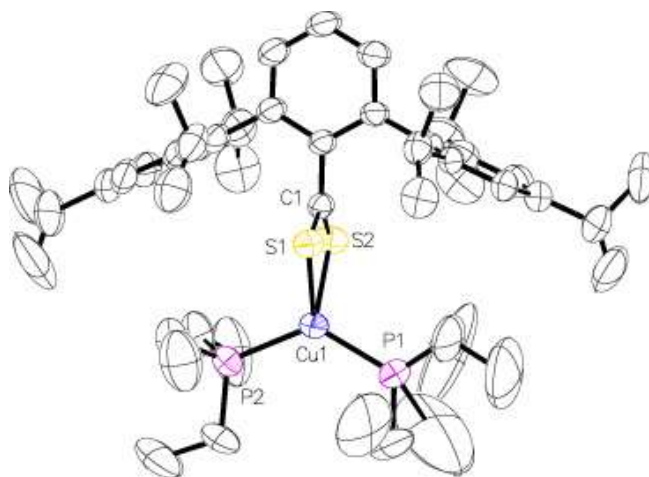


Figure A-7. Thermal ellipsoid 30% probability plot of **5**. All hydrogen atoms are omitted for clarity. Selected bond lengths: C1-S1: 1.65864(3) Å; C1-S2: 1.67355(3) Å; Cu1-S1: 2.44188(3) Å; Cu1-S2: 2.43358(3) Å; Cu1-P1: 2.2175(10) Å; Cu1-P2: 2.2361(10) Å;

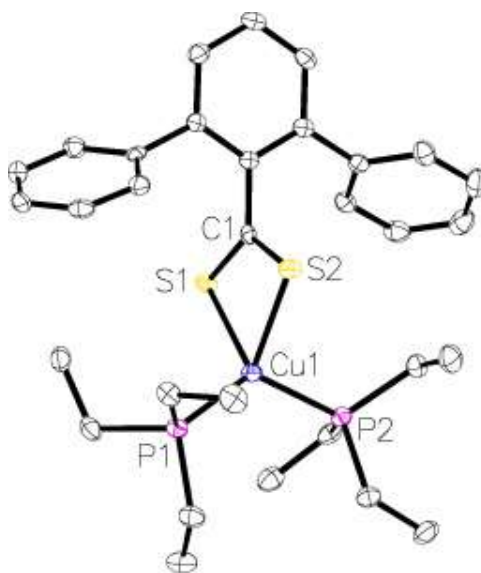


Figure A-8. Thermal ellipsoid plot of **7** shown at the 50% probability level. All hydrogen atoms are omitted for clarity. Selected bond length C1-S1: 1.68312(8) Å; C1-S2: 1.6780(1) Å; Cu1-S1: 2.45045(11) Å; Cu1-S2: 2.42886(12) Å; Cu1-P1: 2.2316(6) Å;

Cu1-P2: 2.2335(6) Å; P1-Cu1-P2: 125.81(2)°; S1-Cu1-S2: 73.25(2)°; S1-Cu1-P1: 115.10(2)°; S2-Cu1-P2: 105.33(2)°.

Complex **8** contains a two-coordinate copper center with a C1-Cu1-P1 bond angle of 168.380(3)°. Cu₂[2,6-(Mes)₂C₆H₃]₂ has been reported with a Cu1-C1 bond distance of 1.927(5) Å.²⁰⁸ This is nearly identical to the 1.9282(4) Å bond length in **8**. In addition, the analog of **8** with PPh₃ is known and it contains C1-Cu1-P1 bond angle of 168.82(8)° and Cu1-C1 bond distance of 1.922(3) Å.²¹⁹ Complex **9** is a three-coordinate trigonal planar copper compound with one Cu-C bond of 1.9720(2) Å and all C-Cu-P bond angles of 120°.

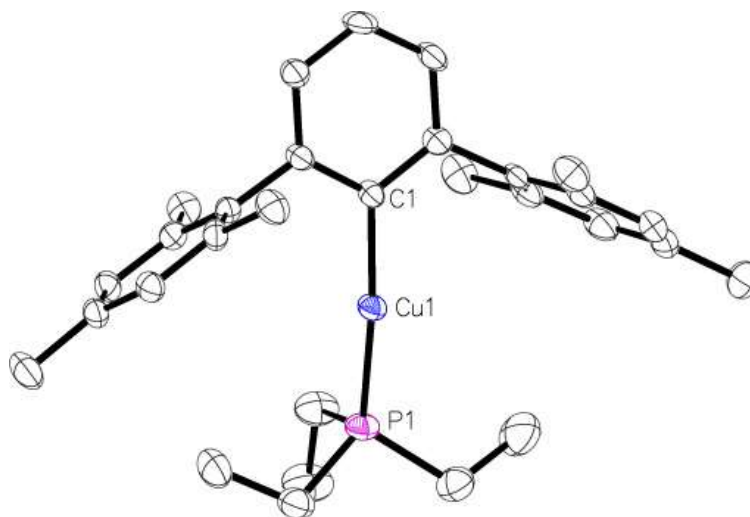


Figure A-9. Thermal ellipsoid plot of **8** shown at the 50% probability level. All hydrogen atoms and residue solvent molecule are omitted for clarity. Selected bond lengths and angles: C1-Cu1: 1.9282(4) Å; P1-Cu1: 2.2003(4) Å; C1-Cu1-P1: 168.380(3)°.

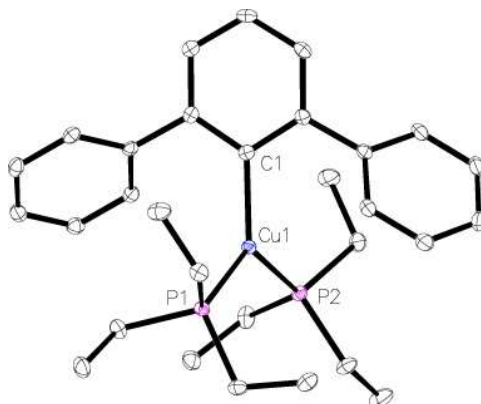


Figure A-10. Thermal ellipsoid plot of **9** shown at the 50% probability level. All hydrogen atoms are omitted for clarity. Selected bond lengths and angles: C1-Cu1: 1.9790(2) Å; Cu1-P1: 2.2495(4) Å; Cu1-P2: 2.558(2) Å; P1-Cu1-P2: 119.526(6)°; C1-Cu1-P2: 119.790(11)°; C1-Cu1-P1: 120.682(6)°.

Complexes **10**, Figure A-11, and **11**, Figure A-12, are structural analogs with three copper(I) centers and three mesityl-terphenyl ligands. The geometry around each copper is angular with E-Cu-E (E = S, Se) bond angles between 155-160°. Complex **11** is structurally similar to the previously reported $[\text{}^i\text{Pr}_3\text{PCuSPh}]_3$ ²²⁰ and $(\mu\text{-SPh})_3\text{Cu}_3(\text{PPh}_3)_4$.²²¹ Few copper-selenium clusters have been reported, but the Cu-Se bond distances in **11** of 2.32 Å are comparable to 2.370(2) to 2.412(2) Å in $\{\text{Cu}[\text{Se}(2,4,6\text{-}^i\text{Pr}_3\text{C}_6\text{H}_2)]\}_6$.²²²

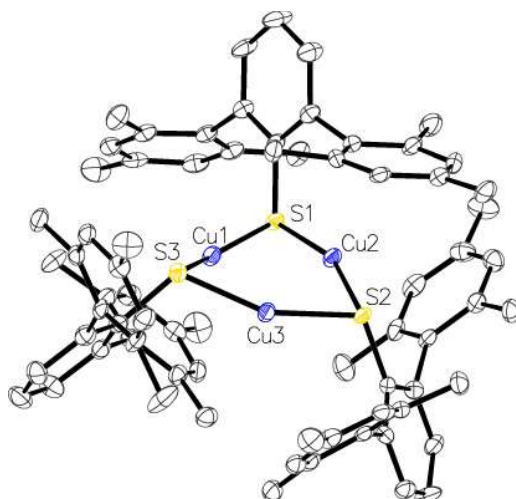


Figure A-11. Thermal ellipsoid plot of **10** shown at the 50% probability level. All hydrogen atoms are omitted for clarity. Selected bond lengths and angles: Cu1-S1: 2.21032(10) Å; Cu2-S1: 2.21033(14) Å; Cu2-S2: 2.22210(13) Å; Cu3-S2: 2.19521(10) Å; Cu3-S3: 2.20693(11) Å, Cu1-S3: 2.20536(11) Å; Cu1-Cu2: 2.92243(16) Å; Cu1-Cu3: 2.85052 Å; Cu3-Cu2: 2.87843(14) Å; S1-Cu1-S3: 155.1371(17)°; S2-Cu3-S3: 157.8052(15)°; S1-Cu2-S2: 159.3547(14)°.

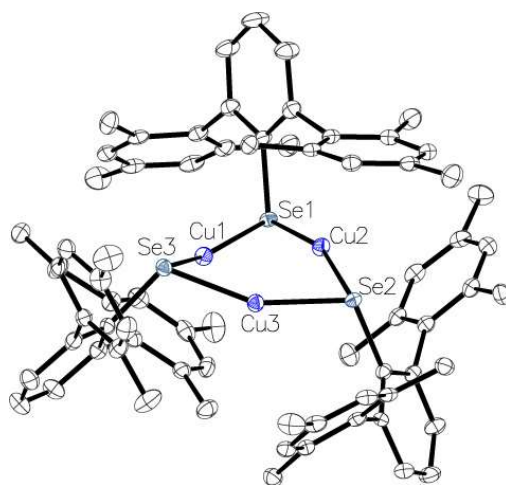


Figure A-12. Thermal ellipsoid plot of **11** shown at the 50% probability level. All hydrogen atoms are omitted for clarity. Selected bond lengths and angles: Cu1-Se1:

2.3154(5) Å; Cu2-Se1: 2.3176(5) Å; Cu1-Se3: 2.3113(5) Å; Cu3-Se3: 2.3190(6) Å; Cu3-Se2: 2.3190(6) Å; Cu2-Se2: 2.3334(5) Å; Cu1-Cu2: 2.7946(8) Å; Cu2-Cu3: 2.6769(7) Å; Cu1-Cu3: 2.6537(5) Å; Se1-Cu1-Se3: 154.501(6)°; Se2-Cu3-Se3: 157.013(8)°; Se1-Cu2-Se2: 160.8907(19)°.

Complexes **12** and **13** are three-coordinate complexes, which feature the copper center coordinated through a chalcogenide, phosphorus, and an ipso-carbon interaction. There is no evidence for the ipso-carbon interaction in solution. The Cu1-S1 bond distance of 2.1734(10) Å is close to the 2.1470(8) Å distance in the 3,4,7,8-tetramethyl-1,10-phenanthroline (tmphen) 2,6-diphenyl-thiophenolatocopper(I) complex²²³ as well as 2.194(1) Å in (Trip)CuPPh₃.²¹⁷ The C1-S1-Cu1 bond angle of 103.53(7)° is comparable to the 102.99(13)° to the corresponding C-S-Cu angle in (Trip)CuPPh₃, but larger than the 98.7(1)° in (tmphen)Cu[S(2,4,6-Me₃C₆H₂)], tmphen = 3,4,7,8-tetramethyl-1,10-phenanthroline.²²³ The C1-Se1-Cu1 angle in **13** is larger, 97.56(6)°, due to the larger size of selenium versus sulfur. The ipso-carbon interactions, Cu1-C13, in **12** and **13** of 2.378(3) and 2.28020(12) Å are similar to those seen in [Cu(2,6-(Mes)₂C₆H₃)₂] of 2.295(4) and 2.123(4) Å or 2.298(2) and 2.271(2) Å in [Cu(C₆F₅)₄(η²-toluene)₂].²²⁴

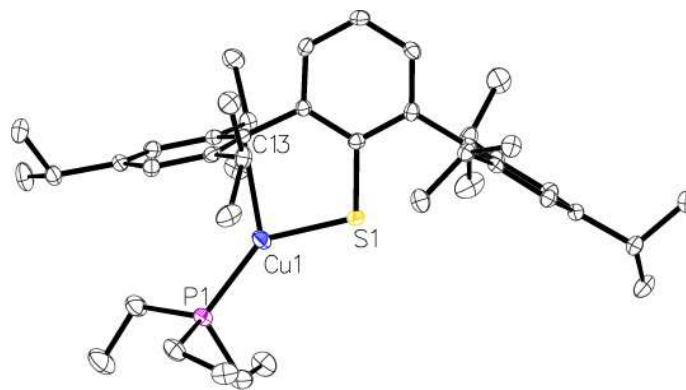


Figure A-13. Thermal ellipsoid plot of **12** shown at the 50% probability level. All hydrogen atoms are omitted for clarity. Selected bond distances: Cu1-S1: 2.1734(10) Å; Cu1-C13: 2.378(3) Å; Cu1-P1: 2.1882(10) Å; S1-Cu1-C13: 87.03(8)°; C1-S1-Cu1: 103.53(7)°.

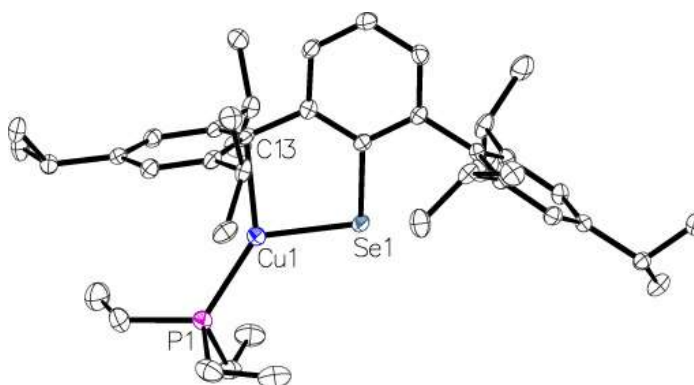


Figure A-14. Thermal ellipsoid plot of **13** shown at the 50% probability level. All hydrogen atoms are omitted for clarity. Selected bond length Cu1-Se1: 2.30182(12) Å, Cu1-C13: 2.28020(12) Å; Cu1-P1: 2.20287(13) Å; Se1-Cu1-C13: 89.276(4)°; C1-Se1-Cu1: 97.56(6)°.

Conclusion

Several copper(I) complexes have been synthesized with chalcogen-substituted terphenyl-based ligands to produce mono-, di-, tri-, and tetranuclear complexes. This

afforded complexes that mimic the active site of several copper-containing proteins such as Atx1 and CusA. The steric properties, in tandem with varying equivalents of PEt_3 , forced copper into geometries of near-linear, angular, trigonal planar, and tetrahedral. When the unsubstituted terphenyl ligand was employed, carbon disulfide insertion into the copper-carbon bond was observed, while this was not the case with the mesityl and triisopropyl-derivatives. The chemistry of the terphenyl ligand has been largely unexplored compared to the mesityl and triisopropyl-derivatives and the coordination chemistry and reactivity of this species is under further investigation.

Appendix B: Reactivity of U(IV) Phosphido Complexes with Organic Azide and Isocyanide.

Introduction

Insertion or migratory insertion reactions are a fundamental class of reactions that are invoked in many important industrial processes. This is true in Ziegler-Natta polymerization, hydroamination, and hydroformylation.

Experimental Section

General Considerations. All syntheses were carried out under inert atmosphere of dinitrogen using standard Schlenk and glovebox techniques. Solvents were purified in MBRAUN solvent purification system prior to use. Tert-butyl isocyanide (Aldrich), azidotrimethylsilane (Aldrich), $\text{KN}(\text{SiMe}_3)_2$ (Aldrich) were used as received. $(\text{C}_5\text{Me}_5)_2\text{ThCl}_2$,¹² $(\text{C}_5\text{Me}_5)_2\text{UCl}_2$,¹² $(\text{C}_5\text{Me}_5)_2\text{U}(\text{CH}_3)\text{I}$, $\text{Mg}(\text{}^{13}\text{CH}_3)_2$ ²²⁵, $(\text{C}_5\text{Me}_5)_2\text{Th}(\text{CH}_3)[\text{P}(\text{C}_6\text{H}_2\text{Me}_3\text{-}2,4,6)(\text{SiMe}_3)]$ were prepared according to literature procedures. $\text{KP}(\text{C}_6\text{H}_5)(\text{SiMe}_3)$ was prepared from $\text{HP}(\text{C}_6\text{H}_5)(\text{SiMe}_3)$ and $\text{KN}(\text{SiMe}_3)_2$ in toluene and collected by filtration over medium porous frit. Elemental analyses were performed by Microanalysis Facility, College of Chemistry, University of California, Berkeley. C_6D_6 (Cambridge) was dried over molecular sieves and degassed with three cycles of freeze-pump-thaw. ^1H and ^{13}C NMR experiment were performed on either Bruker Avance III 500 or 600 MHz spectrometer. ^1H and ^{13}C NMR spectrum are reported in ppm referenced internally to solvent impurity⁵⁷. ^{31}P and ^{29}Si NMR experiment were performed on Bruker AVII+ 300MHz spectrometer. ^{31}P and ^{29}Si NMR are reported

in ppm referenced external to 85% H₃PO₄ and tetramethylsilane, respectively. Infrared spectra were recorded as KBr pellets on Perkin-Elmer Spectrum One FT-IR spectrometer.

Synthesis of (C₅Me₅)₂Th[P(C₆H₅)(SiMe₃)]₂. Toluene (10 mL) was added to a mixture of (C₅Me₅)₂ThCl₂ (200 mg, 0.35 mmol) and KP(C₆H₅)(SiMe₃) (154 mg, 0.7 mmol). The resulting cloudy red solution was let to stir overnight and filtered over a pipette plugged with Celite. Volatiles were removed *in vacuo* to yield an orange solid (253 mg, 84%). X-ray quality crystals of (C₅Me₅)₂Th[P(C₆H₅)(SiMe₃)]₂ were grown from a concentrated diethyl ether solution at -45 °C. ¹H NMR (C₆D₆, 600 MHz, 298 K): δ 7.74 (br-t, 4H, *J* = 6.3 Hz, *o*-Ph), 7.22 (t, 4H, ³*J*_{H-H} = 7.2 Hz, *m*-Ph), 7.12 (t, 2H, ³*J*_{H-H} = 7.2 Hz, *p*-Ph), 2.08 (s, 30H, C₅Me₅), 0.56 (d, 18H, ²*J*_{H-P} = 4.2 Hz, SiMe₃). ¹³C{¹H} NMR (C₆D₆, 150 MHz, 298 K): 140.4 (d, ¹*J*_{C-P} = 7.2 Hz), 140.2 (t, ²*J*_{C-P} = 3.15 Hz), 128.1, 127.9, 126.6, 12.8, 3.7 (t, *J*_{C-P} = 6 Hz). ³¹P{¹H} NMR (C₆D₆, 120 MHz): δ 72.7. ²⁹Si INEPT NMR (C₆D₆, 60 MHz): δ 5.62 (dd, *J*_{Si-P} = 1.63 Hz, *J*_{Si-P} = 2.18 Hz). IR (KBr, cm⁻¹): 2951 (m), 2898 (s), 2856 (m), 1576 (w), 1472 (w), 1431 (m), 1378 (w), 1247 (s), 1098 (s), 1024 (s), 897 (w), 835 (vs), 734 (m), 697 (m), 625 (w), 579 (w), 540 (w). Anal. Calcd for C₃₈H₅₈P₂Si₂Th₁: C, 52.76; H, 6.76. Found: C, 52.72; H, 6.65.

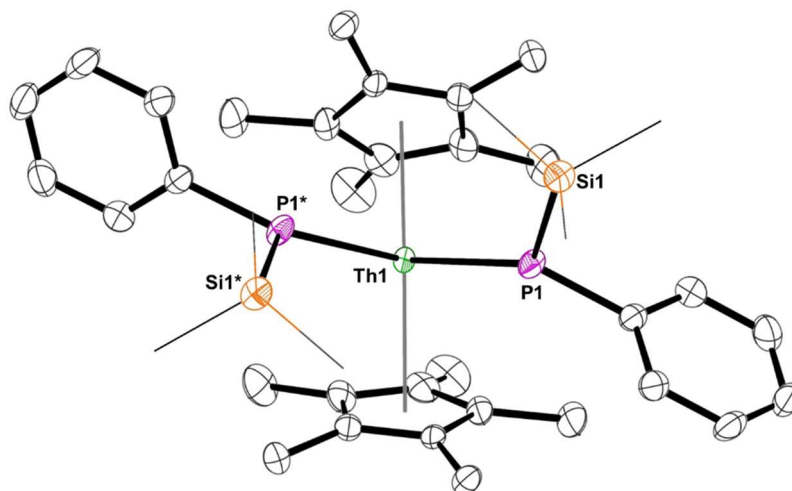


Figure B-1. Thermal ellipsoid plot of $(C_5Me_5)_2Th[P(C_6H_5)(SiMe_3)]_2$ shown at the 50% probability level. All hydrogen atoms are omitted for clarity.

Synthesis of $(C_5Me_5)_2U[(P(C_6H_5)(SiMe_3))]_2$. $(C_5Me_5)_2U[(P(C_6H_5)(SiMe_3))]_2$ was prepared in a manner similar to $(C_5Me_5)_2Th[(P(C_6H_5)(SiMe_3))]_2$ using $(C_5Me_5)_2UCl_2$ (126 mg, 0.22 mmol), $KP(C_6H_5)(SiMe_3)$ (144 mg, 0.65 mmol), and toluene (5 mL). The resulting deep brown solution was stirred overnight at room temperature and filtered over a pipette plugged with Celite. Volatiles were removed *in vacuo* to yield a dark brown solid. The residue was redissolved in pentane and filtered through Celite. (75 mg, 40%). 1H NMR (C_6D_6 , 600 MHz, 298 K): δ 13.5 (s, 30H, C_5Me_5), -2.48 (s, 2H, Ph), -3.74 (s, 4H, Ph), -8.94 (s, 18H, $SiMe_3$), -28.6 (br-s, 4H, Ph). IR (KBr, cm^{-1}): 2655 (m), 2905 (br-s), 2859 (m), 1577 (w), 1474 (w), 1439 (br-m), 1378 (w), 1244 (m), 1137 (br-w), 1081 (w), 1064 (m), 1022 (m), 974 (w), 929 (br-w), 840 (vs), 750 (w), 727 (w), 695 (w), 630 (w). Anal. Calcd for $C_{38}H_{58}P_2Si_2U_1$: C, 52.40; H, 6.71. Found: C, 52.08; H, 6.52.

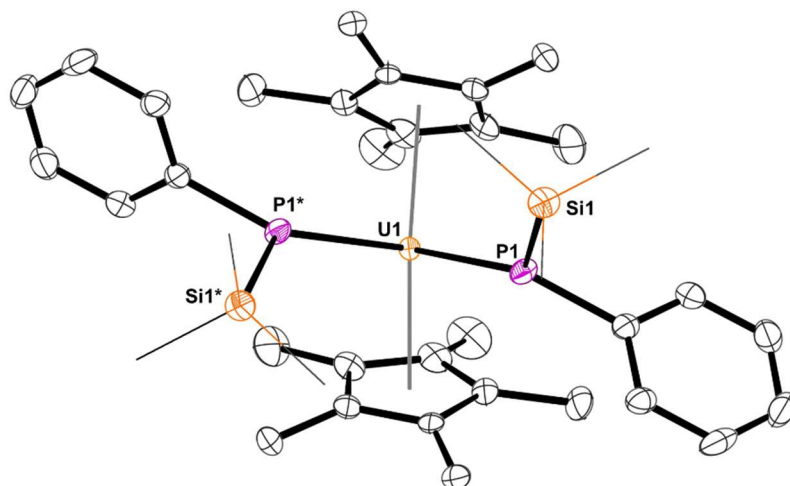


Figure B-2. Thermal ellipsoid plot of $(C_5Me_5)_2Th[P(C_6H_5)(SiMe_3)]_2$ shown at the 50% probability level. All hydrogen atoms are omitted for clarity.

Synthesis of $(C_5Me_5)_2Th(CN^tBu)[(\eta^2-N,C)-(^tBu)NCPPh]$. A solution of $(C_5Me_5)_2Th[P(C_6H_5)(SiMe_3)]_2$ (72 mg, 0.08 mmol) in methylcyclohexane (5 mL) was placed in a $-45\text{ }^\circ\text{C}$ freezer for 30 minutes prior to the next step. To this solution, an excess amount of tert-butyl isocyanide (0.15 mL, 1.3 mmol) was added dropwise. The mixture was let to stir at room temperature overnight. Volatiles were removed *in vacuo* to yield an orange solid. An analytically pure sample of $(C_5Me_5)_2Th(CN^tBu)(\eta^2-N,C)-(^tBu)NCPPh$ was obtained after recrystallization in 1,2 dimethoxymethane (36 mg, 56%). X-ray quality crystals of $(C_5Me_5)_2Th(CN^tBu)(\eta^2-N,C)-(^tBu)NCPPh$ were grown from a concentrated 1,2 dimethoxymethane solution at $-45\text{ }^\circ\text{C}$. 1H NMR (C_6D_6 , 600 MHz, 298 K): δ 8.22 (t, 2H, $J = 6$ Hz, *o*-Ph), 7.42 (t, 2H, $J = 7.8$ Hz, *m*-Ph), 7.19 (t, 1H, $J = 7.2$ Hz, *p*-Ph), 2.05 (s, 30H, C_5Me_5), 1.72 (d, 9H, $J = 1.2$ Hz, $[(H_3C)_3C]NCPPh$), 0.9 (s, 9H, $(H_3C)_3CNC$). $^{13}C\{^1H\}$ NMR (C_6D_6 , 150 Hz, 298 K): 265.4 (d, $^1J_{C-P} = 76.8$ Hz), 155.7 (d,

$^1J_{C-P} = 51.6$ Hz), 131.5 (d, $^3J_{C-P} = 18.6$ Hz), 127.7 (d, $^2J_{C-P} = 6.3$ Hz), 123.8, 122.7, 61.6, 57.2, 29.7 (d, $^4J_{C-P} = 12.8$ Hz), 28.9, 12.0. $^{31}P\{^1H\}$ NMR (C_6D_6 , 120 MHz): δ 58.5. IR (KBr, cm^{-1}): 2966 (s), 2902 (s), 2860 (s), 2188 (vs), 1575 (m), 1470 (m), 1450 (m), 1436 (m), 1373 (m), 1355 (m), 1295 (vs), 1266 (s), 1235 (m), 1197 (s), 1086 (br-m), 1061 (m), 1023 (s), 936 (m), 838 (w), 825 (w), 802 (br-w), 749 (m), 736 (s), 698 (s), 638 (w), 590 (w), 546 (w), 525 (w). Anal. Calcd for $C_{36}H_{53}N_2P_1Th_1$: C, 55.66; H, 6.88; N, 3.61. Found: C, 55.42; H, 7.01; N, 3.54.

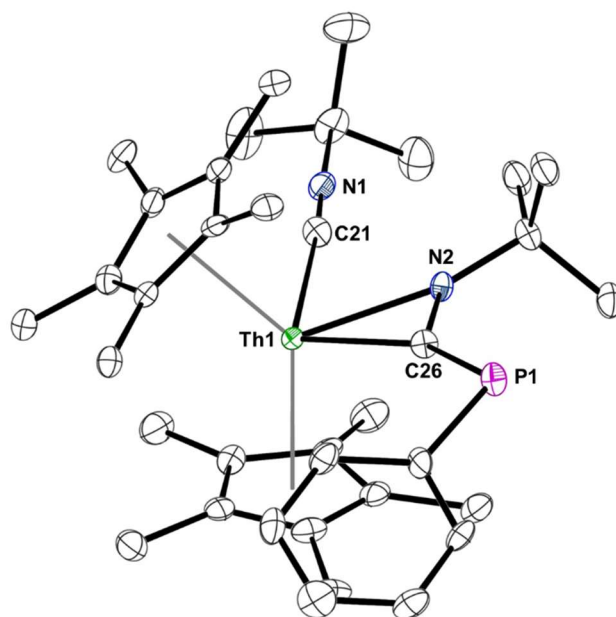


Figure B-3. Thermal ellipsoid plot of $(C_5Me_5)_2Th(CN^tBu)[(\eta^2-N,C)-(^tBuNCPPh)]$ shown at the 50% probability level. All hydrogen atoms are omitted for clarity.

Synthesis of $(C_5Me_5)_2U(CN^tBu)[(\eta^2-N,C)-(^tBuNCPPh)]$. $(C_5Me_5)_2U(CN^tBu)(\eta^2-N,C)-(^tBuNCPPh)$ was prepared in a manner similar to $(C_5Me_5)_2Th(CN^tBu)(\eta^2-N,C)-(^tBuNCPPh)$ using $(C_5Me_5)_2U[(P(C_6H_5)(SiMe_3))_2]$ (241 mg, 0.28 mmol), tert-butyl

isocyanide (0.1 mL, 0.88 mmol), and pentane (5 mL). An Analytically pure sample of $(C_5Me_5)_2U(CN^tBu)(\eta^2-N,C)-(^tBuNCPPh)$ was obtained after recrystallization in diethyl ether (87 mg, 40%). X-ray quality crystals of $(C_5Me_5)_2U(CN^tBu)(\eta^2-N,C)-(^tBuNCPPh)$ were grown from a concentrated pentane solution at $-45\text{ }^\circ\text{C}$. ^1H NMR (C_6D_6 , 500 MHz, 298 K): δ 28.5 (s, 9H, ^tBu), 4.10 (s, 2H, Ph), 1.50 (s, 30H, C_5Me_5), -1.50 (s, 1H, Ph), -14.7 (s, 9H, ^tBu), -46.5 (s, 2H, Ph). $^{31}\text{P}\{^1\text{H}\}$ NMR (C_6D_6 , 120 MHz): δ 198.3. IR (KBr, cm^{-1}): 2967 (s), 2912 (s), 2171 (vs), 1438 (m), 1375 (m), 1262 (m), 1205 (br-m), 1082 (br-m), 1023 (m), 903 (w), 884 (w), 803 (br-m), 751 (w), 694 (w), 676 (w), 577 (w). Satisfactory elemental analysis could not be obtained after multiple attempts.

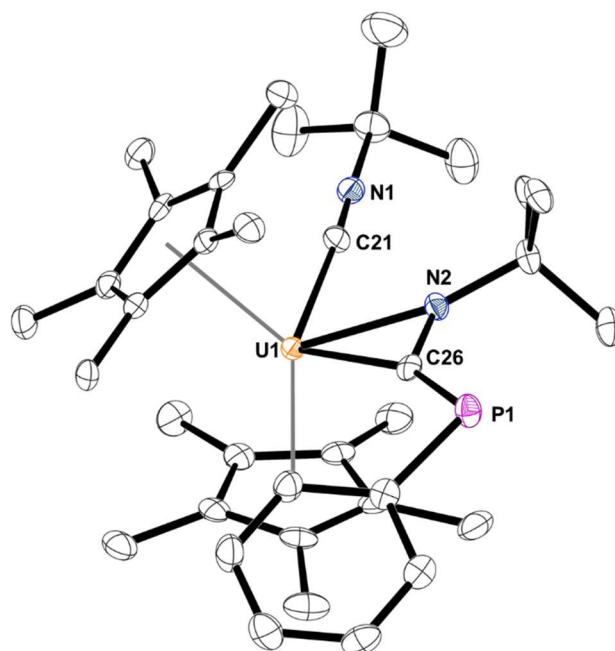


Figure B-4. Thermal ellipsoid plot of $(C_5Me_5)_2Th(CN^tBu)[(\eta^2-N,C)-(^tBuNCPPh)]$ shown at the 50% probability level. All hydrogen atoms are omitted for clarity.

Synthesis of $(C_5Me_5)_2U(CH_3)[P(C_6H_2Me_3-2,4,6)(SiMe_3)]$. To a scintillation vial charged with $(C_5Me_5)_2U(CH_3)I$ (252 mg, 0.39 mmol), toluene (3 mL), and a magnetic stir bar, $KP(C_6H_2Me_3-2,4,6)(SiMe_3)$ (102 mg, 0.39 mmol) in toluene (5 mL) was added at room temperature. The solution was stirred at room temperature overnight, after which it was filtered through Celite. The solvent was removed to yield $(C_5Me_5)_2U[P(C_6H_2Me_3-2,4,6)(SiMe_3)](CH_3)$ as a deep red powder (285 mg, 99%). X-ray quality crystals of $(C_5Me_5)_2U[P(C_6H_2Me_3-2,4,6)(SiMe_3)](CH_3)$ were grown from a concentrated diethyl ether solution at $-45\text{ }^\circ\text{C}$. $^1\text{H NMR}$ (C_6D_6 , 500 MHz, 298 K): δ 9.45 (s, 30H, $C_5(CH_3)_5$), 2.46 (s, 2H, *m*-Mes), -0.20 (s, 3H, CH_3 -*p*-Mes), -6.78 (s, 6H, CH_3 -*o*-Mes), -14.3 (s, 9H, $Si(CH_3)_3$), -125.0 (s, 3H, U- CH_3). IR (KBr, cm^{-1}): 2949 (m), 2908 (s), 2867 (m), 1438 (m), 1376 (m), 1237 (m), 1102 (w), 1044 (w), 1020 (w), 936 (w), 880 (w), 836 (vs), 749 (w). Anal. Calcd for $C_{33}H_{53}SiPU$: C, 53.07; H, 7.15. Found: C, 52.91; H, 7.04.

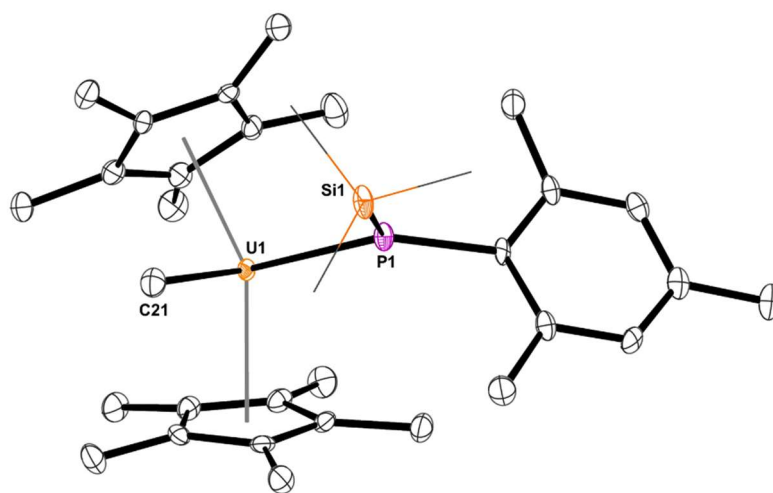


Figure B-5. Thermal ellipsoid plot of $(C_5Me_5)_2U(CH_3)[P(C_6H_2Me_3-2,4,6)(SiMe_3)]$ shown at the 50% probability level. All hydrogen atoms are omitted for clarity.

Synthesis of $(C_5Me_5)_2Th[t^BuNCCH_2C=N^tBuCN^tBu]$. A solution of $(C_5Me_5)_2Th(CH_3)[P(C_6H_2Me_{3-2,4,6})(SiMe_3)]$ (147 mg, 0.2 mmol) in pentane was placed in a $-45^\circ C$ freezer for 30 minutes prior to the next step. To this solution, tert-butyl isocyanide (50 mg, 0.6 mmol) was added dropwise. The mixture was let to stir at room temperature overnight. The volatiles were removed *in vacuo* to yield an orange solid. An analytically pure sample of $(C_5Me_5)_2Th[t^BuNCCH_2C=N^tBuCN^tBu]$ was obtained after recrystallization in pentane (43 mg, 28%). X-ray quality crystals of $(C_5Me_5)_2Th[t^BuNCCH_2C=N^tBuCN^tBu]$ were grown from a concentrated pentane solution at $-45^\circ C$. 1H NMR (C_6D_6 , 500 MHz, 298 K): δ 3.69 (s, 2H, CH_2), 2.06 (s, 30H, $C_5(CH_3)_5$), 1.81 (s, 9H, $(H_3C)_3CNC$), 1.50 (s, 9H, $(H_3C)_3CNC$), 1.36 (s, 9H, $(H_3C)_3CNC$). $^{13}C\{^1H\}$ NMR (C_6D_6 , 175 Hz, 298 K): 157.5, 132.3, 125.0, 112.3, 58.2, 57.9, 56.0, 47.1, 34.6, 33.9, 32.4, 13.0. IR (KBr, cm^{-1}): 2960 (vs), 2907 (vs), 2864 (s), 2825 (w), 1670 (s), 1595 (w), 1492 (s), 1452 (w), 1424 (w), 1386 (w), 1355 (m), 1315 (s), 1258 (w), 1229 (w), 1203 (vs), 1118 (w), 1086 (w), 1024 (w), 982 (w), 966 (w), 919 (w), 846 (w), 799 (m), 768 (m). Anal. Calcd for $C_{36}H_{59}N_3Th_1$: C, 56.45; H 7.76; N, 5.49. Found: C, 56.13; H, 7.77; N, 5.19.

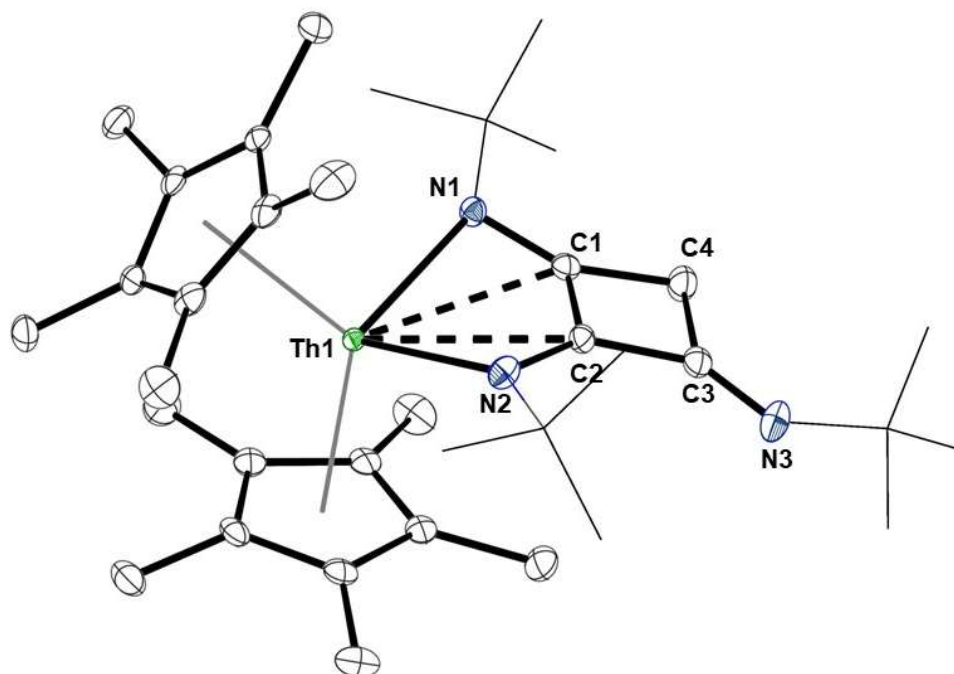


Figure B-6. Thermal ellipsoid plot of $(C_5Me_5)_2Th[tBuNCCH_2C=NtBuCNtBu]$ shown at the 50% probability level. All hydrogen atoms are omitted for clarity.

Synthesis of $(C_5Me_5)_2U[tBuNCCH_2C=NtBuCNtBu]$. $(C_5Me_5)_2U[tBuNCCH_2C=NtBuCNtBu]$ was prepared in a manner similar to $(C_5Me_5)_2Th[tBuNCCH_2C=NtBuCNtBu]$ using $(C_5Me_5)_2U(CH_3)[P(C_6H_2Me_3-2,4,6)(SiMe_3)]$ (241 mg, 0.32 mmol), tert-butyl isocyanide (80 mg, 0.96 mmol), and pentane (10 mL). An analytically pure sample of $(C_5Me_5)_2U[tBuNCCH_2C=NtBuCNtBu]$ was obtained after recrystallization in diethyl ether (87 mg, 35%). X-ray quality crystals of $(C_5Me_5)_2U[tBuNCCH_2C=NtBuCNtBu]$ were grown from a concentrated pentane solution $-45\text{ }^\circ\text{C}$. 1H NMR (C_6D_6 , 600 MHz, 298 K): δ 31.6 (s, 2H, CH_2), 8.47 (s, 30H, $C_5(CH_3)_5$), 6.41 (s, 9H, $(H_3C)_3CNC$), -12.5 (s, 9H, $(H_3C)_3CNC$), -24.7 (s, 9H, $(H_3C)_3CNC$). IR (KBr, cm^{-1}): 2962 (vs), 2908 (br-s), 1668 (s), 1598 (w), 1560 (w), 1492 (m), 1454 (m), 1385 (w), 1357 (m), 1322 (m), 1261 (m), 1200

(vs), 1088 (br-m), 1023 (m), 957 (w), 915 (w), 845 (m), 800 (m), 767 (w). Anal. Calcd for $C_{36}H_{59}N_3U_1$: C, 56.02; H, 7.70; N, 5.44. Found: C, 55.78; H, 7.56; N, 5.14.

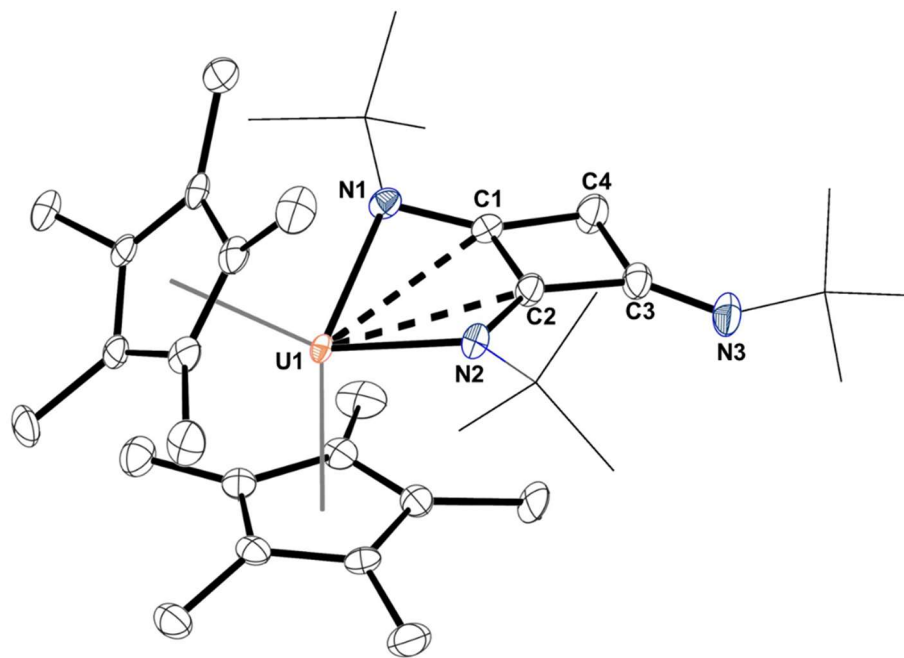


Figure B-7. Thermal ellipsoid plot of $(C_5Me_5)_2Th[tBuNCCH_2C=NtBuCNtBu]$ shown at the 50% probability level. All hydrogen atoms are omitted for clarity.

Synthesis of $(C_5Me_5)_2U(\kappa^2-N,N)-[(N(SiMe_3))_2P(C_6H_2Me_3-2,4,6)]$. To a scintillation vial charged with $(C_5Me_5)_2U(CH_3)[P(C_6H_2Me_3-2,4,6)(SiMe_3)]$ (250 mg, 0.33 mmol), dimethoxyethane (7 mL), and a stir bar, azidotrimethylsilane (73mg, 0.63 mmol) was added. Gas evolution was observed immediately. The solution was let to stir at room temperature overnight. After which, the solvent was removed *in vacuo* to yield a dark brown solid. Recrystallization from a concentrated diethyl ether solution (-40 °C) yielded dark brown crystals, which were dried *in vacuo* (175 mg, 66%). X-ray quality crystals were obtained from a concentrated diethyl ether solution at -40 °C. 1H NMR (C_6D_6 , 500

MHz, 298 K): 33.7 (s, 3H, CH_3 -Mes), 12.0 (s, 1H, CH -Mes), 10.7 (s, 15H, $C_5(CH_3)_5$), 7.98 (s, 1H, CH -Mes), 5.66 (s, 3H, CH_3 -Mes), 5.01 (s, 15H, $C_5(CH_3)_5$), 3.70 (s, 3H, CH_3 -Mes), -21.2 (s, 18H, $-SiMe_3$). $^{31}P\{^1H\}$ NMR (C_6D_6 , 120 MHz): δ -174.8. ^{29}Si INEPT NMR (C_6D_6 , 60 MHz): δ 222.9. IR (KBr, cm^{-1}): 2949 (m), 2904 (br-m), 2856 (w), 1437 (br-w), 1376 (w), 1244 (s), 1083 (br-w), 1021 (br-w), 954 (w), 891 (s), 837 (vs), 765 (w), 689 (w), 668 (m). Anal. Calcd for $C_{35}H_{59}N_2PSi_2U$: C, 50.48; H, 7.14; N, 3.48. Found: C, 50.30; H, 7.27; N, 3.17.

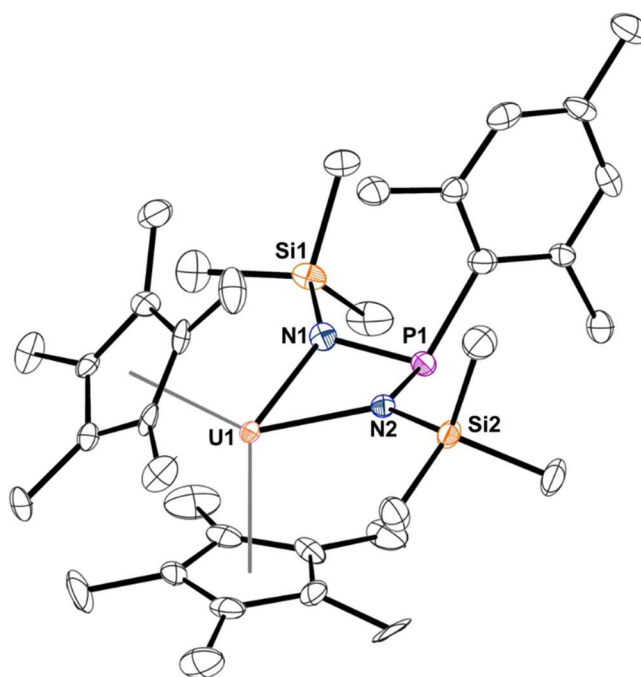


Figure B-8. Thermal ellipsoid plot of $(C_5Me_5)_2U(\kappa^2-N,N)-[(N(SiMe_3)_2P(C_6H_2Me_3-2,4,6))]$ shown at the 50% probability level. All hydrogen atoms are omitted for clarity.

Synthesis of $(C_5Me_5)_2U(CH_3)[P(C_6H_5)(SiMe_3)]$. To a scintillation vial charged with $K[P(C_6H_5)(SiMe_3)]$ (40 mg, 0.18 mmol) and toluene (5 mL), $(C_5Me_5)_2U(CH_3)(Cl)$ (100 mg, 0.18 mmol) in toluene (5 mL) was added. The solution was let to stir at room

temperature overnight. After which, it was filtered through Celite and the solvent was removed *in vacuo* to yield a dark brown solid (107 mg, 85%). ^1H NMR (C_6D_6 , 600 MHz, 298 K): 11.4 (s, 30H, $\text{C}_5(\text{CH}_3)_5$), -4.21 (s, 1H, *p*-Ph), -5.35 (s, 2H, *m*-Ph), -14.6 (s, 9H, - SiMe_3), -35.6 (s, 2H, *p*-Ph), -190.2 (s, 3H, - CH_3). IR (KBr, cm^{-1}): 2903 (vs), 2858 (s), 2725 (w), 1578 (m), 1473 (m), 1432 (br-m), 1378 (m), 1259 (w), 1242 (s), 1102 (s), 1081 (s), 1022 (s), 889 (w), 837 (vs), 747 (w), 726 (w), 693 (w), 629 (w). Anal. Calcd for $\text{C}_{30}\text{H}_{47}\text{PSiU}$: C, 51.13; H, 6.72. Found: C, 50.67; H, 6.26.

Synthesis of $(\text{C}_5\text{Me}_5)_2\text{U}(\text{CH}_3)[-\text{N}=\text{P}(\text{SiMe}_3)_2(\text{C}_6\text{H}_5)]$. $(\text{C}_5\text{Me}_5)_2\text{U}(\text{CH}_3)[-\text{N}=\text{P}(\text{SiMe}_3)_2(\text{C}_6\text{H}_5)]$ was synthesized in a fashion similar to $(\text{C}_5\text{Me}_5)_2\text{U}(\kappa^2\text{-N,N})-[(\text{N}(\text{SiMe}_3)_2)\text{P}(\text{C}_6\text{H}_2\text{Me}_3\text{-}2,4,6)]$ using $(\text{C}_5\text{Me}_5)_2\text{U}(\text{CH}_3)[\text{P}(\text{C}_6\text{H}_5)(\text{SiMe}_3)]$ (148 mg, 0.21 mmol), azidotrimethylsilane (38 mg, 0.33), and diethyl ether. Recrystallization from a concentrated diethyl ether solution (-40 °C) yielded brown crystals which were dried *in vacuo* (30 mg, 18%). X-ray quality crystals were obtained from a concentrated diethyl ether solution at -40 °C. ^1H NMR (C_6D_6 , 500 MHz, 298 K): δ 23.7 (s, 2H, *o*-Ph), 11.0 (s, 18H, - SiMe_3), 9.10 (br-s, 1H, *p*-Ph), 8.9 (br-s, 2H, *m*-Ph), -1.83 (s, 30H, $\text{C}_5(\text{CH}_3)_5$), -194.4 (s, 3H, - CH_3). $^{31}\text{P}\{^1\text{H}\}$ NMR (C_6D_6 , 120 MHz): δ 518.0. IR (KBr, cm^{-1}): 2953 (m), 2901 (s), 2854 (m), 1436 (w), 1376 (w), 1246 (m), 1088 (m), 1046 (vs), 1023 (m), 933 (m), 882 (m), 839 (vs), 749 (w), 697 (w). Anal. Calcd for $\text{C}_{33}\text{H}_{56}\text{NPSi}_2\text{U}$: C, 50.05; H, 7.13; N, 1.77. Found: C, 49.86; H, 6.91; N, 1.72.

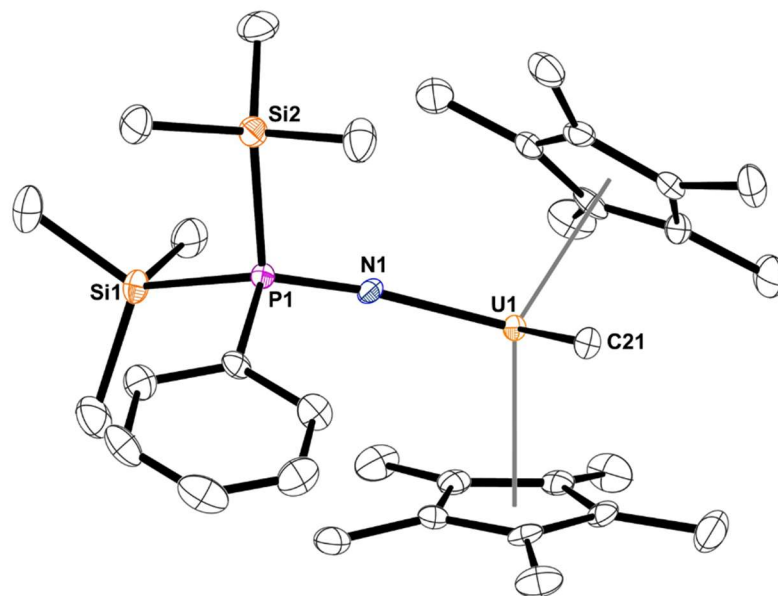


Figure B-9. Thermal ellipsoid plot of (C₅Me₅)₂U(CH₃)[-N=P(SiMe₃)₂(C₆H₅)] shown at the 50% probability level. All hydrogen atoms are omitted for clarity.

References

1. Fox, A. R.; Bart, S. C.; Meyer, K.; Cummins, C. C., Towards uranium catalysts. *Nature* **2008**, *455*, 341.
2. Cotton, S., Lanthanide and actinide chemistry. **2013**.
3. Kaltsoyannis, N., Does Covalency Increase or Decrease across the Actinide Series? Implications for Minor Actinide Partitioning. *Inorg. Chem.* **2013**, *52* (7), 3407-3413.
4. Lukens, W. W.; Speldrich, M.; Yang, P.; Duignan, T. J.; Autschbach, J.; Kogerler, P., The roles of 4f- and 5f-orbitals in bonding: a magnetochemical, crystal field, density functional theory, and multi-reference wavefunction study. *Dalton Trans.* **2016**, *45* (28), 11508-11521.
5. Fortier, S.; Walensky, J. R.; Wu, G.; Hayton, T. W., High-Valent Uranium Alkyls: Evidence for the Formation of $U^{VI}(CH_2SiMe_3)_6$. *J. Am. Chem. Soc.* **2011**, *133* (30), 11732-11743.
6. Schrock, R. R.; Hoveyda, A. H., Molybdenum and Tungsten Imido Alkylidene Complexes as Efficient Olefin-Metathesis Catalysts. *Angew. Chem. Int. Ed.* **2003**, *42* (38), 4592-4633.
7. Hoffman, B. M.; Lukoyanov, D.; Yang, Z.-Y.; Dean, D. R.; Seefeldt, L. C., Mechanism of Nitrogen Fixation by Nitrogenase: The Next Stage. *Chem. Rev.* **2014**, *114* (8), 4041-4062.
8. Waterman, R., Metal-phosphido and -phosphinidene complexes in P-E bond-forming reactions. *Dalton Trans.* **2009**, (1), 18-26.

9. Pohlki, F.; Doye, S., The catalytic hydroamination of alkynes. *Chem. Soc. Rev.* **2003**, *32* (2), 104-114.
10. Hayton, T. W., Metal-ligand multiple bonding in uranium: structure and reactivity. *Dalton Trans.* **2010**, *39* (5), 1145-1158.
11. Broach, R. W.; Schultz, A. J.; Williams, J. M.; Brown, G. M.; Manriquez, J. M.; Fagan, P. J.; Marks, T. J., Molecular Structure of an Unusual Organoactinide Hydride Complex Determined Solely by Neutron Diffraction. *Science* **1979**, *203* (4376), 172-174.
12. Fagan, P. J.; Manriquez, J. M.; Maatta, E. A.; Seyam, A. M.; Marks, T. J., Synthesis and properties of bis(pentamethylcyclopentadienyl) actinide hydrocarbyls and hydrides. A new class of highly reactive f-element organometallic compounds. *J. Am. Chem. Soc.* **1981**, *103* (22), 6650-6667.
13. Arnold, P. L.; Love, J. B.; Patel, D., Pentavalent uranyl complexes. *Coord. Chem. Rev.* **2009**, *253* (15), 1973-1978.
14. Fortier, S.; Hayton, T. W., Oxo ligand functionalization in the uranyl ion (UO₂²⁺). *Coord. Chem. Rev.* **2010**, *254* (3), 197-214.
15. Cramer, R. E.; Maynard, R. B.; Paw, J. C.; Gilje, J. W., A uranium-carbon multiple bond. Crystal and molecular structure of (η⁵-C₅H₅)₃UHP(CH₃)₂(C₆H₅). *J. Am. Chem. Soc.* **1981**, *103* (12), 3589-3590.
16. Crabtree, R. H., *The organometallic chemistry of the transition metals*. 2014.
17. Ephritikhine, M., Uranium carbene compounds. *C. R. Chim.* **2013**, *16* (4), 391-405.

18. Cramer, R. E.; Maynard, R. B.; Paw, J. C.; Gilje, J. W., Carbon monoxide insertion into a uranium carbon double bond. The structure of $(\eta^5\text{-C}_5\text{H}_5)_3\text{U}(\eta^2\text{-OCCH})\text{P}(\text{CH}_3)(\text{C}_6\text{H}_5)_2$. *Organometallics* **1982**, *1* (6), 869-871.
19. Cramer, R. E.; Jeong, J. H.; Gilje, J. W., Uranium-carbon multiple-bond chemistry. 9. The insertion of phenyl isocyanate into the uranium-carbon bond of $\text{Cp}^3\text{U}:\text{CHP}(\text{Ph})(\text{R})(\text{Me})$ to form $\text{Cp}^3\text{U}[(\text{NPh})(\text{O})\text{CCHP}(\text{Ph})(\text{R})(\text{Me})]$. *Organometallics* **1987**, *6* (9), 2010-2012.
20. Cramer, R. E.; Panchanatheswaran, K.; Gilje, J. W., Uranium carbon multiple-bond chemistry. 3. Insertion of acetonitrile and the formation of a uranium nitrogen multiple bond. *J. Am. Chem. Soc.* **1984**, *106* (6), 1853-1854.
21. Tourneux, J.-C.; Berthet, J.-C.; Thuery, P.; Mezailles, N.; Le Floch, P.; Ephritikhine, M., Easy access to uranium nucleophilic carbene complexes. *Dalton Trans.* **2010**, *39* (10), 2494-2496.
22. Cantat, T.; Arliguie, T.; Noël, A.; Thuéry, P.; Ephritikhine, M.; Floch, P. L.; Mézailles, N., The U=C Double Bond: Synthesis and Study of Uranium Nucleophilic Carbene Complexes. *J. Am. Chem. Soc.* **2009**, *131* (3), 963-972.
23. Mills, D. P.; Cooper, O. J.; Tuna, F.; McInnes, E. J. L.; Davies, E. S.; McMaster, J.; Moro, F.; Lewis, W.; Blake, A. J.; Liddle, S. T., Synthesis of a Uranium(VI)-Carbene: Reductive Formation of Uranyl(V)-Methanides, Oxidative Preparation of a $[\text{R}_2\text{C}=\text{U}=\text{O}]^{2+}$ Analogue of the $[\text{O}=\text{U}=\text{O}]^{2+}$ Uranyl Ion ($\text{R} = \text{Ph}_2\text{PNSiMe}_3$), and Comparison of the Nature of $\text{U}^{\text{IV}}=\text{C}$, $\text{U}^{\text{V}}=\text{C}$, and $\text{U}^{\text{VI}}=\text{C}$ Double Bonds. *J. Am. Chem. Soc.* **2012**, *134* (24), 10047-10054.

24. Cooper, O. J.; McMaster, J.; Lewis, W.; Blake, A. J.; Liddle, S. T., Synthesis and structure of $[U\{C(PPh_2NMe_3)_2\}_2]$ (Mes = 2,4,6-Me₃C₆H₂): A homoleptic uranium bis(carbene) complex with two formal U=C double bonds. *Dalton Trans.* **2010**, 39 (21), 5074-5076.
25. Ma, G.; Ferguson, M. J.; McDonald, R.; Cavell, R. G., Actinide Metals with Multiple Bonds to Carbon: Synthesis, Characterization, and Reactivity of U(IV) and Th(IV) Bis(iminophosphorano)methandiide Pincer Carbene Complexes. *Inorg. Chem.* **2011**, 50 (14), 6500-6508.
26. Smiles, D. E.; Wu, G.; Hrobárik, P.; Hayton, T. W., Synthesis, Thermochemistry, Bonding, and ¹³C NMR Chemical Shift Analysis of a Phosphorano-Stabilized Carbene of Thorium. *Organometallics* **2017**, 36 (23), 4519-4524.
27. Fortier, S.; Walensky, J. R.; Wu, G.; Hayton, T. W., Synthesis of a Phosphorano-Stabilized U(IV)-Carbene via One-Electron Oxidation of a U(III)-Ylide Adduct. *J. Am. Chem. Soc.* **2011**, 133 (18), 6894-6897.
28. Kiplinger, J. L.; Morris, D. E.; Scott, B. L.; Burns, C. J., Enhancing the reactivity of uranium(vi) organoimido complexes with diazoalkanes. *Chem. Commun.* **2002**, (1), 30-31.
29. Lam, O. P.; Feng, P. L.; Heinemann, F. W.; O'Connor, J. M.; Meyer, K., Charge-Separation in Uranium Diazomethane Complexes Leading to C-H Activation and Chemical Transformation. *J. Am. Chem. Soc.* **2008**, 130 (9), 2806-2816.
30. Wroblewski, D. A.; Ryan, R. R.; Wasserman, H. J.; Salazar, K. V.; Paine, R. T.; Moody, D. C., Synthesis and characterization of

- bis(diphenylphosphido)bis(pentamethylcyclopentadienyl)thorium(IV), $[(\eta^5\text{-C}_5(\text{CH}_3)_5)_2\text{Th}(\text{PPh}_2)_2]$. *Organometallics* **1986**, *5* (1), 90-94.
31. Blake, P. C.; Lappert, M. F.; Atwood, J. L.; Zhang, H., The synthesis and characterisation, including X-ray diffraction study, of $[\text{Th}\{\eta\text{-C}_5\text{H}_3(\text{SiMe}_3)_2\}_3]$; the first thorium(III) crystal structure. *J. Chem. Soc., Chem. Commun.* **1986**, (15), 1148-1149.
32. Ren, W.; Song, H.; Zi, G.; Walter, M. D., A bipyridyl thorium metallocene: synthesis, structure and reactivity. *Dalton Trans.* **2012**, *41* (19), 5965-5973.
33. Alonso, F.; Beletskaya, I. P.; Yus, M., Transition-Metal-Catalyzed Addition of Heteroatom-Hydrogen Bonds to Alkynes. *Chem. Rev.* **2004**, *104* (6), 3079-3160.
34. Daly, S. R.; Piccoli, P. M. B.; Schultz, A. J.; Todorova, T. K.; Gagliardi, L.; Girolami, G. S., Synthesis and Properties of a Fifteen-Coordinate Complex: The Thorium Aminodiboranate $[\text{Th}(\text{H}_3\text{BNMe}_2\text{BH}_3)_4]$. *Angew. Chem. Int. Ed.* **2010**, *49* (19), 3379-3381.
35. Anderson, N. H.; Odoh, S. O.; Yao, Y.; Williams, U. J.; Schaefer, B. A.; Kiernicki, J. J.; Lewis, A. J.; Goshert, M. D.; Fanwick, P. E.; Schelter, E. J.; Walensky, J. R.; Gagliardi, L.; Bart, S. C., Harnessing redox activity for the formation of uranium tris(imido) compounds. *Nat. Chem.* **2014**, *6* (10), 919-926.
36. Summerscales, O. T.; Cloke, F. G. N.; Hitchcock, P. B.; Green, J. C.; Hazari, N., Reductive Cyclotrimerization of Carbon Monoxide to the Deltate Dianion by an Organometallic Uranium Complex. *Science* **2006**, *311* (5762), 829-831.
37. Li, J.; Bursten, B. E.; Liang, B.; Andrews, L., Noble Gas-Actinide Compounds: Complexation of the CUO Molecule by Ar, Kr, and Xe Atoms in Noble Gas Matrices. *Science* **2002**, *295* (5563), 2242-2245.

38. Arnold, P. L.; Patel, D.; Wilson, C.; Love, J. B., Reduction and selective oxo group silylation of the uranyl dication. *Nature* **2008**, *451* (7176), 315-317.
39. Evans, W. J.; Miller, K. A.; DiPasquale, A. G.; Rheingold, A. L.; Stewart, T. J.; Bau, R., A Crystallizable f-Element Tuck-In Complex: The Tuck-in Tuck-over Uranium Metallocene [(C₅Me₅)U{μ-η⁵:η¹:η¹-C₅Me₃(CH₂)₂}(μ-H)₂U(C₅Me₅)₂]. *Angew. Chem. Int. Ed.* **2008**, *47* (27), 5075-5078.
40. Evans, W. J.; Montalvo, E.; Kozimor, S. A.; Miller, K. A., Multi-Electron Reduction from Alkyl/Hydride Ligand Combinations in U⁴⁺ Complexes. *J. Am. Chem. Soc.* **2008**, *130* (37), 12258-12259.
41. Gardner, B. M.; McMaster, J.; Lewis, W.; Blake, A. J.; Liddle, S. T., A Crystallizable Dinuclear Tuck-In-Tuck-Over Tuck-Over Dialkyl Tren Uranium Complex and Double Dearylation of BPh₄⁻ To Give the BPh₂-Functionalized Metallocycle [U{N(CH₂CH₂NSiMe₃)₂(CH₂CH₂NSiMe₂CHBPh₂)}(THF)]. *J. Am. Chem. Soc.* **2009**, *131* (30), 10388-10389.
42. Pagano, J. K.; Dorhout, J. M.; Waterman, R.; Czerwinski, K. R.; Kiplinger, J. L., Phenylsilane as a safe, versatile alternative to hydrogen for the synthesis of actinide hydrides. *Chem. Commun.* **2015**, *51* (98), 17379-17381.
43. Ephritikhine, M., Recent Advances in Organoactinide Chemistry As Exemplified by Cyclopentadienyl Compounds. *Organometallics* **2013**, *32* (9), 2464-2488.
44. Pool, J. A.; Scott, B. L.; Kiplinger, J. L., A New Mode of Reactivity for Pyridine N-Oxide: C-H Activation with Uranium(IV) and Thorium(IV) Bis(alkyl) Complexes. *J. Am. Chem. Soc.* **2005**, *127* (5), 1338-1339.

45. Haskel, A.; Straub, T.; Eisen, M. S., Organoactinide-Catalyzed Intermolecular Hydroamination of Terminal Alkynes. *Organometallics* **1996**, *15* (18), 3773-3775.
46. Tourneux, J.-C.; Berthet, J.-C.; Cantat, T.; Thuéry, P.; Mézailles, N.; Ephritikhine, M., Exploring the Uranyl Organometallic Chemistry: From Single to Double Uranium–Carbon Bonds. *J. Am. Chem. Soc.* **2011**, *133* (16), 6162-6165.
47. Tourneux, J.-C.; Berthet, J.-C.; Cantat, T.; Thuéry, P.; Mézailles, N.; Le Floch, P.; Ephritikhine, M., Uranium(IV) Nucleophilic Carbene Complexes. *Organometallics* **2011**, *30* (11), 2957-2971.
48. Lu, E.; Cooper, O. J.; McMaster, J.; Tuna, F.; McInnes, E. J. L.; Lewis, W.; Blake, A. J.; Liddle, S. T., Synthesis, Characterization, and Reactivity of a Uranium(VI) Carbene Imido Oxo Complex. *Angew. Chem. Int. Ed.* **2014**, *53* (26), 6696-6700.
49. Lu, E.; Lewis, W.; Blake, A. J.; Liddle, S. T., The Ketimide Ligand is Not Just an Inert Spectator: Heteroallene Insertion Reactivity of an Actinide–Ketimide Linkage in a Thorium Carbene Amide Ketimide Complex. *Angew. Chem. Int. Ed.* **2014**, *53* (35), 9356-9359.
50. Gregson, M.; Lu, E.; Mills, D. P.; Tuna, F.; McInnes, E. J. L.; Hennig, C.; Scheinost, A. C.; McMaster, J.; Lewis, W.; Blake, A. J.; Kerridge, A.; Liddle, S. T., The inverse-trans-influence in tetravalent lanthanide and actinide bis(carbene) complexes. *Nat. Commun.* **2017**, *8*, 14137.
51. Cooper, O. J.; Mills, D. P.; McMaster, J.; Moro, F.; Davies, E. S.; Lewis, W.; Blake, A. J.; Liddle, S. T., Uranium–Carbon Multiple Bonding: Facile Access to the Pentavalent Uranium Carbene $[U\{C(PPh_2NSiMe_3)_2\}(Cl)_2(I)]$ and Comparison of $U^V=C$ and $U^{IV}=C$ Bonds. *Angew. Chem. Int. Ed.* **2011**, *50* (10), 2383-2386.

52. Lu, E.; Cooper, O. J.; Tuna, F.; Wooles, A. J.; Kaltsoyannis, N.; Liddle, S. T., Uranium–Carbene–Imido Metalla-Allenenes: Ancillary-Ligand-Controlled cis-/trans-Isomerisation and Assessment of trans Influence in the $R_2C=U^{IV}=NR'$ Unit ($R=Ph_2PNSiMe_3$; $R'=CPh_3$). *Chem. Eur. J.* **2016**, *22* (33), 11559-11563.
53. Lu, E.; Tuna, F.; Lewis, W.; Kaltsoyannis, N.; Liddle, S. T., Uranium Metalla-Allenenes with Carbene Imido $R_2C=U^{IV}=NR'$ Units ($R=Ph_2PNSiMe_3$; $R'=CPh_3$): Alkali-Metal-Mediated Push–Pull Effects with an Amido Auxiliary. *Chem. Eur. J.* **2016**, *22* (33), 11554-11558.
54. Cooper, O. J.; Mills, D. P.; McMaster, J.; Tuna, F.; McInnes, E. J. L.; Lewis, W.; Blake, A. J.; Liddle, S. T., The Nature of the U=C Double Bond: Pushing the Stability of High-Oxidation-State Uranium Carbenes to the Limit. *Chem. Eur. J.* **2013**, *19* (22), 7071-7083.
55. Levine, D. S.; Tilley, T. D.; Andersen, R. A., Evidence for the Existence of Group 3 Terminal Methylidene Complexes. *Organometallics* **2017**, *36* (1), 80-88.
56. Cramer, R. E.; Maynard, R. B.; Paw, J. C.; Gilje, J. W., Crystal and molecular structure of $(\eta^5-C_5H_5)_3U = CHP(CH_3)_2(C_6H_5)$. A compound with a uranium-carbon multiple bond. *Organometallics* **1983**, *2* (10), 1336-1340.
57. Fulmer, G. R.; Miller, A. J. M.; Sherden, N. H.; Gottlieb, H. E.; Nudelman, A.; Stoltz, B. M.; Bercaw, J. E.; Goldberg, K. I., NMR Chemical Shifts of Trace Impurities: Common Laboratory Solvents, Organics, and Gases in Deuterated Solvents Relevant to the Organometallic Chemist. *Organometallics* **2010**, *29* (9), 2176-2179.
58. Suite, A., *Bruker AXS Inc.* **2007**, *Madison, Wisconsin, USA, 2007*.

59. Sheldrick, G., A short history of SHELX. *Acta Crystallogr. A* **2008**, *64* (1), 112-122.
60. Dolomanov, O. V.; Bourhis, L. J.; Gildea, R. J.; Howard, J. A. K.; Puschmann, H., OLEX2: a complete structure solution, refinement and analysis program. *J. Appl. Cryst.* **2009**, *42* (2), 339-341.
61. Frisch, M. J.; Trucks, G. W.; Schlegel, H. B.; Scuseria, G. E.; Robb, M. A.; Cheeseman, J. R.; Scalmani, G.; Barone, V.; Petersson, G. A.; Nakatsuji, H.; Li, X.; Caricato, M.; Marenich, A. V.; Bloino, J.; Janesko, B. G.; Gomperts, R.; Mennucci, B.; Hratchian, H. P.; Ortiz, J. V.; Izmaylov, A. F.; Sonnenberg, J. L.; Williams; Ding, F.; Lipparini, F.; Egidi, F.; Goings, J.; Peng, B.; Petrone, A.; Henderson, T.; Ranasinghe, D.; Zakrzewski, V. G.; Gao, J.; Rega, N.; Zheng, G.; Liang, W.; Hada, M.; Ehara, M.; Toyota, K.; Fukuda, R.; Hasegawa, J.; Ishida, M.; Nakajima, T.; Honda, Y.; Kitao, O.; Nakai, H.; Vreven, T.; Throssell, K.; Montgomery Jr., J. A.; Peralta, J. E.; Ogliaro, F.; Bearpark, M. J.; Heyd, J. J.; Brothers, E. N.; Kudin, K. N.; Staroverov, V. N.; Keith, T. A.; Kobayashi, R.; Normand, J.; Raghavachari, K.; Rendell, A. P.; Burant, J. C.; Iyengar, S. S.; Tomasi, J.; Cossi, M.; Millam, J. M.; Klene, M.; Adamo, C.; Cammi, R.; Ochterski, J. W.; Martin, R. L.; Morokuma, K.; Farkas, O.; Foresman, J. B.; Fox, D. J. *Gaussian 16*, Wallingford, CT, 2016.
62. Moritz, A.; Cao, X.; Dolg, M., Quasirelativistic energy-consistent 5f-in-core pseudopotentials for divalent and tetravalent actinide elements. *Theor. Chem. Acc.* **2007**, *118* (5), 845-854.

63. Hehre, W. J.; Ditchfield, R.; Pople, J. A., Self—Consistent Molecular Orbital Methods. XII. Further Extensions of Gaussian—Type Basis Sets for Use in Molecular Orbital Studies of Organic Molecules. *J. Chem. Phys.* **1972**, *56* (5), 2257-2261.
64. Bergner, A.; Dolg, M.; Küchle, W.; Stoll, H.; Preuß, H., Ab initio energy-adjusted pseudopotentials for elements of groups 13–17. *Mol. Phys.* **1993**, *80* (6), 1431-1441.
65. Martin, J. M. L.; Sundermann, A., Correlation consistent valence basis sets for use with the Stuttgart–Dresden–Bonn relativistic effective core potentials: The atoms Ga–Kr and In–Xe. *J. Chem. Phys.* **2001**, *114* (8), 3408-3420.
66. Becke, A. D., Density-functional thermochemistry. III. The role of exact exchange. *J. Chem. Phys.* **1993**, *98* (7), 5648-5652.
67. Dobson, J. F.; Vignale, G.; Das, M. P., *Electronic Density Functional Theory: Recent Progress and New Directions*. Springer US: 1998.
68. Reed, A. E.; Curtiss, L. A.; Weinhold, F., Intermolecular interactions from a natural bond orbital, donor-acceptor viewpoint. *Chem. Rev.* **1988**, *88* (6), 899-926.
69. Scharf, L. T.; Gessner, V. H., Metalated Ylides: A New Class of Strong Donor Ligands with Unique Electronic Properties. *Inorg. Chem.* **2017**.
70. Lu, E.; Cooper, O. J.; McMaster, J.; Tuna, F.; McInnes, E. J. L.; Lewis, W.; Blake, A. J.; Liddle, S. T., Synthesis, Characterization, and Reactivity of a Uranium(VI) Carbene Imido Oxo Complex. *Angew. Chem. Int. Ed.* **2014**, *126* (26), 6814-6818.
71. Lu, E.; Cooper, O. J.; Tuna, F.; Wooles, A. J.; Kaltsoyannis, N.; Liddle, S. T., Uranium–Carbene–Imido Metalla-Allenenes: Ancillary-Ligand-Controlled cis-/trans-Isomerisation and Assessment of trans Influence in the $R_2C=U^{IV}=NR'$ Unit (R=Ph₂PNSiMe₃; R'=CPh₃). *Chem. Eur. J.* **2016**, *22* (33), 11559-11563.

72. Lu, E.; Tuna, F.; Lewis, W.; Kaltsoyannis, N.; Liddle, S. T., Uranium Metalla-Allenenes with Carbene Imido $R_2C=U^{IV}=NR'$ Units ($R=Ph_2PNSiMe_3$; $R'=CPh_3$): Alkali-Metal-Mediated Push–Pull Effects with an Amido Auxiliary. *Chem. Eur. J.* **2016**, *22* (33), 11554-11558.
73. Cooper, O. J.; Mills, D. P.; McMaster, J.; Tuna, F.; McInnes, E. J. L.; Lewis, W.; Blake, A. J.; Liddle, S. T., The Nature of the U=C Double Bond: Pushing the Stability of High-Oxidation-State Uranium Carbenes to the Limit. *Chem. Eur. J.* **2013**, *19* (22), 7071-7083.
74. Ren, W.; Zi, G.; Walter, M. D., Synthesis, Structure, and Reactivity of a Thorium Metallocene Containing a 2,2'-Bipyridyl Ligand. *Organometallics* **2012**, *31* (2), 672-679.
75. Rabinovich, D.; Schimek, G. L.; Pennington, W. T.; Nielsen, J. B.; Abney, K. D., Dibromobis(η^5 -pentamethylcyclopentadienyl)thorium(IV). *Acta Crystallogr. C* **1997**, *53* (12), 1794-1797.
76. Mrutu, A.; Barnes, C. L.; Bart, S. C.; Walensky, J. R., Bringing Redox Reactivity to a Redox Inactive Metal Center – E–I (E = C, Si) Bond Cleavage with a Thorium Bis(α -diimine) Complex. *Eur. J. Inorg. Chem.* **2013**, *2013* (22-23), 4050-4055.
77. Castro, L.; Yahia, A.; Maron, L., Are 5f Electrons Really Active in Organoactinide Reactivity? Some Insights from DFT Studies. *ChemPhysChem* **2010**, *11* (5), 990-994.
78. Castro, L.; Yahia, A.; Maron, L., A DFT study of the reactivity of actinidocenes (U, Np and Pu) with pyridine and pyridine N-oxide derivatives. *Dalton Trans.* **2010**, *39* (29), 6682-6692.

79. Jantunen, K. C.; Burns, C. J.; Castro-Rodriguez, I.; Da Re, R. E.; Golden, J. T.; Morris, D. E.; Scott, B. L.; Taw, F. L.; Kiplinger, J. L., Thorium(IV) and Uranium(IV) Ketimide Complexes Prepared by Nitrile Insertion into Actinide–Alkyl and –Aryl Bonds. *Organometallics* **2004**, *23* (20), 4682-4692.
80. Behrle, A. C.; Castro, L.; Maron, L.; Walensky, J. R., Formation of a Bridging Phosphinidene Thorium Complex. *J. Am. Chem. Soc.* **2015**, *137* (47), 14846-14849.
81. Seyferth, D.; Hughes, W. B.; Heeren, J. K., Studies in Phosphinemethylene Chemistry. X. The Reaction of Organolithium Reagents with Alkyltriphenylphosphonium Halides. The Mechanism of Phosphinemethylene Formation¹. *J. Am. Chem. Soc.* **1965**, *87* (13), 2847-2854.
82. Hayton, T. W., Recent developments in actinide-ligand multiple bonding. *Chem. Commun.* **2013**, *49* (29), 2956-2973.
83. Neidig, M. L.; Clark, D. L.; Martin, R. L., Covalency in f-element complexes. *Coord. Chem. Rev.* **2013**, *257* (2), 394-406.
84. Vitova, T.; Pidchenko, I.; Fellhauer, D.; Bagus, P. S.; Joly, Y.; Pruessmann, T.; Bahl, S.; Gonzalez-Robles, E.; Rothe, J.; Altmaier, M.; Denecke, M. A.; Geckeis, H., The role of the 5f valence orbitals of early actinides in chemical bonding. *Nat. Commun.* **2017**, *8*, 16053.
85. Rungthanaphatsophon, P.; Bathelier, A.; Castro, L.; Behrle, A. C.; Barnes, C. L.; Maron, L.; Walensky, J. R., Formation of Methane versus Benzene in the Reactions of $(C_5Me_5)_2Th(CH_3)_2$ with $[CH_3PPh_3]X$ (X=Cl, Br, I) Yielding Thorium-Carbene or Thorium-Ylide Complexes. *Angew. Chem. Int. Ed.* **2017**, *56* (42), 12925-12929.

86. Mao, W.; Xiang, L.; Maron, L.; Leng, X.; Chen, Y., Nonchelated Phosphoniomethylidene Complexes of Scandium and Lutetium. *J. Am. Chem. Soc.* **2017**, *139* (49), 17759-17762.
87. Cary, S. K.; Vasiliu, M.; Baumbach, R. E.; Stritzinger, J. T.; Green, T. D.; Diefenbach, K.; Cross, J. N.; Knappenberger, K. L.; Liu, G.; Silver, M. A.; DePrince, A. E.; Polinski, M. J.; Van Cleve, S. M.; House, J. H.; Kikugawa, N.; Gallagher, A.; Arico, A. A.; Dixon, D. A.; Albrecht-Schmitt, T. E., Emergence of californium as the second transitional element in the actinide series. *Nat. Commun.* **2015**, *6*, 6827.
88. Silver, M. A.; Cary, S. K.; Stritzinger, J. T.; Parker, T. G.; Maron, L.; Albrecht-Schmitt, T. E., Covalency-Driven Dimerization of Plutonium(IV) in a Hydroxamate Complex. *Inorg. Chem.* **2016**, *55* (11), 5092-5094.
89. Jones, M. B.; Gaunt, A. J.; Gordon, J. C.; Kaltsoyannis, N.; Neu, M. P.; Scott, B. L., Uncovering f-element bonding differences and electronic structure in a series of 1 : 3 and 1 : 4 complexes with a diselenophosphinate ligand. *Chem. Sci.* **2013**, *4* (3), 1189-1203.
90. Ingram, K. I. M.; Tassell, M. J.; Gaunt, A. J.; Kaltsoyannis, N., Covalency in the f Element–Chalcogen Bond. Computational Studies of $M[N(EPR_2)_2]_3$ ($M = La, Ce, Pr, Pm, Eu, U, Np, Pu, Am, Cm$; $E = O, S, Se, Te$; $R = H, iPr, Ph$). *Inorg. Chem.* **2008**, *47* (17), 7824-7833.
91. Gaunt, A. J.; Reilly, S. D.; Enriquez, A. E.; Scott, B. L.; Ibers, J. A.; Sekar, P.; Ingram, K. I. M.; Kaltsoyannis, N.; Neu, M. P., Experimental and Theoretical Comparison of Actinide and Lanthanide Bonding in $M[N(EPR_2)_2]_3$ Complexes ($M = U, Pu, La, Ce$; $E = S, Se, Te$; $R = Ph, iPr, H$). *Inorg. Chem.* **2008**, *47* (1), 29-41.

92. Kelley, M. P.; Su, J.; Urban, M.; Luckey, M.; Batista, E. R.; Yang, P.; Shafer, J. C., On the Origin of Covalent Bonding in Heavy Actinides. *J. Am. Chem. Soc.* **2017**, *139* (29), 9901-9908.
93. Behrle, A. C.; Barnes, C. L.; Kaltsoyannis, N.; Walensky, J. R., Systematic Investigation of Thorium(IV)- and Uranium(IV)-Ligand Bonding in Dithiophosphonate, Thioselenophosphinate, and Diselenophosphonate Complexes. *Inorg. Chem.* **2013**, *52* (18), 10623-10631.
94. Clark, A. E.; Martin, R. L.; Hay, P. J.; Green, J. C.; Jantunen, K. C.; Kiplinger, J. L., Electronic Structure, Excited States, and Photoelectron Spectra of Uranium, Thorium, and Zirconium Bis(Ketimido) Complexes $(C_5R_5)_2M[-NCPH_2]_2$ (M = Th, U, Zr; R = H, CH₃). *J. Phys. Chem. A* **2005**, *109* (24), 5481-5491.
95. Hilton, D. J.; Prasankumar, R. P.; Schelter, E. J.; Thorsmølle, V. K.; Trugman, S. A.; Shreve, A. P.; Kiplinger, J. L.; Morris, D. E.; Taylor, A. J., Ultrafast Spectroscopy of the Uranium(IV) and Thorium(IV) Bis(ketimido) Complexes $(C_5Me_5)_2An[-N=C(Ph)(CH_2Ph)]_2$ (An = Th, U). *J. Phys. Chem. A* **2008**, *112* (34), 7840-7847.
96. Da Re, R. E.; Jantunen, K. C.; Golden, J. T.; Kiplinger, J. L.; Morris, D. E., Molecular Spectroscopy of Uranium(IV) Bis(ketimido) Complexes. Rare Observation of Resonance-Enhanced Raman Scattering from Organoactinide Complexes and Evidence for Broken-Symmetry Excited States. *J. Am. Chem. Soc.* **2005**, *127* (2), 682-689.
97. Cantat, T.; Graves, C. R.; Jantunen, K. C.; Burns, C. J.; Scott, B. L.; Schelter, E. J.; Morris, D. E.; Hay, P. J.; Kiplinger, J. L., Evidence for the Involvement of 5f Orbitals in the Bonding and Reactivity of Organometallic Actinide Compounds: Thorium(IV) and

Uranium(IV) Bis(hydrazonato) Complexes. *J. Am. Chem. Soc.* **2008**, *130* (51), 17537-17551.

98. Lukens, W. W.; Edelstein, N. M.; Magnani, N.; Hayton, T. W.; Fortier, S.; Seaman, L. A., Quantifying the σ and π Interactions between U(V) f Orbitals and Halide, Alkyl, Alkoxide, Amide and Ketimide Ligands. *J. Am. Chem. Soc.* **2013**, *135* (29), 10742-10754.

99. Minasian, S. G.; Keith, J. M.; Batista, E. R.; Boland, K. S.; Clark, D. L.; Kozimor, S. A.; Martin, R. L.; Shuh, D. K.; Tylliszczak, T., New evidence for 5f covalency in actinocenes determined from carbon K-edge XAS and electronic structure theory. *Chem. Sci.* **2014**, *5* (1), 351-359.

100. Minasian, S. G.; Keith, J. M.; Batista, E. R.; Boland, K. S.; Kozimor, S. A.; Martin, R. L.; Shuh, D. K.; Tylliszczak, T.; Vernon, L. J., Carbon K-Edge X-ray Absorption Spectroscopy and Time-Dependent Density Functional Theory Examination of Metal–Carbon Bonding in Metallocene Dichlorides. *J. Am. Chem. Soc.* **2013**, *135* (39), 14731-14740.

101. Minasian, S. G.; Keith, J. M.; Batista, E. R.; Boland, K. S.; Clark, D. L.; Conradson, S. D.; Kozimor, S. A.; Martin, R. L.; Schwarz, D. E.; Shuh, D. K.; Wagner, G. L.; Wilkerson, M. P.; Wolfsberg, L. E.; Yang, P., Determining Relative f and d Orbital Contributions to M–Cl Covalency in MCl_6^{2-} (M = Ti, Zr, Hf, U) and $UOCl_5^-$ Using Cl K-Edge X-ray Absorption Spectroscopy and Time-Dependent Density Functional Theory. *J. Am. Chem. Soc.* **2012**, *134* (12), 5586-5597.

102. Kozimor, S. A.; Yang, P.; Batista, E. R.; Boland, K. S.; Burns, C. J.; Clark, D. L.; Conradson, S. D.; Martin, R. L.; Wilkerson, M. P.; Wolfsberg, L. E., Trends in

Covalency for d- and f-Element Metallocene Dichlorides Identified Using Chlorine K-Edge X-ray Absorption Spectroscopy and Time-Dependent Density Functional Theory. *J. Am. Chem. Soc.* **2009**, *131* (34), 12125-12136.

103. Formanuk, A.; Ariciu, A.-M.; Ortu, F.; Beekmeyer, R.; Kerridge, A.; Tuna, F.; McInnes, E. J. L.; Mills, D. P., Actinide covalency measured by pulsed electron paramagnetic resonance spectroscopy. *Nat. Chem.* **2016**, *9*, 578.

104. Smiles, D. E.; Wu, G.; Hrobárik, P.; Hayton, T. W., Use of ^{77}Se and ^{125}Te NMR Spectroscopy to Probe Covalency of the Actinide-Chalcogen Bonding in $[\text{Th}(\text{E}_n)\{\text{N}(\text{SiMe}_3)_2\}_3]^-$ (E = Se, Te; n = 1, 2) and Their Oxo-Uranium(VI) Congeners. *J. Am. Chem. Soc.* **2016**, *138* (3), 814-825.

105. Bader, R. F. W., *Atoms in molecules : a quantum theory*. Clarendon: Oxford, 2003.

106. Wellington, J. P. W.; Kerridge, A.; Kaltsoyannis, N., Should environmental effects be included when performing QTAIM calculations on actinide systems? A comparison of QTAIM metrics for $\text{Cs}_2\text{UO}_2\text{Cl}_4$, $\text{U}(\text{Se}_2\text{PPh}_2)_4$ and $\text{Np}(\text{Se}_2\text{PPh}_2)_4$ in gas phase, COSMO and PEECM. *Polyhedron* **2016**, *116*, 57-63.

107. Huang, Q.-R.; Kingham, J. R.; Kaltsoyannis, N., The strength of actinide-element bonds from the quantum theory of atoms-in-molecules. *Dalton Trans.* **2015**, *44* (6), 2554-2566.

108. te Velde, G.; Bickelhaupt, F. M.; Baerends, E. J.; Fonseca Guerra, C.; van Gisbergen, S. J. A.; Snijders, J. G.; Ziegler, T., Chemistry with ADF. *J. Comput. Chem.* **2001**, *22* (9), 931-967.

109. Lenthe, E. v.; Baerends, E. J.; Snijders, J. G., Relativistic regular two-component Hamiltonians. *J. Chem. Phys.* **1993**, *99* (6), 4597-4610.
110. Lenthe, E. v.; Baerends, E. J.; Snijders, J. G., Relativistic total energy using regular approximations. *J. Chem. Phys.* **1994**, *101* (11), 9783-9792.
111. Lenthe, E. v.; Ehlers, A.; Baerends, E.-J., Geometry optimizations in the zero order regular approximation for relativistic effects. *J. Chem. Phys.* **1999**, *110* (18), 8943-8953.
112. Van Lenthe, E.; Baerends, E. J., Optimized Slater-type basis sets for the elements 1–118. *J. Comput. Chem.* **2003**, *24* (9), 1142-1156.
113. Glendening, E. D.; Landis, C. R.; Weinhold, F., NBO 6.0: Natural bond orbital analysis program. *J. Comput. Chem.* **2013**, *34* (16), 1429-1437.
114. Evans, W. J.; Walensky, J. R.; Ziller, J. W., Reactivity of Methyl Groups in Actinide Metallocene Amidinate and Triazenido Complexes with Silver and Copper Salts. *Organometallics* **2010**, *29* (1), 101-107.
115. Behrle, A. C.; Kerridge, A.; Walensky, J. R., Dithio- and Diselenophosphate Thorium(IV) and Uranium(IV) Complexes: Molecular and Electronic Structures, Spectroscopy, and Transmetalation Reactivity. *Inorg. Chem.* **2015**, *54* (24), 11625-11636.
116. Ren, W.; Deng, X.; Zi, G.; Fang, D.-C., The Th=C double bond: an experimental and computational study of thorium poly-carbene complexes. *Dalton Trans.* **2011**, *40* (38), 9662-9664.
117. Trnka, T. M.; Bonanno, J. B.; Bridgewater, B. M.; Parkin, G., Bis(permethyindenyl) Complexes of Thorium: Synthesis, Structure, and Reactivity. *Organometallics* **2001**, *20* (15), 3255-3264.

118. Spirlet, M. R.; Rebizant, J.; Apostolidis, C.; Kanellakopoulos, B., Bis(cyclopentadienyl) actinide(IV) compounds. I. The structure of dichlorobis(pentamethyl- η^5 -cyclopentadienyl)uranium(IV) and dichlorobis(pentamethyl- η^5 -cyclopentadienyl)thorium(IV). *Acta Crystallogr. C* **1992**, *48* (12), 2135-2137.
119. Söderlind, P.; Eriksson, O.; Johansson, B.; Wills, J. M., Electronic properties of f-electron metals using the generalized gradient approximation. *Phys. Rev. B* **1994**, *50* (11), 7291-7294.
120. Erker, G.; Czisch, P.; Mynott, R.; Tsay, Y. H.; Krueger, C., Reaction of zirconocene complexes with phosphorous ylides: evidence for the formation of $\text{Cp}_2\text{Zr}(\text{C}_6\text{H}_5)\text{CHPPh}_3$ from diphenylzirconocene and CH_2PPh_3 by an aryne mechanism. *Organometallics* **1985**, *4* (7), 1310-1312.
121. Hunter, W. E.; Hrcir, D. C.; Bynum, R. V.; Penttila, R. A.; Atwood, J. L., The search for dimethylzirconocene. Crystal structures of dimethylzirconocene, dimethylhafnocene, chloromethylzirconocene, and (μ -oxo)bis(methylzirconocene). *Organometallics* **1983**, *2* (6), 750-755.
122. Bruno, J. W.; Smith, G. M.; Marks, T. J.; Fair, C. K.; Schultz, A. J.; Williams, J. M., Carbon-hydrogen activation mechanisms and regioselectivity in the cyclometalation reactions of bis(pentamethylcyclopentadienyl)thorium dialkyl complexes. *J. Am. Chem. Soc.* **1986**, *108* (1), 40-56.
123. Seaman, L. A.; Walensky, J. R.; Wu, G.; Hayton, T. W., In Pursuit of Homoleptic Actinide Alkyl Complexes. *Inorg. Chem.* **2013**, *52* (7), 3556-3564.

124. Fraenkel, G.; Chow, A.; Winchester, W. R., Structure and dynamic behavior of solvated neopentyl lithium monomers, dimers, and tetramers: proton, carbon-13 and lithium-6 NMR. *J. Am. Chem. Soc.* **1990**, *112* (17), 6190-6198.
125. Fortier, S.; Melot, B. C.; Wu, G.; Hayton, T. W., Homoleptic Uranium(IV) Alkyl Complexes: Synthesis and Characterization. *J. Am. Chem. Soc.* **2009**, *131* (42), 15512-15521.
126. Arnold, P. L., Uranium-mediated activation of small molecules. *Chem. Commun.* **2011**, *47* (32), 9005-9010.
127. Anderson, N. H.; Odoh, S. O.; Yao, Y.; Williams, U. J.; Schaefer, B. A.; Kiernicki, J. J.; Lewis, A. J.; Goshert, M. D.; Fanwick, P. E.; Schelter, E. J.; Walensky, J. R.; Gagliardi, L.; Bart, S. C., Harnessing redox activity for the formation of uranium tris(imido) compounds. *Nature Chemistry* **2014**, *6*, 919.
128. Evans, W. J.; Kozimor, S. A.; Ziller, J. W., Molecular Octa-Uranium Rings with Alternating Nitride and Azide Bridges. *Science* **2005**, *309* (5742), 1835-1838.
129. Mullane, K. C.; Lewis, A. J.; Yin, H.; Carroll, P. J.; Schelter, E. J., Anomalous One-Electron Processes in the Chemistry of Uranium Nitrogen Multiple Bonds. *Inorg. Chem.* **2014**, *53* (17), 9129-9139.
130. Wildman, E. P.; Balázs, G.; Wooles, A. J.; Scheer, M.; Liddle, S. T., Thorium–phosphorus triamidoamine complexes containing Th–P single- and multiple-bond interactions. *Nat. Commun.* **2016**, *7*, 12884.
131. Ren, W.; Zi, G.; Fang, D.-C.; Walter, M. D., Thorium Oxo and Sulfido Metallocenes: Synthesis, Structure, Reactivity, and Computational Studies. *J. Am. Chem. Soc.* **2011**, *133* (33), 13183-13196.

132. Smiles, D. E.; Wu, G.; Kaltsoyannis, N.; Hayton, T. W., Thorium-ligand multiple bonds via reductive deprotection of a trityl group. *Chem. Sci.* **2015**, *6* (7), 3891-3899.
133. Vilanova, S. P.; Alayoglu, P.; Heidarian, M.; Huang, P.; Walensky, J. R., Metal–Ligand Multiple Bonding in Thorium Phosphorus and Thorium Arsenic Complexes. *Chem. Eur. J.* **2017**, *23* (66), 16748-16752.
134. King, D. M.; Tuna, F.; McInnes, E. J. L.; McMaster, J.; Lewis, W.; Blake, A. J.; Liddle, S. T., Synthesis and Structure of a Terminal Uranium Nitride Complex. *Science* **2012**, *337* (6095), 717-720.
135. Hayton, T. W.; Boncella, J. M.; Scott, B. L.; Palmer, P. D.; Batista, E. R.; Hay, P. J., Synthesis of Imido Analogs of the Uranyl Ion. *Science* **2005**, *310* (5756), 1941-1943.
136. Graves, C. R.; Scott, B. L.; Morris, D. E.; Kiplinger, J. L., Facile Access to Pentavalent Uranium Organometallics: One-Electron Oxidation of Uranium(IV) Imido Complexes with Copper(I) Salts. *J. Am. Chem. Soc.* **2007**, *129* (39), 11914-11915.
137. Spencer, L. P.; Yang, P.; Scott, B. L.; Batista, E. R.; Boncella, J. M., Uranium(VI) Bis(imido) Chalcogenate Complexes: Synthesis and Density Functional Theory Analysis. *Inorg. Chem.* **2009**, *48* (6), 2693-2700.
138. Hayton, T. W.; Boncella, J. M.; Scott, B. L.; Batista, E. R.; Hay, P. J., Synthesis and Reactivity of the Imido Analogues of the Uranyl Ion. *J. Am. Chem. Soc.* **2006**, *128* (32), 10549-10559.
139. Bell, N. L.; Maron, L.; Arnold, P. L., Thorium Mono- and Bis(imido) Complexes Made by Reprotonation of cyclo-Metalated Amides. *J. Am. Chem. Soc.* **2015**, *137* (33), 10492-10495.

140. Kiernicki, J. J.; Ferrier, M. G.; Lezama Pacheco, J. S.; La Pierre, H. S.; Stein, B. W.; Zeller, M.; Kozimor, S. A.; Bart, S. C., Examining the Effects of Ligand Variation on the Electronic Structure of Uranium Bis(imido) Species. *J. Am. Chem. Soc.* **2016**, *138* (42), 13941-13951.
141. Warner, B. P.; Scott, B. L.; Burns, C. J., A Simple Preparative Route to Bis(imido)uranium(VI) Complexes by the Direct Reductions of Diazenes and Azides. *Angew. Chem. Int. Ed.* **1998**, *37* (7), 959-960.
142. Evans, W. J.; Traina, C. A.; Ziller, J. W., Synthesis of Heteroleptic Uranium ($\mu\text{-}\eta^6\text{:}\eta^6\text{-C}_6\text{H}_6\text{)}^{2-}$ Sandwich Complexes via Facile Displacement of $(\eta^5\text{-C}_5\text{Me}_5)^{1-}$ by Ligands of Lower Hapticity and Their Conversion to Heteroleptic Bis(imido) Compounds. *J. Am. Chem. Soc.* **2009**, *131* (47), 17473-17481.
143. Arney, D. S. J.; Burns, C. J.; Smith, D. C., Synthesis and structure of the first uranium(VI) organometallic complex. *J. Am. Chem. Soc.* **1992**, *114* (25), 10068-10069.
144. Arney, D. S. J.; Burns, C. J., Synthesis and structure of high-valent organouranium complexes containing terminal monooxo functional groups. *J. Am. Chem. Soc.* **1993**, *115* (21), 9840-9841.
145. Arney, D. S. J.; Burns, C. J., Synthesis and Properties of High-Valent Organouranium Complexes Containing Terminal Organoimido and Oxo Functional Groups. A New Class of Organo-f-Element Complexes. *J. Am. Chem. Soc.* **1995**, *117* (37), 9448-9460.
146. Jilek, R. E.; Tomson, N. C.; Shook, R. L.; Scott, B. L.; Boncella, J. M., Preparation and Reactivity of the Versatile Uranium(IV) Imido Complexes

U(NAr)Cl₂(R₂bpy)₂ (R = Me, tBu) and U(NAr)Cl₂(tppo)₃. *Inorg. Chem.* **2014**, *53* (18), 9818-9826.

147. Jilek, R. E.; Spencer, L. P.; Kuiper, D. L.; Scott, B. L.; Williams, U. J.; Kikkawa, J. M.; Schelter, E. J.; Boncella, J. M., A General and Modular Synthesis of Monoimidouranium(IV) Dihalides. *Inorg. Chem.* **2011**, *50* (10), 4235-4237.

148. Jilek, R. E.; Spencer, L. P.; Lewis, R. A.; Scott, B. L.; Hayton, T. W.; Boncella, J. M., A Direct Route to Bis(imido)uranium(V) Halides via Metathesis of Uranium Tetrachloride. *J. Am. Chem. Soc.* **2012**, *134* (24), 9876-9878.

149. Evans, W. J.; Kozimor, S. A.; Ziller, J. W., [(C₅Me₅)₂U][(μ -Ph)₂BPh₂] as a four electron reductant. *Chem. Commun.* **2005**, (37), 4681-4683.

150. Kraft, S. J.; Fanwick, P. E.; Bart, S. C., Carbon–Carbon Reductive Elimination from Homoleptic Uranium(IV) Alkyls Induced by Redox-Active Ligands. *J. Am. Chem. Soc.* **2012**, *134* (14), 6160-6168.

151. Evans, W. J.; Davis, B. L., Chemistry of Tris(pentamethylcyclopentadienyl) f-Element Complexes, (C₅Me₅)₃M. *Chem. Rev.* **2002**, *102* (6), 2119-2136.

152. Garner, M. E.; Arnold, J., Reductive Elimination of Diphosphine from a Thorium–NHC–Bis(phosphido) Complex. *Organometallics* **2017**, *36* (23), 4511-4514.

153. Gaunt, A. J.; Scott, B. L.; Neu, M. P., Homoleptic uranium(III) imidodiphosphinochalcogenides including the first structurally characterised molecular trivalent actinide-Se bond. *Chem. Commun.* **2005**, (25), 3215-3217.

154. Gaunt, A. J.; Scott, B. L.; Neu, M. P., A Molecular Actinide–Tellurium Bond and Comparison of Bonding in [M^{III}{N(TePiPr₂)₂}₃] (M=U, La). *Angew. Chem. Int. Ed.* **2006**, *45* (10), 1638-1641.

155. Ingram, K. I. M.; Kaltsoyannis, N.; Gaunt, A. J.; Neu, M. P., Covalency in the f-element–chalcogen bond: Computational studies of $[M(N(EPH_2)_2)_3]$ ($M = La, U, Pu$; $E = O, S, Se, Te$). *J. Alloys Compd.* **2007**, *444-445*, 369-375.
156. Roger, M.; Barros, N.; Arliguie, T.; Thuéry, P.; Maron, L.; Ephritikhine, M., $U(SMes^*)_n$, ($n = 3, 4$) and $Ln(SMes^*)_3$ ($Ln = La, Ce, Pr, Nd$): Lanthanide(III)/Actinide(III) Differentiation in Agostic Interactions and an Unprecedented η^3 Ligation Mode of the Arylthiolate Ligand, from X-ray Diffraction and DFT Analysis. *J. Am. Chem. Soc.* **2006**, *128* (27), 8790-8802.
157. Arliguie, T.; Lescop, C.; Ventelon, L.; Leverd, P. C.; Thuéry, P.; Nierlich, M.; Ephritikhine, M., C–H and C–S Bond Cleavage in Uranium(III) Thiolato Complexes. *Organometallics* **2001**, *20* (17), 3698-3703.
158. Matson, E. M.; Fanwick, P. E.; Bart, S. C., Formation of Trivalent U–C, U–N, and U–S Bonds and Their Reactivity toward Carbon Dioxide and Acetone. *Organometallics* **2011**, *30* (21), 5753-5762.
159. Roger, M.; Belkhiri, L.; Thuéry, P.; Arliguie, T.; Fourmigué, M.; Boucekkine, A.; Ephritikhine, M., Lanthanide(III)/Actinide(III) Differentiation in Mixed Cyclopentadienyl/Dithiolene Compounds from X-ray Diffraction and Density Functional Theory Analysis. *Organometallics* **2005**, *24* (21), 4940-4952.
160. Jensen, M. P.; Bond, A. H., Comparison of Covalency in the Complexes of Trivalent Actinide and Lanthanide Cations. *J. Am. Chem. Soc.* **2002**, *124* (33), 9870-9877.

161. Matson, E. M.; Forrest, W. P.; Fanwick, P. E.; Bart, S. C., Functionalization of Carbon Dioxide and Carbon Disulfide Using a Stable Uranium(III) Alkyl Complex. *J. Am. Chem. Soc.* **2011**, *133* (13), 4948-4954.
162. Behrle, A. C.; Walensky, J. R., Insertion of tBuNC into thorium-phosphorus and thorium-arsenic bonds: phosphazaallene and arsaazaallene moieties in f element chemistry. *Dalton Trans.* **2016**, *45* (24), 10042-10049.
163. Arney, D. S. J.; Schnabel, R. C.; Scott, B. C.; Burns, C. J., Preparation of Actinide Phosphinidene Complexes: Steric Control of Reactivity. *J. Am. Chem. Soc.* **1996**, *118* (28), 6780-6781.
164. Duttera, M. R.; Day, V. W.; Marks, T. J., Organoactinide phosphine/phosphite coordination chemistry. Facile hydride-induced dealkoxylation and the formation of actinide phosphinidene complexes. *J. Am. Chem. Soc.* **1984**, *106* (10), 2907-2912.
165. Gardner, B. M.; Balázs, G.; Scheer, M.; Tuna, F.; McInnes, E. J. L.; McMaster, J.; Lewis, W.; Blake, A. J.; Liddle, S. T., Triamidoamine–Uranium(IV)-Stabilized Terminal Parent Phosphide and Phosphinidene Complexes. *Angew. Chem. Int. Ed.* **2014**, *53* (17), 4484-4488.
166. Rookes, T. M.; Wildman, E. P.; Balázs, G.; Gardner, B. M.; Wooles, A. J.; Gregson, M.; Tuna, F.; Scheer, M.; Liddle, S. T., Actinide–Pnictide (An–Pn) Bonds Spanning Non-Metal, Metalloid, and Metal Combinations (An=U, Th; Pn=P, As, Sb, Bi). *Angew. Chem. Int. Ed.* **2018**, *57* (5), 1332-1336.
167. Becker, G.; Mundt, O.; Rössler, M.; Schneider, E., Bildung und Eigenschaften von Acylphosphanen. VI. Synthese von Alkyl- und Arylbis (trimethylsilyl)- sowie Alkyl und Aryltrimethylsilylphosphanen. *Z. Anorg. Allg. Chem.* **1978**, *443* (1), 42-52.

168. Gilman, H.; Pacevitz, H. A.; Baine, O., Benzylalkali Compounds¹. *J. Am. Chem. Soc.* **1940**, *62* (6), 1514-1520.
169. Avens, L. R.; Burns, C. J.; Butcher, R. J.; Clark, D. L.; Gordon, J. C.; Schake, A. R.; Scott, B. L.; Watkin, J. G.; Zwick, B. D., Mono(pentamethylcyclopentadienyl)uranium(III) Complexes: Synthesis, Properties, and X-ray Structures of $(\eta\text{-C}_5\text{Me}_5)\text{U}(\text{THF})_3$, $(\eta\text{-C}_5\text{Me}_5)\text{U}(\text{py})_3$, and $(\eta\text{-C}_5\text{Me}_5)\text{U}[\text{N}(\text{SiMe}_3)_2]_2$. *Organometallics* **2000**, *19* (4), 451-457.
170. Warner, B. P.; Scott, B. L.; Burns, C. J., A simple preparative route to bis(imido)-uranium(VI) complexes by the direct reductions of diazenes and azides. *Angew. Chem. Int. Ed.* **1998**, *37* (7), 959-960.
171. Sheldrick, G., SHELXT - Integrated space-group and crystal-structure determination. *Acta Crystallogr. A* **2015**, *71* (1), 3-8.
172. Sheldrick, G., Crystal structure refinement with SHELXL. *Acta Crystallogr. C* **2015**, *71* (1), 3-8.
173. Thorn, A.; Dittrich, B.; Sheldrick, G. M., Enhanced rigid-bond restraints. *Acta Crystallogr. A* **2012**, *68* (4), 448-451.
174. Spek, A., PLATON SQUEEZE: a tool for the calculation of the disordered solvent contribution to the calculated structure factors. *Acta Crystallogr. C* **2015**, *71* (1), 9-18.
175. Windorff, C. J.; Evans, W. J., ²⁹Si NMR Spectra of Silicon-Containing Uranium Complexes. *Organometallics* **2014**, *33* (14), 3786-3791.

176. Evans, W. J.; Mueller, T. J.; Ziller, J. W., Lanthanide versus Actinide Reactivity in the Formation of Sterically Crowded $[(C_5Me_5)_3ML_n]$ Nitrile and Isocyanide Complexes. *Chem. Eur. J.* **2010**, *16* (3), 964-975.
177. Matson, E. M.; Breshears, A. T.; Kiernicki, J. J.; Newell, B. S.; Fanwick, P. E.; Shores, M. P.; Walensky, J. R.; Bart, S. C., Trivalent Uranium Phenylchalcogenide Complexes: Exploring the Bonding and Reactivity with CS_2 in the Tp^*_2UEPh Series (E = O, S, Se, Te). *Inorg. Chem.* **2014**, *53* (24), 12977-12985.
178. Walensky, J. R.; Martin, R. L.; Ziller, J. W.; Evans, W. J., Importance of Energy Level Matching for Bonding in Th^{3+} - Am^{3+} Actinide Metallocene Amidinates, $(C_5Me_5)_2[iPrNC(Me)NiPr]An$. *Inorg. Chem.* **2010**, *49* (21), 10007-10012.
179. Ortu, F.; Formanuk, A.; Innes, J. R.; Mills, D. P., New vistas in the molecular chemistry of thorium: low oxidation state complexes. *Dalton Trans.* **2016**, *45* (18), 7537-7549.
180. Lam, O. P.; Anthon, C.; Heinemann, F. W.; O'Connor, J. M.; Meyer, K., Structural and Spectroscopic Characterization of a Charge-Separated Uranium Benzophenone Ketyl Radical Complex. *J. Am. Chem. Soc.* **2008**, *130* (20), 6567-6576.
181. Hall, S. W.; Huffman, J. C.; Miller, M. M.; Avens, L. R.; Burns, C. J.; Sattelberger, A. P.; Arney, D. S. J.; England, A. F., Synthesis and characterization of bis(pentamethylcyclopentadienyl)uranium(IV) and -thorium(IV) compounds containing the bis(trimethylsilyl)phosphide ligand. *Organometallics* **1993**, *12* (3), 752-758.
182. Hou, Z.; Stephan, D. W., Generation and reactivity of the first mononuclear early metal phosphinidene complex, $Cp^*_2Zr:P(C_6H_2Me_3-2,4,6)$. *J. Am. Chem. Soc.* **1992**, *114* (25), 10088-10089.

183. Erickson, K. A.; Kagan, B. D.; Scott, B. L.; Morris, D. E.; Kiplinger, J. L., Revisiting the bis(dimethylamido) metallocene complexes of thorium and uranium: improved syntheses, structure, spectroscopy, and redox energetics of $(C_5Me_5)_2An(NMe_2)_2$ ($An = Th, U$). *Dalton Trans.* **2017**, 46 (34), 11208-11213.
184. Bartlett, R. A.; Olmstead, M. M.; Power, P. P.; Sigel, G. A., Synthesis and spectroscopic and x-ray structural studies of the mesitylphosphines Ph_2Mes and $PHMes_2$ ($Mes = 2,4,6-Me_3C_6H_2$) and their lithium salts $[Li(THF)_3PHMes]$ and $[Li(OEt)_2PMes_2]_2$. *Inorg. Chem.* **1987**, 26 (12), 1941-1946.
185. Ishiyama, T.; Mizuta, T.; Miyoshi, K.; Nakazawa, H., Synthesis and Characterization of Some Zirconium and Hafnium Complexes with a Phosphide-Pendant Cyclopentadienyl Ligand. *Organometallics* **2003**, 22 (5), 1096-1105.
186. Lin, Z.; Marks, T. J., Metal, bond energy, and ancillary ligand effects on actinide-carbon σ -bond hydrogenolysis. A kinetic and mechanistic study. *J. Am. Chem. Soc.* **1987**, 109 (26), 7979-7985.
187. Toscano, P. J.; Marks, T. J., Dicyclopentadienyldimethylthorium/silica surface chemistry. High-resolution carbon-13 CPMAS NMR evidence for alkylation of surface silicon sites. *Langmuir* **1986**, 2 (6), 820-823.
188. ADF2017, SCM, Theoretical Chemistry, Vrije Universiteit, Amsterdam, The Netherlands, <http://www.scm.com>.
189. Perdew, J. P.; Burke, K.; Ernzerhof, M., Generalized Gradient Approximation Made Simple. *Phys. Rev. Lett.* **1996**, 77 (18), 3865-3868.

190. Yanai, T.; Tew, D. P.; Handy, N. C., A new hybrid exchange–correlation functional using the Coulomb-attenuating method (CAM-B3LYP). *Chem. Phys. Lett.* **2004**, *393* (1), 51-57.
191. Yasui, S.; Ogawa, Y.; Shioji, K.; Mishima, M.; Yamazaki, S., Dramatic Effect of Atmosphere on Product Distribution from Steady-State Photolysis of Triarylphosphines. *Bull. Chem. Soc. Jpn.* **2014**, *87* (9), 988-996.
192. Elrod, L. T.; Boxwala, H.; Haq, H.; Zhao, A. W.; Waterman, R., As–As Bond Formation via Reductive Elimination from a Zirconocene Bis(dimesitylarsenide) Compound. *Organometallics* **2012**, *31* (14), 5204-5207.
193. Pyykkö, P., Additive Covalent Radii for Single-, Double-, and Triple-Bonded Molecules and Tetrahedrally Bonded Crystals: A Summary. *J. Phys. Chem. A* **2015**, *119* (11), 2326-2337.
194. Kiplinger, J. L.; John, K. D.; Morris, D. E.; Scott, B. L.; Burns, C. J., [(C₅Me₅)₂U(Me)(OTf)]₂: A New Reagent for Uranium Metallocene Chemistry. Preparation of the First Actinide Hydrazonato Complexes. *Organometallics* **2002**, *21* (21), 4306-4308.
195. Rookes, T. M.; Wildman, E. P.; Balázs, G.; Gardner, B. M.; Wooles, A. J.; Gregson, M.; Tuna, F.; Scheer, M.; Liddle, S. T., Actinide–Pnictide (An–Pn) Bonds Spanning Non-Metal, Metalloid, and Metal Combinations (An=U, Th; Pn=P, As, Sb, Bi). *Angew. Chem. Int. Ed.* **2018**, *57* (5), 1332-1336.
196. Edwards, P. G.; Harman, M.; Hursthouse, M. B.; Parry, J. S., The synthesis and crystal structure of the thorium tetraphosphido complex, Th[P(CH₂CH₂PMe₂)₂]₄, an

actinide complex with only metal-phosphorus ligand bonds. *J. Chem. Soc., Chem. Commun.* **1992**, (19), 1469-1470.

197. Settineri, N. S.; Arnold, J., Insertion, protonolysis and photolysis reactivity of a thorium monoalkyl amidinate complex. *Chem. Sci.* **2018**, 9 (10), 2831-2841.

198. Viesser, R. V.; Ducati, L. C.; Tormena, C. F.; Autschbach, J., The unexpected roles of σ and π orbitals in electron donor and acceptor group effects on the ^{13}C NMR chemical shifts in substituted benzenes. *Chem. Sci.* **2017**, 8 (9), 6570-6576.

199. Ford, P. C.; Cariati, E.; Bourassa, J., Photoluminescence Properties of Multinuclear Copper(I) Compounds. *Chem. Rev.* **1999**, 99 (12), 3625-3648.

200. Chen, C.; Weng, Z.; Hartwig, J. F., Synthesis of Copper(I) Thiolate Complexes in the Thioetherification of Aryl Halides. *Organometallics* **2012**, 31 (22), 8031-8037.

201. Fier, P. S.; Luo, J.; Hartwig, J. F., Copper-Mediated Fluorination of Arylboronate Esters. Identification of a Copper(III) Fluoride Complex. *J. Am. Chem. Soc.* **2013**, 135 (7), 2552-2559.

202. Rogers, J.; Dowsett, A. B.; Dennis, P. J.; Lee, J. V.; Keevil, C. W., Influence of Temperature and Plumbing Material Selection on Biofilm Formation and Growth of *Legionella-Pneumophila* in a Model Potable Water-System Containing Complex Microbial-Flora. *Appl. Environ. Microb.* **1994**, 60 (5), 1585-1592.

203. Ranford, J. D.; Sadler, P. J.; Tocher, D. A., Cytotoxicity and antiviral activity of transition-metal salicylato complexes and crystal structure of Bis(diisopropylsalicylato)(1,10-phenanthroline)copper(II). *J. Chem. Soc., Dalton Trans.* **1993**, (22), 3393-3399.

204. Festa, R. A.; Thiele, D. J., Copper: An essential metal in biology. *Curr. Biol.* **2011**, *21* (21), R877-R883.
205. Pufahl, R. A.; Singer, C. P.; Peariso, K. L.; Lin, S.-J.; Schmidt, P. J.; Fahrni, C. J.; Culotta, V. C.; Penner-Hahn, J. E.; O'Halloran, T. V., Metal Ion Chaperone Function of the Soluble Cu(I) Receptor Atx1. *Science* **1997**, *278* (5339), 853-856.
206. Long, F.; Su, C.-C.; Zimmermann, M. T.; Boyken, S. E.; Rajashankar, K. R.; Jernigan, R. L.; Yu, E. W., Crystal structures of the CusA efflux pump suggest methionine-mediated metal transport. *Nature* **2010**, *467* (7314), 484-488.
207. Lane, A. C.; Barnes, C. L.; Antholine, W. E.; Wang, D.; Fiedler, A. T.; Walensky, J. R., Di- and Trinuclear Mixed-Valence Copper Amidinate Complexes from Reduction of Iodine. *Inorg. Chem.* **2015**, *54* (17), 8509-8517.
208. Niemeyer, M., σ -Carbon versus π -Arene Interactions in the Solid-State Structures of Trimeric and Dimeric Copper Aryls (CuAr)_n (n = 3, Ar = 2,6-Ph₂C₆H₃; n = 2, Ar = 2,6-Mes₂C₆H₃). *Organometallics* **1998**, *17* (21), 4649-4656.
209. Ives, C.; Fillis, E. L.; Hagadorn, J. R., Lithium, titanium and vanadium dithiocarboxylates. *Dalton Trans.* **2003**, (4), 527-531.
210. Niemeyer, M.; Power, P. P., Donor-Free Alkali Metal Thiolates: Synthesis and Structure of Dimeric, Trimeric, and Tetrameric Complexes with Sterically Encumbered Terphenyl Substituents. *Inorg. Chem.* **1996**, *35* (25), 7264-7272.
211. Ellison, J. J.; Ruhlandt-Senge, K.; Hope, H. H.; Power, P. P., Synthesis and Characterization of the New Selenolate Ligand -SeC₆H₃-2,6-Mes₂ (Mes = C₆H₂-2,4,6-Me₃) and Its Two-Coordinate Zinc and Manganese Derivatives: Factors Affecting

Bending in Two-Coordinate Metal Complexes with Aryl-Substituted Ligands. *Inorg. Chem.* **1995**, *34* (1), 49-54.

212. Mann, F. G.; Purdie, D.; Wells, A. F., 329. The constitution of complex metallic salts. Part V. The constitution of the phosphine and arsine derivatives of cuprous iodide. The configuration of the co-ordinated cuprous complex. *J. Chem. Soc.* **1936**, (0), 1503-1513.

213. Niemeyer, M.; Power, P. P., Synthesis and characterization of some group 1 and 2 metal derivatives of the crowding terphenyl thiolate and selenolate ligands —EC₆H₃-2,6-Trip₂ (E = S or Se; Trip = 2,4,6-i-Pr₃C₆H₂-). *Inorg. Chim. Acta* **1997**, *263* (1-2), 201-207.

214. Saednya, A.; Hart, H., Two Efficient Routes to m-Terphenyls from 1,3-Dichlorobenzenes. *Synthesis* **1996**, *1996* (12), 1455-1458.

215. Shen, V. K.; Siderius, D. W.; Krekelberg, W. P.; Eds., *NIST Standard Reference Database Number 101* September 2015 ed.; 2015.

216. Lane, A. C.; Vollmer, M. V.; Laber, C. H.; Melgarejo, D. Y.; Chiarella, G. M.; Fackler, J. P.; Yang, X.; Baker, G. A.; Walensky, J. R., Multinuclear Copper(I) and Silver(I) Amidinate Complexes: Synthesis, Luminescence, and CS₂ Insertion Reactivity. *Inorg. Chem.* **2014**, *53* (21), 11357-11366.

217. Groysman, S.; Holm, R. H., A Series of Mononuclear Quasi-Two-Coordinate Copper(I) Complexes Employing a Sterically Demanding Thiolate Ligand. *Inorg. Chem.* **2009**, *48* (2), 621-627.

218. Jayarathne, U.; Parmelee, S. R.; Mankad, N. P., Small Molecule Activation Chemistry of Cu–Fe Heterobimetallic Complexes Toward CS₂ and N₂O. *Inorg. Chem.* **2014**, *53* (14), 7730-7737.
219. Niemeyer, M., Reaktion von Kupferarylen mit Imidazol-2-ylidenen oder Triphenylphosphan - Bildung von 1:1-Addukten mit zweifach koordinierten Kupferatomen. *Z. Anorg. Allg. Chem.* **2003**, *629* (9), 1535-1540.
220. Kluge, O.; Grummt, K.; Biedermann, R.; Krautscheid, H., Trialkylphosphine-Stabilized Copper(I) Phenylchalcogenolate Complexes - Crystal Structures and Copper–Chalcogenolate Bonding. *Inorg. Chem.* **2011**, *50* (11), 4742-4752.
221. Dance, I. G.; Fitzpatrick, L. J.; Scudder, M. L., The stereochemistry of (μ-SR)₃M₃ cyclic molecules, with reference to the molecular structures of (μ-SPh)₃Cu₃(PPh₃)₄ and [(μ-SPh)₃Fe₃Cl₆]₃. *J. Chem. Soc., Chem. Commun.* **1983**, (9), 546-548.
222. Ohlmann, D.; Pritzkow, H.; Grutzmacher, H.; Anthamatten, M.; Glaser, R., A hexanuclear copper arylselenolate: synthesis, structure and proposal for its rearrangement. *J. Chem. Soc., Chem. Commun.* **1995**, (10), 1011-1012.
223. F. Stange, A.; Kaim, W., Highly dissymmetric chelate coordination of 3,4,7,8-tetramethyl-1,10-phenanthroline to CuI(SR). *Chem. Commun.* **1998**, (4), 469-470.
224. Sundararaman, A.; Lalancette, R. A.; Zakharov, L. N.; Rheingold, A. L.; Jäkle, F., Structural Diversity of Pentafluorophenylcopper Complexes. First Evidence of π-Coordination of Unsupported Arenes to Organocopper Aggregates. *Organometallics* **2003**, *22* (17), 3526-3532.
225. Kurogi, T.; Carroll, P. J.; Mindiola, D. J., A radical coupled pathway to a stable and terminally bound titanium methylenide. *Chem. Commun.* **2017**, *53* (24), 3412-3414.

Vita

Pokpong Rungthanaphatsophon was born and raised in Bangkok, Thailand. Prior to his graduate career at the University of Missouri-Columbia, he attended Chulalongkorn University as an undergraduate in Applied Chemistry. During his senior year, at Chulalongkorn University, he went to Florida State University as an undergraduate researcher in Joseph B. Schlhoff's lab. In the Spring of 2012, Pokpong received a Bachelor's of Science in Applied Chemistry.

In the Fall of 2013, Pokpong started his graduate career at the University of Missouri-Columbia, under the supervision of Dr. Justin Walensky. Pokpong successfully defended his thesis in the spring of 2018.